AE 521

DeHond

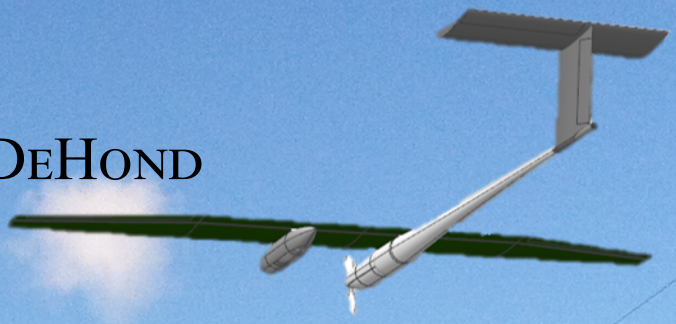

AIAA Undergraduate Individual Aircraft Design Competition 2018 - 2019

Advisor: Dr. R. Barrett-Gonzalez AIAA # 022393

Author: Jacob Rogers AIAA # 902069

The University of Kansas

Aerospace Engineering Department

10 May 2019

Table of Contents

List of Figures

List of Tables

List of Symbols

Symbol	Description	Units
a	Acceleration	ft/s^2
A	Aspect Ratio	~
b	Span	ft
$\bar{c}$	Mean Geometric Chord	ft
C_D	Coefficient of Drag	~
C_{Do}	Zero Lift Drag Coefficeint	~
C_L	Aircraft Lift Coefficient	~
C_l	Airfoil Lift Coefficient	~
D	Drag	lbf
D_{ff}	Date of First Flight	
e	Oswald Efficiency Factor	~
g	Acceleration due to Gravity	ft/s^2
GW	Gross Weight	lbf
L	Lift	lbf
m	mass	kg
n	Load Factor	~
P	Power	shp,hp
P	Pressure	psf
R	Range	nmi
S	Wing Area	ft^2
T	Thrust	lbf
T/W	Thrust to Weight Ratio	~
V	True Airspeed	kts, ft/s
$\bar{V}$	Volume Coefficient	~
W	Weight	lbf
W/S	Wing Loading	psf
x	Axis along Fuselage	ft or in
X	Distance from C.G.	in

Symbol	Description	Units
Greek Symbols		
α	Angle of Attack	rad or deg
β	Sideslip Angle	rad or deg
δ	Deflection Angle	rad or deg
ε	Wash Angle	rad or deg
Λ	Sweep Angle	rad or deg
λ	Taper Ratio	~
ρ	Air Density	lbf-s^2/ft^4
μ	Dynamic Viscosity	lbf-s/ft^2

Subscripts

D	Drag
e	Empty or Elevator
f	Fuselage
F	Fuel
h	Horizontal Tail
i	Incidence
l	Airfoil Lift
L	Wing Lift
m	Pitching Moment
MAX	Maximum
n	Yawing Moment
PL	Payload
r	Root or Rudder
S	Stall
t	Tip
TO	Take-off
v	Vertical Tail
w	Wing
wett	Wetted Area
wf	Wing-fuselage

Acronyms

AAA	Advanced Aircraft Analysis
AC	Aerodynamic Center
AID	Aircraft Intuitive Design
B.L.	Butt Line
C.G.	Center of Gravity
EO	Electro-Optical
FLIR	Forward Looking Infrared
F.S.	Fuselage Station
KE	Kinetic Energy
LiDAR	Light Detection and Ranging
MGC	Mean Geometric Chord
OE	Operating Empty Weight
RFP	Request for Proposal
RHA	Rolled Homogeneous Armor
STAMPED	Statistical Time and Market Predictive Engineering Design
UAV	Unmanned Aerial Vehicle
W.L.	Water Line

1. INTRODUCTION, MISSION SPECIFICATION AND MISSION PROFILE

This report has been created in response to the Request for Proposal (RFP) from the American Institute of Aeronautics and Astronautics (AIAA) for a power line inspection UAV. Power or transmission lines have been historically inspected with the use of helicopters carrying infrared and electrooptical sensors to inspect the lines. Inspections conducted in this manner result in high cost and put human life in danger, so many companies have begun to migrate what inspections they can to UAV platforms.

The RFP specifies that the aircraft must be able to inspect 100 linear miles of transmission lines in a single working day. The UAV will be supported by a 2018 Ford F-150 SuperCrew; the aircraft must be able to be transported within the vehicle or the vehicle's bed. The aircraft is also required to carry several sensors which make up the payload (Ref. 1).

1.1 MISSION SPECIFICATIONS

Table 1.1 below outlines the key requirements listed in the RFP as well as the payload necessary to perform the specified mission (Ref. 1). The most current reference was published in August 2018 and can be found here: https://www.aiaa.org.

Table 1.1: Power Line Inspection UAV Requirements (Ref. 1)

Performance Requirements	
Range	100 Linear Miles
Payload	3.4 LB_F LiDAR (Ref. 2) 0.09 LB_F GPS-Based Autopilot (Ref. 3) .06 LB_F ADS-B Flight Transponder (Ref. 4)
Minimum Payload	~4
Ceiling/Floor	400/150 FT AGL
Entry Into Service	2020

1.2 MISSION PROFILE, PERFORMANCE, PAYLOAD RANGE REQUIREMENTS

The mission profile for a line inspection UAV includes takeoff, climb out and cruise. The aircraft needs to be capable of cruising out 50 miles, making a 180° turn, and cruising 50 miles back to its launching station. From this point the aircraft will swap out batteries and return to the air for another flight to complete 100 miles of line inspected. A simple representation of the flight profile and circuit are shown below in Fig. 1.1. and Fig. 1.2, respectively. In addition to the mandatory payload requirement listed above in Table 1.1, the RFP listed optional payload as a Long Wave

Infrared fixed camera to detect transmission line temperature and a high-resolution still camera to improve the data collected by the LiDAR. The selection of additional sensors was left open to the Designer.

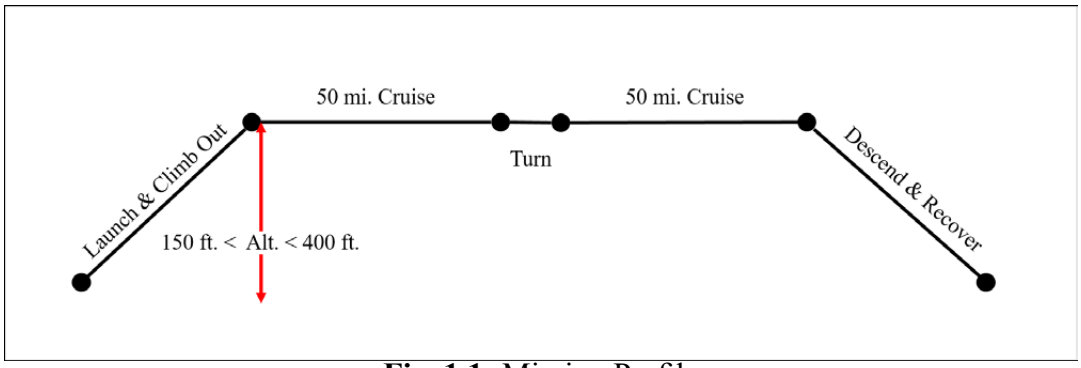

Fig. 1.1: Mission Profile

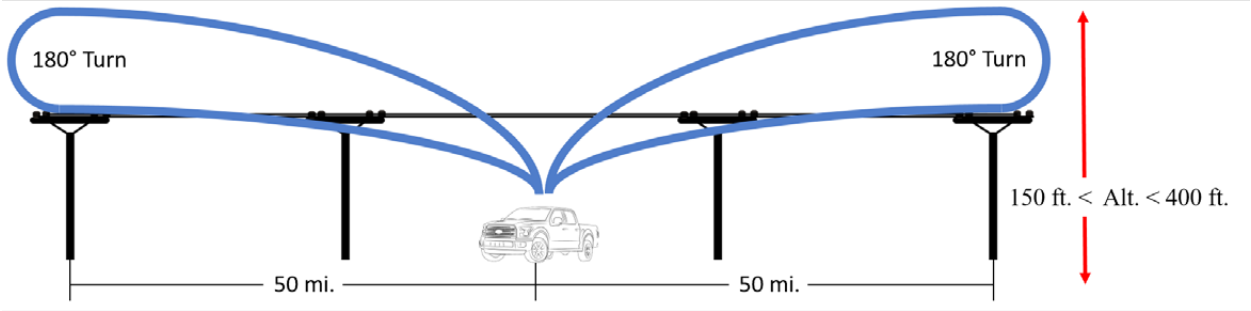

Fig. 1.2: Flight Circuit

1.3 Overall Design Method and Process

Preliminary sizing for this aircraft was accomplished using the *Airplane Design Book Part I* by Dr. Jan Roskam (Ref. 5). Adobe InDesign was used to write and compile the report into one singular book. Calculations were made using spreadsheets within Microsoft Excel and MATLAB was used for running calculations requiring multiple iterations. Preliminary sizing of the aircraft followed the process listed below.

1. Mission Specification Identified

- Mission requirements specified in RFP define what the aircraft needed to be capable of

2. Historical Overview

- List of UAVs compiled which achieve a similar range and maximum takeoff weight

3. Statistical Time and Market Predictive Engineering Design (STAMPED) Analysis

- Using the list of UAVs gathered in the previous step, STAMPED Analysis was performed to find a trend of recent market competitors

2. Historical Review

In this section the Designer will highlight several UAVs that have the capability of fulfilling a similar role to the aircraft outlined in the RFP. These aircraft were used as reference points in the STAMPED Analysis process that will be discussed later.

2.1 Power Line Inspection History

Power line inspection has been conducted largely by ground and air crews until recently as UAVs have begun to fill a large role in this market. Prior to the rise of the civilian UAVs, power companies relied on helicopter crews, flying as low as 300 feet, to inspect the power lines (Ref. 6). Not only are these practices costly, but they also pose a danger to human life. In January of 2009, while conducting a mock inspection, a Hughes OH-6A crashed after striking the ground wires of a power line. This tragic accident in North Carolina left the certified flight instructor with serious injuries and killed the commercial pilot that was certifying for future inspections (Ref. 7). While this type of accident is far from the norm, it is something that can be simply avoided by using smaller, autonomous, and much less expensive aircraft to inspect power lines.

Fig. 2.1: Helicopter Power Line Inspection (Ref. 8)

Beyond just a flight safety hazard, using UAVs to inspect power lines also keeps human operators safely on the ground further away from high-voltage equipment. UAVs can also offer the capability to perform this function remotely and likely in the future fully autonomously. Such operations could reduce labor costs in inspections and would limit the need for human technicians around high voltage power lines.

Fig. 2.2: Inspection Helicopter Crash (Ref. 9)

2.2 Market Competition

Aircraft of similar weight and endurance to the Mission Specification were selected as the market competition. Many of the aircraft that will be discussed in this section do not have the specific role of power line inspection, but do fill a utility role that would allow these UAVs to also accomplish the mission specified by the RFP. Table 2.1, below lists important characteristics of the aircraft discussed and aircraft used for STAMPED Analysis.

The Penguin C, designed and produced by UAVFactory, is a long range and high endurance UAV. This aircraft can integrate with a multitude of electrooptical (EO), infrared (IR), and light detection and ranging (LiDAR) sensors making it a versatile surveillance and inspection UAV. The Penguin can fly for up to 20 hours or out to 60 miles while powered by a 2-Stroke, fuel injected, piston engine (Ref. 10).

Fig. 2.3: Penguin C (Ref. 10)

UAVE Limited's Prion Mk3 boasts a range of over 600 miles and an endurance of over 10 hours. The company has several ideas for roles their aircraft can fill, one being LiDAR surveying. The Prion Mk3 would be an excellent candidate for this RFP as it has a large operational radius and can carry approximately 30 lb_f of payload. This UAV also features a fuel injected reciprocating engine, however the aircraft weighs over 55 lb_f when configured for survey missions (Ref. 11).

Fig. 2.4: Prion Mk3 (Ref. 11)

Delair's DT26x is an aircraft that would nearly be capable of fulfilling this RFP, for this reason it was one of the aircraft surveyed in the STAMPED Analysis discussed in chapter 4. The DT26x is sold as an all in one aircraft containing a HD Camera, a RIEGL LiDAR, and a GPS. With all this payload the maximum takeoff weight is listed at 37.5 lb_f. The aircraft is catapult assisted on takeoff, and since all the sensors are internally stored it is able to belly land (Ref. 12).

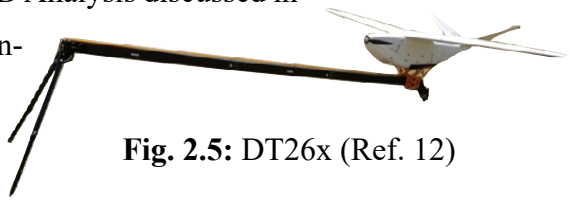

Fig. 2.5: DT26x (Ref. 12)

On the extreme is the Trans-Atlantic Model 5 which made a 38-hour flight between Newfoundland and Ireland, nearly a 1900 Nm flight. The aircraft was powered by a small 2-Stroke engine which used less than five pounds of fuel. Unfortunately, the aircraft was very limited in payload capacity; around a tenth of a pound (Ref. 13).

Table 2.1: Historical Data (Ref. 10 - 25)

Aircraft	Range (miles)	Wing Loading W/S (psf)	Empty-to-Takeoff Weight Ratio W_E/W_{TO}
AL-20	620	4.08	0.52
AR-4 Evolution	75	2.75	0.80
CSV-20	31	6.20	0.5
DT26X	93	-	1.0
Penguin B	-	5.53	0.47
Penguin BE Electric	-	4.29	0.60
Penguin C	60	5.28	0.44
Prion Mk3	600	3.23	0.64
Puma	11	1.73	0.86
Raven	6	2.38	0.73
ScanEagle	932	5.91	0.64
Sensintel Coyote	50	7.78	0.93
Silent Falcon	62	1.28	0.75
SilverFox	20	-	0.87
TAM-5	1890	0.71	0.43
Warmate	75	-	0.73

3. DESIGN VECTOR & WEIGHTS ESTABLISHMENT

The basis of the design came from the RFP (Ref. 1) and attempting to find a design that would fulfil the requirements of the proposal without needlessly exceeding them. In addition to the RFP, FAA Part 107 regulations apply to small civil UAVs. FAA Part 107 has regulations on operating altitudes and maximum speeds that apply to civil UAVs. With these requirements defined and data collected from other aircraft the STAMPED Analysis could be performed.

3.1 OBJECTIVE FUNCTION

Fig. 3.1: WRVEC

After speaking with the White River Valley Electric Cooperative (WRVEC), which provides electricity to the residents of Branson, Missouri, a rough design direction was produced. Several key items that electric distribution companies look to track are: Vegetation growth and encroachment, vegetation identification, and brush density. Tracking of these items allows the companies to better manage the so called “Right of Way” which runs along the transmission lines. Accurate vegetation growth tracking allows these companies to better manage the brush and trees in the area that can impact transmission lines Another significant requirement identified by WRVEC is the ability to fly in degraded weather conditions. The UAV they currently operate is an IP68 rated aircraft meaning that the aircraft is dust tight and water resistant down to 1 meter (~3.3 ft) of water (Ref. 26). Taking these factors into consideration the initial sizing was reworked to better meet items specified by WVREC.

OF=[Carry LiDAR, Fly 100 mi., Meet time req. (1 or 0)]
x[0.3x(Carry EO Camera (1 or 0))
+ 0.3x(Carry IR Camera (1 or 0))
+ 0.2x(IP Rating (percent of IP68))
+ 0.2x(Wind Flight Capability (percent of 20 kt sustained, 35 kt gusting))]

4. STAMPED ANALYSIS

In this section the STAMPED Analysis process used by the Designer will be covered. Statistical Time and Market Predictive Engineering Design (STAMPED) Analysis, is a form of market analysis used to evaluate past leaders in the market to predict the trend of future market leaders.

This technique targets several key variables in design selected by the Designer. Often, these variables will include empty-to-takeoff weight (We/Wto), wingspan (b), wing planform (S), and wetted area (Swett) to name a few. After the Designer has identified these key parameters they can be plotted against competitors and over time, as shown in Fig. 4.1. This method clearly illustrates the dominance of a design parameter in the market over a period leading up to the expected first flight of a future aircraft. The intent of STAMPED Analysis is to facilitate the decision-making process of preliminary design such that the final product is a result of past market trends. If the designer can effectively weight design parameters with respect to market leaders this method can be used to predict how aspects of an aircraft's design will affect its market performance. STAMPED Analysis can also help Designers predict life cycle costs of an aircraft in a given market. This facilitates the integrated product design (IPD) process that allows companies to design with life cycle cost in mind. Doing so can decrease overall cost of supporting an aircraft through its life cycle and help maximize profit.

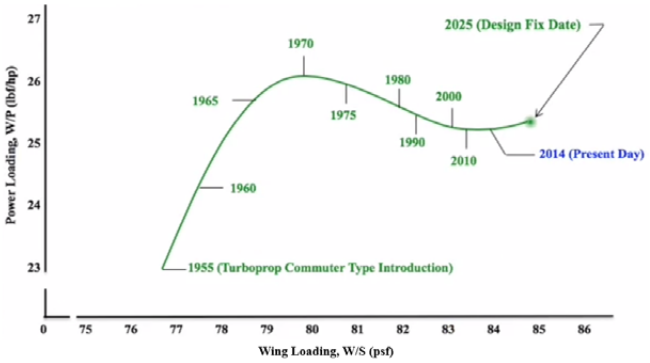

Fig. 4.1: STAMPED Analysis Data (Ref. 27)

STAMPED Analysis was performed in the preliminary sizing of this aircraft. However, little to no market share information was found as many UAV companies do not list such data. While the market share information could not be found pulling design parameters from many different aircraft of similar size and role was still very useful for sizing an aircraft for the mission specified within the RFP. Most commercially available UAVs are used as remote sensing platforms and that is effectively what this RFP is asking for. The Designer selected 16 different aircraft that fit within or near the 55 lb_f maximum takeoff weight and plotted varying aspects of each aircraft against time. This scatter plot was then used to develop a trend for each design parameter.

5. WEIGHT SIZING

STAMPED Analysis was used with data from aircraft discussed in Chapter 2 to determine the weight and weight ratios of the aircraft. All preliminary weights are listed in Table 5.1.

5.1 Maximum Takeoff Weight and Empty-to-Takeoff Weight Ratio Determination

Maximum takeoff weight and empty-to-takeoff weight ratio are two of the most important design parameters for this UAV. Firstly, the maximum takeoff weight is limited to 55 lb_f and secondly a minimum payload capacity has been estimated from the RFP. In the UAV market over the last 18 years, leading up to 2020, empty-to-takeoff weight ratio has remained roughly constant trending slightly downward; Fig. 5.1. For this design the Designer chose to stick closely to the

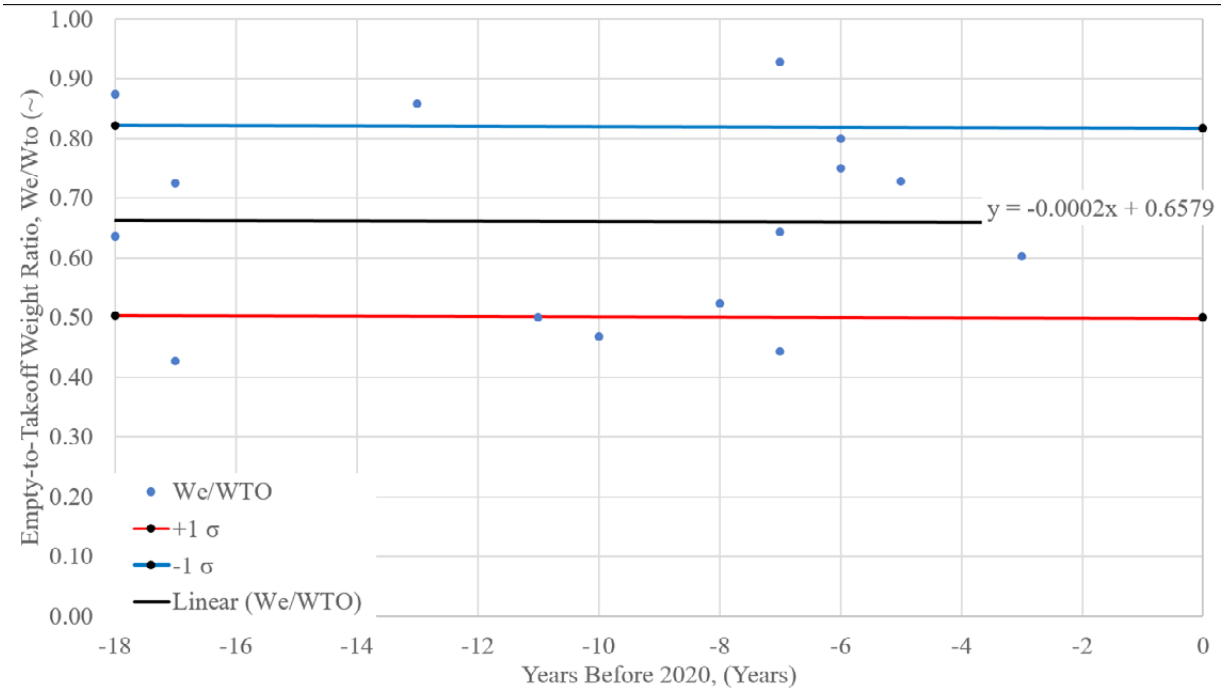

Fig. 5.1: Empty-to-Takeoff Weight Ratio, W_E/W_{TO} (~) (Ref. 10 - 25)

average as the propulsion was planned to be electric and this will drive the empty weight of the aircraft up. The minimum payload weight was approximately five pounds accounting for about 15% of the takeoff weight. The empty-to-takeoff weight ratio chosen was 0.59 which allowed a large enough margin for the payload and to have a sizeable battery. Using STAMPED Analysis, it was shown that maximum takeoff weight has been trending upward since 2002, Fig. 5.2. The initial design approach for aircraft ran along the trend line established from similar market aircraft. After performing iterations to minimize excess empty weight the maximum takeoff weight was

determined to be 36 lb_f. When compared to the aircraft used in the STAMPED Analysis the design point falls just above the trend line leaning toward one standard deviation aggressive. Because the process to determine maximum takeoff weight is iterative it relied on many different factors including powerplant sizing and wing sizing, both of which will be discussed in more depth in

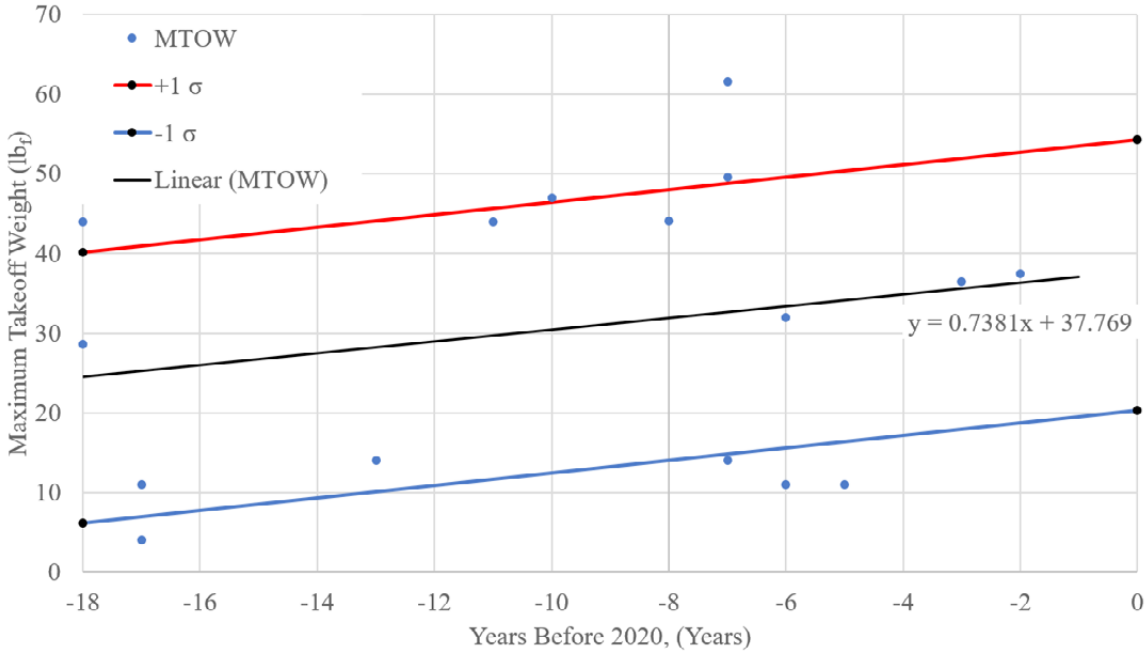

Fig. 5.2: Maximum Takeoff Weight STAMPED Data (Ref. 10 - 25)

the next chapter. Using this empty-to-takeoff weight ratio and the selected takeoff weight gives an empty weight of approximately 21 lb_f. The battery mass was found using an estimation of the needed power to drive the aircraft for the 100-mile flight as well as all auxiliary systems required to be on the aircraft. The battery weight is listed below in Table 5.1; the next chapter will discuss the battery weight was estimated.

Table 5.1: Preliminary Weight Parameters

Maximum Takeoff Weight, MTOW (lb_f)	36
Empty-to-Takeoff Weight Ratio, W_e/W_{TO} (~)	0.59
Empty Weight, W_e (lb_f)	~21.4
Battery Weight, W_{batt} (lb_f)	~9.36
Payload Weight, W_{PL} (lb_f)	~5.4

6. WING AND POWERPLANT SIZING

This chapter will discuss how the aircraft sizing chart was created and why it was created in the manner that is shown below in Fig. 6.3. The sizing chart for this mission profile is very simple; the RFP listed no maneuvering requirements and the FAA's Part 107, similarly, has no constraints on this for small UAVs. Additionally, the takeoff and landing requirements have been removed from the sizing chart because the aircraft will be catapult launched and recover via a parachute.

6.1 Drag Polar Estimation

Normally the drag polar is given for several flight conditions: Clean, takeoff flaps with gear down, takeoff flaps with gear up, landing flaps with gear up, and landing flaps with gear down. However, for this mission specification landing gear and flaps are not going to be used and because of this the drag polar depicted in Fig. 6.1 only plots the "Clean" curve. The zero-lift coefficient of drag, C_{D0}, was calculated using a lift to drag ratio, L/D_{max}, of 19. This number was determined from the STAMPED Analysis process and allows the Designer to estimate C_{D0} without also having to estimate a skin friction coefficient, C_f. For the drag polar shown below the C_{D0} value was set to 0.0185. Fig. 6.1 shows how C_{D0} and C_L were estimated.

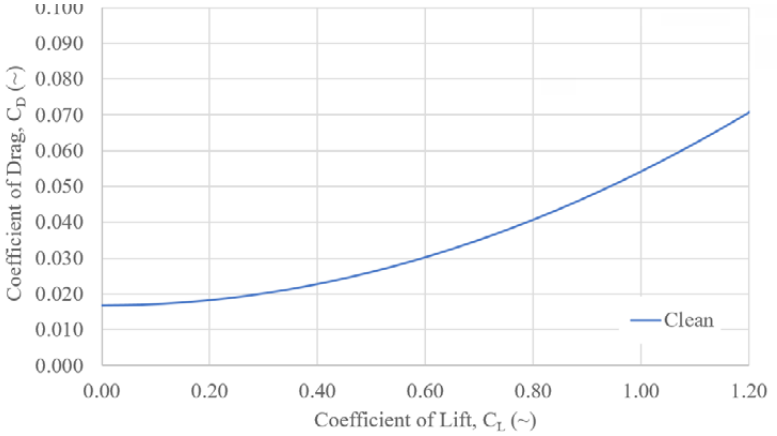

Fig. 6.1: Drag Polar Estimation

6.2 Performance Constraints

(Click to Enlarge)

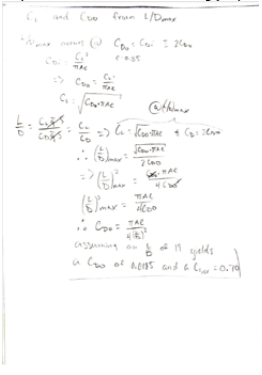

The RFP constrains the takeoff and landing distance and clearly defines the area that the aircraft must be able to takeoff and recover in. As shown in the Fig. 6.2, the aircraft needs to be able to takeoff from an unimproved surface within 500 ft. At the end of the road will be 50 ft tall trees situated 15 ft apart on either side of the road. The runway will be 10 ft wide with "tall" grass is on either side of the road on a 10 ft shoulder (Ref. 1). The required altitude for this mission is listed between 150 ft to 400 ft AGL; while there are no specific climb requirements the aircraft must be able to maintain this altitude during the whole flight. The RFP specifies that the aircraft will fly out 50 miles from the

launch area, make a 180° turn and fly back to the recovery area. There are no restrictions on the bank angle at which this turn is made. Finally, the aircraft must be able to inspect 100 linear miles of transmission lines. Effectively this means the aircraft must be able to fly 200 miles at a speed of greater than 25 mph to meet the time requirement. From both the FAA and the RFP there are ground speed limitation on the aircraft: from the FAA the maximum operating speed of any small UAV is 100 mph (87 kts) and the LiDAR specified by the RFP is limited to approximately 65 – 70 ft/s (~45 mph) depending on the range from the desired target.

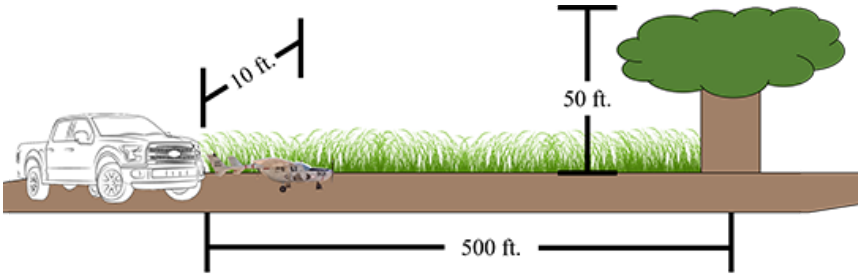

Fig. 6.2: Takeoff Constraint (Ref. 1)

6.3 Catapult Sizing

To simplify the takeoff requirement and save battery power that would otherwise be used to climb to altitude, the aircraft is planned to be catapult launched. To determine the necessary size of the catapult an energy equation was used to solve for the energy needed to launch the aircraft to height and cruise velocity. To easily clear the 50 ft trees at the end of the road the catapult was sized to launch the aircraft to 50 ft AGL; the energy necessary for this is 1800 ft-lbf (2.44 kJ). Next the cruise velocity was determined from L/Dmax to be 65 ft/s and the energy necessary to launch the aircraft to this speed is about 2390 ft-lb_f (3.23 kJ). The total input energy from the catapult is just shy of 4200 ft-lb_f (6 kJ); most commercially available UAV catapults range between 6 – 12 kJ (4425 – 8850 ft-lbf). With this input energy selected the load experience by the aircraft needed to be determined to size the length of the catapult. A load factor of 5 was selected as the maximum allowable as the load would be experienced along the X-body axis of the aircraft. The catapult length was determined to be 25 ft long which releases the aircraft at 87 ft/s. The acceleration was assumed to be constant over the length catapult resulting in an overall load factor of 4.66 that the aircraft will experience at launch.

6.4 Battery Sizing

The battery was sized based on the power necessary at cruise. This cruise cruise velocity was calculated using a $C_{L,cr}$ found from the selected L/D_{max} of 19. The resulting cruise velocity at 10,000 ft was approximately 64 ft/s, this velocity drops to 55 ft/s at sea level. With the velocity calculated the kinetic energy of the aircraft at cruise condition was found and this was used to de-

termine the instantaneous power the motor would need to deliver to the aircraft to keep it in flight. This was found to be about 295 Watts and knowing the cruise velocity and the range the aircraft must fly the total energy needed from the battery could also be found. When sizing the battery a 10 minute reserve at cruise was added to allow the aircraft to deviate in altitude or recover from a deviation in flight path if necessary. With this 10 minute reserve, and the power to run the required equipment the battery is about 727 Watt-hours and weighs approximately 9.4 lb_f.

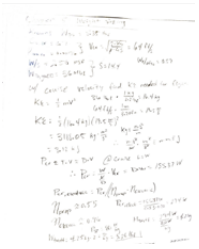

(Click to enlarge)

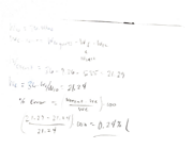

6.5 Sizing Chart Analysis

Fig. 6.3 shows the sizing chart for the preliminary sizing of the power line inspection UAV. Based on STAMPED Analysis and the sizing chart the design point chosen resulted in the following design parameters listed in Table 6.1.

Table 6.1: Aircraft Preliminary Sizing

Wing Loading, W/S (psf)	2.5
Thrust to Weight Ratio, T/W	0.076
Net Thrust, T_{Net} (lb_f)	2.74
Wing Area, S (ft^2)	14.40
Cruise Power, P_{TO} (hp)	0.39
$C_{L,cr}$	0.7

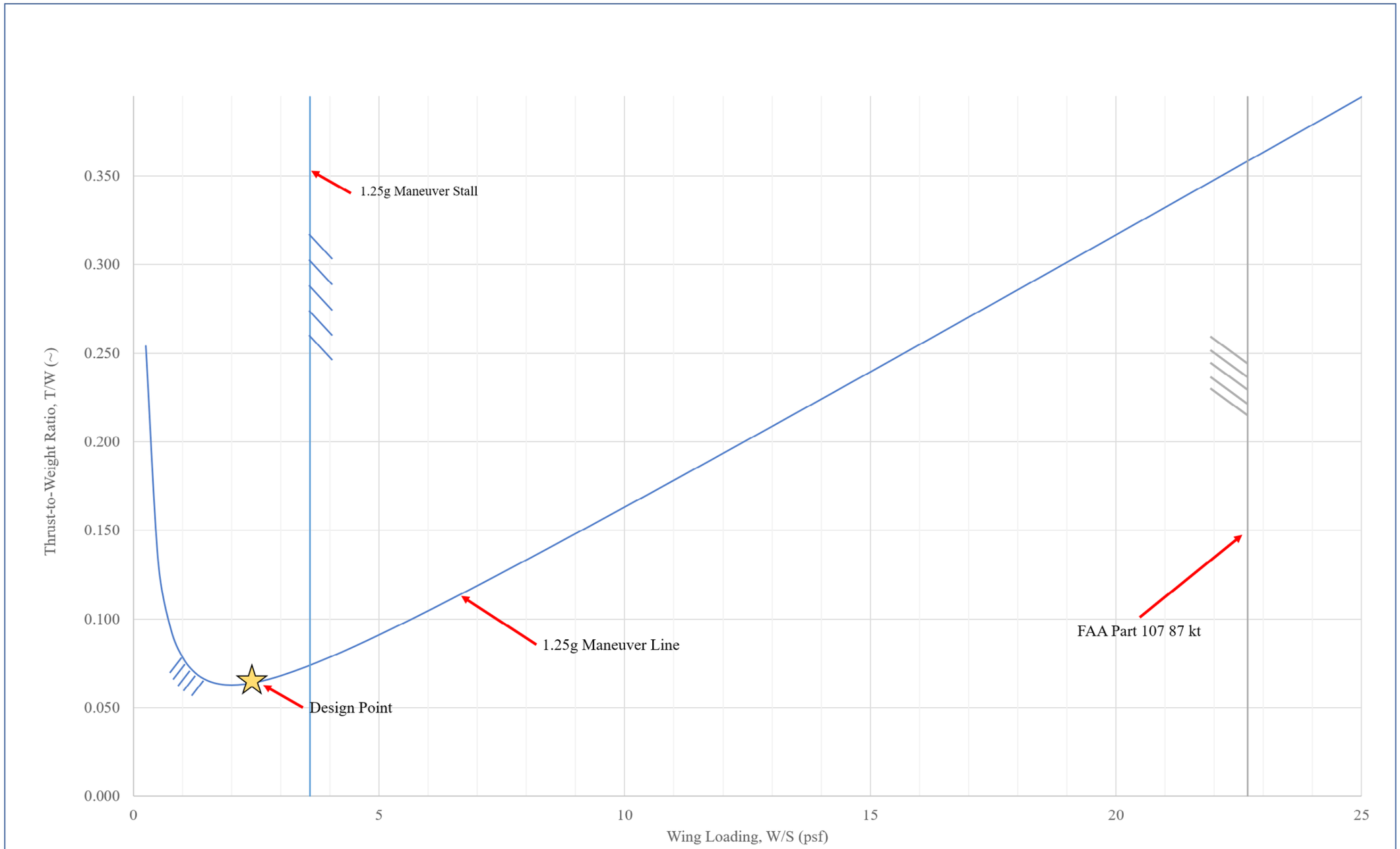

Fig. 6.3: Sizing Chart

7. Class I Configuration Matrix and Initial Downselection

This section will discuss the configurations considered for this mission and how these configurations were downselected to the final design configuration. Procedures followed for this section are from *Airplane Design Part II* (Ref. 28).

7.1. Major Impacts on the Design

The RFP (Ref. 1) lists several requirements that have driven the design and preliminary sizing of this aircraft. The most impactful requirements stated in the RFP and constraints set during the preliminary sizing of the aircraft are listed below.

- Range of 100 statute miles
- Carry LiDAR, Autopilot, and ADS-B
- Launch and recover from 500 ft. unimproved road

7.2. Comparative Study of Aircraft with Similar Performance

An in depth look at several aircraft is covered in Chapter 2 of this report. Of the vehicles examined in Chapter 2 the most similar aircraft were the Penguin B & C. Designed by UAVFactory, these aircraft are both capable of meeting the requirements listed in the RFP and are both very modular which this design aims to be. To achieve the range the endurance specified by the manufacturer both aircraft cruise at a high L/D, approximately 20, and are catapult launched to save energy that would otherwise be needed for climb out.

7.3. Configuration Sweep and Selection

7.3.1. Concept of Operations

The DeHond is designed to fly long endurance missions during which the system will be used to inspect transmission lines. The aircraft is capable of flying 100 statute miles without swapping batteries and during this flight it will power several sensors which will be used to collect data on the transmission lines. To achieve long endurance flight the aircraft will be catapult launched to reduce the altitude that the vehicle would otherwise have to climb. Additionally, the aircraft will cruise at an L/D of 19 at 43 mph. At this cruise speed the aircraft will need to remain within 160 ft of the transmission lines in order to satisfy the point density required by the mission. Based on data gathered on transmission line heights throughout the US the average height of line is roughly 40 ft with the maximum being around 110 ft

Fig. 7.1: Concept of Operations Launch (Ref. 10)

Fig. 7.2: Airbag Recovery System (Ref. 29)

tall. During most missions this will require the aircraft to cruise at under 200 ft and could cruise as high as 270 ft. Once the mission is complete the aircraft will deploy a parachute at roughly 200 ft and will land in the open area available for launch and recovery. While not in use the fuselage and sensor pod can be removed from the wing to allow for easy storage in a cushioned case provided with the aircraft. The wings will break in four sections to make handling easier. The wing will break at the midspan and then both of the three foot wingtips will be removable as well. Finally, the wing will also come with a cushioned storage case to prevent damage during transportation.

7.3.2. SELECTION OF THE OVERALL CONFIGURATION

7.3.2.1. AIRCRAFT CATEGORY

There are multiple categories of aircraft that could meet the mission described in the RFP. However, the RFP is calling for an aircraft that fills a role similar to that of military patrol aircraft which need long range and endurance to monitor wide sweeps of land or water.

7.3.2.2. CONFIGURATION SWEEP

The following aircraft, except for one, were created using the Aircraft Intuitive Design (AID) app for MATLAB (Ref. 30). The last aircraft was created in NX because AID does not facilitate the design of an asymmetric aircraft.

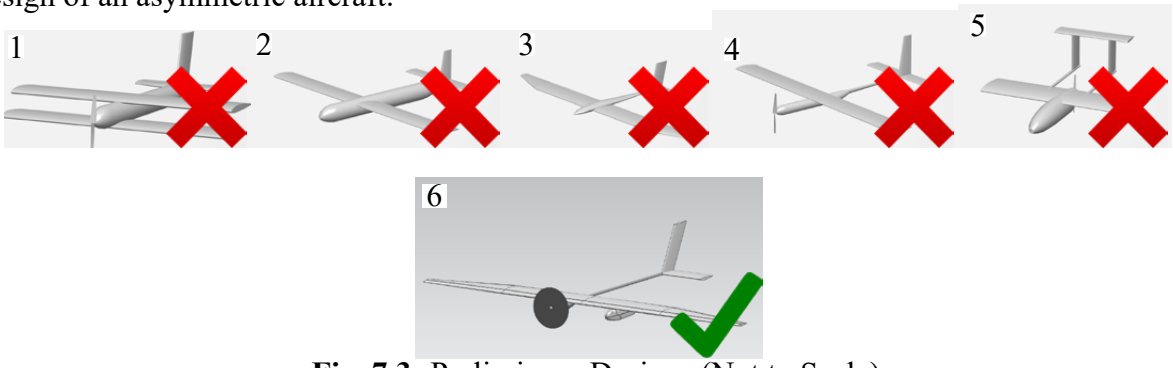

Fig. 7.3: Preliminary Designs (Not to Scale)

7.3.2.3. CONFIGURATION DOWNSELECTION REASONING

In the configuration sweep aircraft were narrowed down based upon the capability of each configuration. Justification for each downselection is shown in Table 7.1.

Table 7.1: Downselection Justification

Design	Justification
1	Low wing obscures visibility of LiDAR
2	Less capable of modularity
3	Low wing obscures visibility of LiDAR
4	Less capable of modularity
5	Not readily modular
6	Selected for high modularity with clear view for LiDAR and FLIR

7.4. Summary and Recommendations

Summary

The major findings in this chapter are:

- Final configuration is an Asymmetric Aircraft;
- Sensors and motor stored separately;
- Modular pod can be replaced with other sensor pods.

Recommendations

The author recommends that:

- A second boom be added through the wing to support the tail, and translate pitching motion better;
- Middle line replaceable unit (LRU) be added to contain parachute and arresting device.

8. LAYOUT OF THE COCKPIT AND THE FUSELAGE

This Chapter will review the design and layout of the fuselage. The fuselage design has largely changed and will be detailed further in later chapters. The design will focus on modularity that will make the DeHond capable of many different mission sets as needed by the operator. All procedures followed for the design of the fuselage come from *Airplane Design Part III* (Ref. 31).

8.1. MAJOR IMPACTS TO THE DESIGN OF THE FUSELAGE

Several items listed in the RFP were identified to have a large impact on the design of the fuselage and sensor pod that would be used to house these items.

8.2. LAYOUT DESIGN OF THE FUSELAGE

This configuration has two separate fuselages, one which will house the motor and the main battery needed to power the motor, and the second which will contain the sensors needed for collecting data on the transmission lines. The powerplant fuselage, shown in Fig. 8.1, was designed to support a tractor propeller and has the battery placed directly behind the motor. This fuselage diameter was directly driven by the height of the battery that had to be stored within it. Sizing to fit the battery resulted in the maximum diameter of this fuselage being 4.5 inches resulting in a fineness ratio of 4.3. This could be improved by extending the length of the powerplant fuselage before tapering into the boom and potentially tapering more gradually out to the end of the boom rather than attaching the boom to back of the fuselage. A ring frame and two bulkheads were added to give the structure rigidity and facilitate connection to the spars of the wing Fig. 8.1. Extending from the end of this fuselage is a tail boom which attaches to the empennage and is hollow to allow wiring to be passed back for the rudder and elevator control.

The second fuselage contains the auxiliary batteries, both placed at the front most section, followed by the LiDAR through the middle. The LiDAR was the largest object that needed to be fit within the pod, so the structure was sized to this sensor. The sensor fuselage has a maximum diameter of 4.9 inches and is 21.8 inches in length resulting in a fineness ratio of 4.45. As mentioned in the previous Paragraph, this fineness ratio could be improved by increasing the overall length of the pod. However, because the LiDAR size is not variable the maximum diameter of the pod cannot be reduced. Behind the LiDAR are several instruments necessary for flight, the eight-channel receiver, autopilot, and ADS-B. These occupy a relatively low amount of volume and can be easily transferred between fuselages as needed per mission requirement. Lastly, the FLIR and HD camera are mounted forward outside of the main pod in a separate compartment. This compartment was originally planned to have retractable windshields; however, a decision was

made to make these shields static and add a window composed of Zinc Sulfide. What is special about Zinc Sulfide is that it allows both visible light and infrared waves to transmit through with limited distortion (Ref. 32). Use of this material as a window for the FLIR and HD camera allows the operator to use both cameras whenever necessary and reduces the profile drag of the sensor pod. Making the structure static around the cameras has the added benefit of reducing mechanical complexity and better protects the cameras. To provide cooling air for the batteries and LiDAR a pitot tube was placed on the front of pod to allow air in while adding little to the profile drag of the body. The sensor fuselage also has two ring frames that support the structure and allow the pod to be attached to the forward and aft spars of the wing.

8.3. Cockpit and Fuselage Summary and Recommendations

Summary

The major findings in this chapter are:

- This design has two fuselages;
- The main fuselage is 103 inches long;
- The sensor pod is 30 inches long;
- The first has a fineness ratio of 4.3;
- The second has a fineness ratio of 4.45.

Recommendations

The author recommends that:

- The receiver, ADS-B, and autopilot be transferred to the powerplant fuselage;
- The length of both fuselages be extended to improve the fineness ratio and reduce drag;
- Replace the pitot tube with a NACA duct for cooling of batteries and systems.

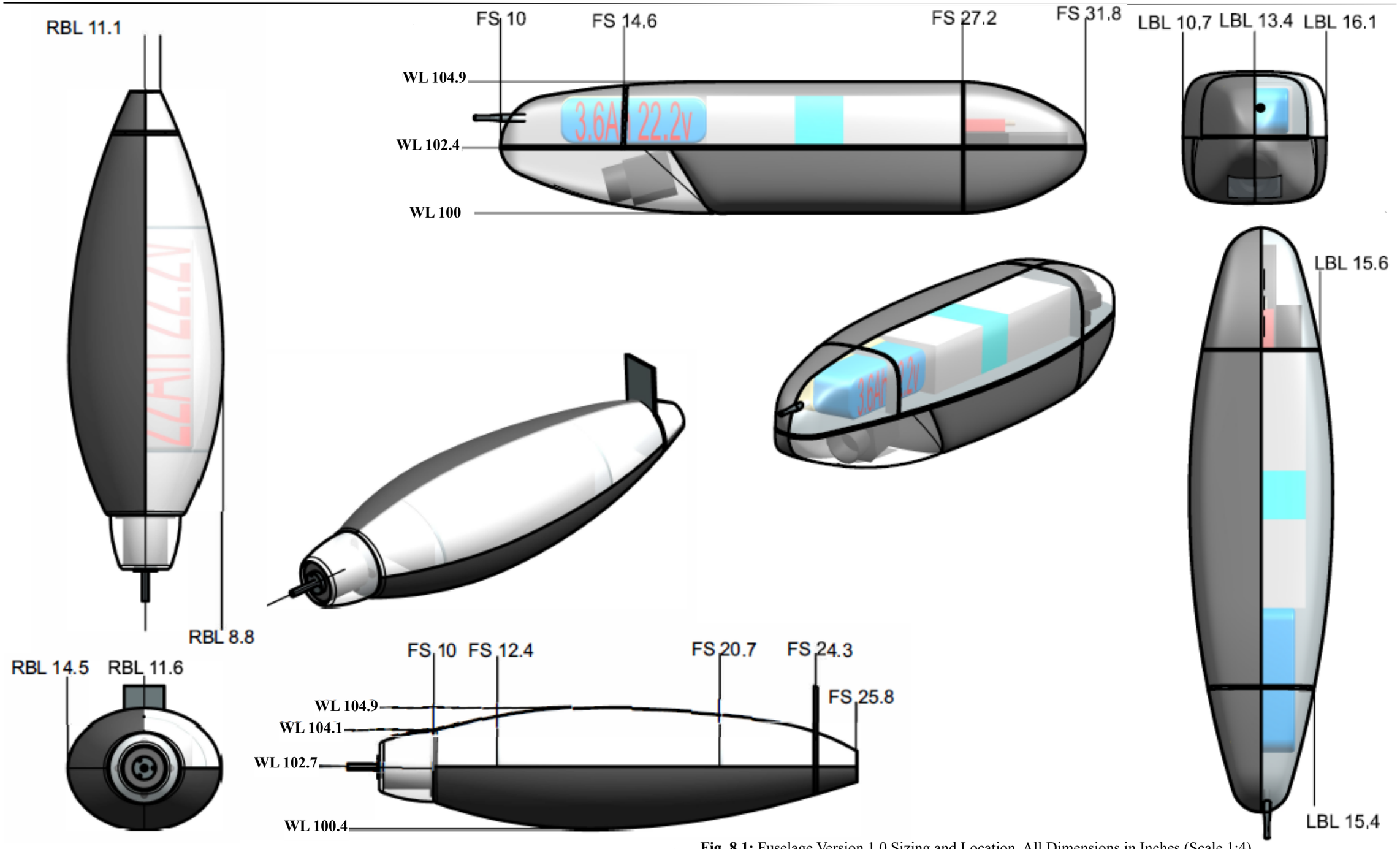

Fig. 8.1: Fuselage Version 1.0 Sizing and Location, All Dimensions in Inches (Scale 1:4)

9. Layout Design of the Propulsion Installation

This Chapter will discuss the selection of the propulsion system and how it was integrated into the design. The propulsion system must be available by 2020 as stated in the RFP (Ref. 1). Procedures followed for the selection of the propulsion system are detailed in *Airplane Design Part II* (Ref. 28)

9.1. Selection and Layout of the Propulsion Installation

The initial selection of the powerplant was based on the needed thrust for flight. This was determined from two different values. Firstly, the thrust needed for cruise was determined by setting lift equal to the weight of the aircraft. From there the L/Dmax from preliminary sizing was used to calculate the drag at cruise. During cruise the aircraft should not be experiencing any acceleration so the thrust was set equal to the drag. This results in approximately 1.9 lbf of thrust for cruise. Additionally, the aircraft was sized to a 1.25g maneuver which results in a thrust-to-weight ratio of 0.076 needed to maintain flight in this maneuvering condition. Thrust was not sized for takeoff due to the catapult system that will be used to launch the aircraft.

Fig. 9.1: Tattu 22 Ah Battery (Ref. 34)

The propulsion system was selected by using a tool called eCalc developed by the German company, Solution for All (Ref. 33). The tool also has a catalog of commercially available batteries and motors accompanied by test data which the user can use to select a motor, battery, and propeller combination. First the maximum takeoff weight of the aircraft minus the weight of the battery was input into eCalc. Next the battery was selected, the first choice was one of the highest capacity batteries available in the catalog. A 22 Ah 25C continuous discharge rate battery was used for the first iteration. This size of battery was selected due to the extended duration for which the aircraft must operate. The motor selection was also based on the long endurance mission so a motor that develops higher torque was chosen for the first iteration. Finally, a propeller of 14-inch diameter and 14-inch pitch was selected and the results calculated.

After a few iterations through eCalc the T-Motor MT3520 and the Tattu 22 Ah 25C LiPo was chosen to supply power to the motor. Running the motor at 67% throttle provided approximately 2.9 lbf of thrust and the design only needs about 1.9 lbf of thrust for cruise. In this configuration the aircraft will have an endurance of just over two and half hours, more than what is needed to complete the 100-mile flight

Fig. 9.2: T-Motor MT3520 (Ref. 35)

at the desired cruise speed. Table 9.1 below details the specifications of the chosen motor.

The Powerplant is mounted directly to a firewall on the forward section of the powerplant fuselage, this should allow for easy installation and swap out of motors if a failure occurs. The motor wires can be run through the firewall to the electronic speed controller (ESC) and the battery. A removable engine cowling was also placed over the motor to reduce drag and with an added duct could facilitate cooling of the motor.

Table 9.1: T-Motor MT3520 Specifications (Ref. 35)

Maximum Endurance Throttle, (%)	67
Thrust-to-Weight Ratio, T/W (~)	0.12:1
Maximum Diameter, (in.)	1.37
Length, L (in.)	1.67
Weight, W (lb_f)	0.45

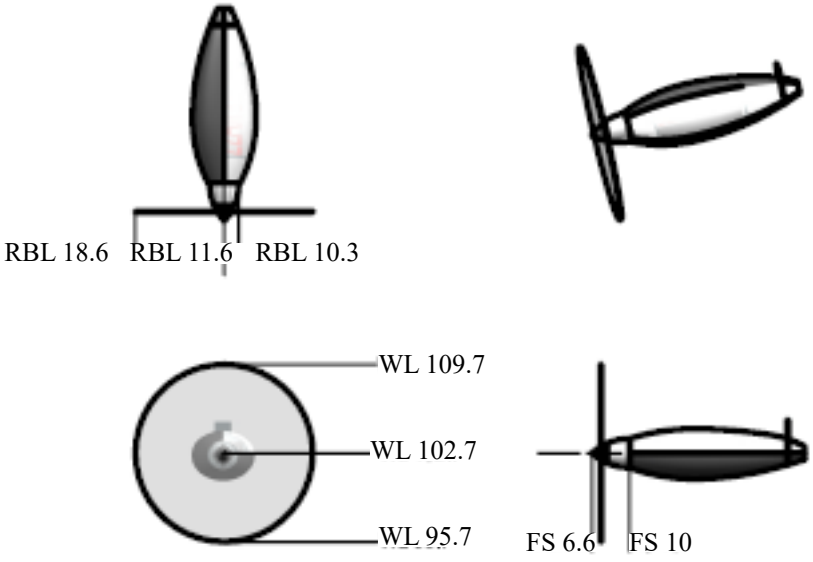

Fig. 9.3: DeHond Version 1.0: Powerplant Three View (Scale 1:20)

9.2. Propulsion Installation Summary and Recommendations

Summary

The major findings in this chapter are:

- Single T-Motors MT-3520
- 67% Throttle provides 2.9 lbf of Thrust
- Motor Thrust-to-Weight ratio (~): 0.12

Recommendations

The author recommends that:

- Dynamic testing of the motor with the aircraft be conducted;
- Integrating a NACA duct or conventional inlet will allow for better cooling of the motor.

10. CLASS I LAYOUT OF THE WING

This Chapter will discuss the design and layout of wing. All procedures used for designing the wing and other selection of certain aspects of the wing come from Airplane Design Part II (Ref. 31).

10.1. WING DESIGN LAYOUT

Many of the major design characteristics of the wing were decided in Chapter 6. The wing loading and wingspan were determined from STAMPED analysis done in Chapter 4. Using the information from these prior Chapters resulted in a wing area of 14.4 ft^2 and an aspect ratio of 10. The values listed below were derived from the equivalent wing calculated using AAA (Ref. 36).

Table 11.1: Salient Wing Characteristics

$\Lambda_{c/4}$	-3 deg
λ_w	0.31
i	0 deg
AR	10.08
Γ	0 deg

The actual wing is a cranked wing but will have similar flight characteristics to that of the equivalent wing while still taking the desired geometry that allows for easier installation of fuselage pods and should make stowage easier as well. A high aspect ratio and low taper ratio were selected because of the long range specified by the RFP. The aircraft needs to be able to cruise for a long period of time so it is beneficial to reduce drag as much as possible. Increasing the aspect ratio will help to reduce the induced drag at any given lifting condition and a taper ratio of approximately 0.4 will behave similarly to an elliptical wing in terms of lift distribution. The downside of a taper ratio is it can add to the cost of manufacturing if ribs are used because differently sized ribs will need to be made for the outboard sections of the wing.

A cranked wing was selected to satisfy the mounting requirements of the two fuselage pods. The inboard half of the wing is straight with no taper meaning the pods can be mounted anywhere along the wing and have a spar to mount to without having to move the location of the mounting brackets on the fuselage pods. To maintain the aspect ratio of the desired wing the root chord was sized to be 1.4 ft and the outer cranked sections taper down to 0.56 ft. The airfoil selected for this wing is the Eppler 403 which is a general-purpose airfoil. It was selected because for cruise the aircraft only requires a CL of 0.7. Additionally, the aircraft will be catapult launched and recover

by parachute so the only C_L requirement is coming from cruise. The AAA model of the cranked and equivalent wing is shown in Fig. 10.1. Fig. 10.2 shows the CAD models of the cranked wing.

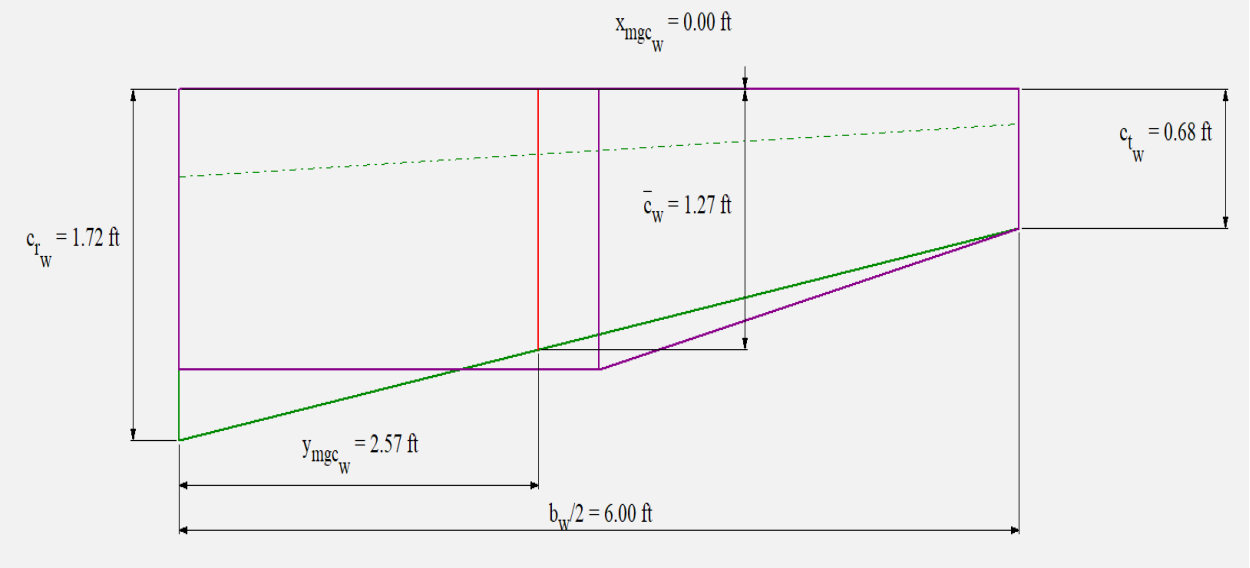

Fig. 10.1: AAA Generated Wing Planform, Scale 1:25 (Ref. 36)

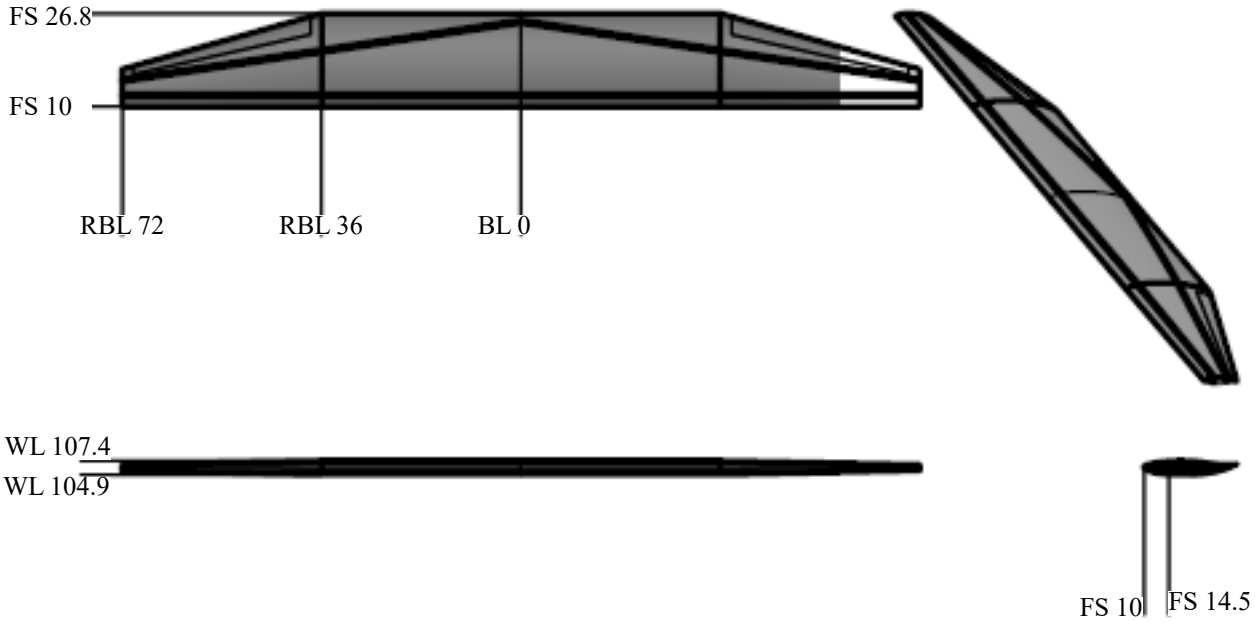

Fig. 10.2: DeHond Version 1.0:Wing Three View, All Dimension in Inches (Scale 1:40)

10.2. WING DESIGN SUMMARY AND RECOMMENDATIONS

Summary

The following values were determined to be:

- Wingspan = 12ft
- Surface Area = 14.4 ft^2
- Dihedral Angle, Γ (degrees) = 0°
- Wing aspect ratio, AR = 10.08
- Taper Ratio = 0.31
- Mean Geometric Chord, $\bar{c}$ (ft.) = 1.27 ft
- Wing airfoil is Eppler 403

Recommendations

The author recommends that:

- The aft spar be made parallel to the forward spar during the inboard straight section of the wing;
- The wing root and tip chords be modified to achieve an equivalent wing taper ratio of 0.4 while still maintaining an equivalent wing aspect ratio of 10.

11. Class I Design of the High Lift Devices

This Chapter will discuss why high lift devices were not used for this design and show hand calculations proving why this decision was made. Procedures followed for the design of high lift devices come from *Airplane Design Part III* (Ref. 31).

11.1. Design of High Lift Devices

This aircraft will be catapult launched and recover via a parachute landing system. For this reason $C_{Lmax,TO}$ and $C_{Lmax,L}$ are not needed. The aircraft needs to only achieve a C_L of 0.7 in flight to cruise at a L/Dmax of 19. For this reason, flaps will not be needed at cruise or any other segment of the mission. However, a conservative approach was used in the determination if flaps should be added to this design. The aircraft was shown to not need flaps for a maximum lift coefficient condition of 1.2. This is proven in the hand calculations by determining how much lift the equivalent wing has. This is accomplished by first finding how much lift an equivalent unswept wing would generate. Then the lift from the unswept wing is corrected for the sweep of the chosen wing. The C_{Lmax} of this equivalent wing was shown to be 1.24 which is greater than the needed 1.2. Because the wing generates more than enough lift high lift devices are not needed. The aircraft was designed such that it would be long coupled; the length between the quarter chord of the root to the quarter chord of the horizontal tail is greater than five times the size of the mean geometric chord (M.G.C). This was done so that the empennage has a longer lever arm when acting on the center of gravity (CG). This gives the design a few benefits, the first being that with a greater lever arm less elevator and rudder deflection is necessary for longitudinal and directional control. Secondly, because less elevator input is needed to trim there is a smaller down force acting on the aircraft effectively increasing the overall amount of lift generated at a trim condition. This makes it so that flaps are not needed to achieve a C_{Lmax} of 1.2. Another added benefit is with lower elevator deflections profile drag is also decreased.

(Click to Enlarge) (Click to Enlarge)

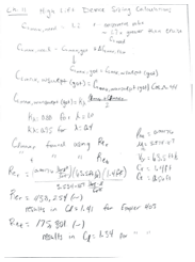

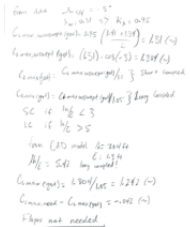

11.2. HIGH LIFT DEVICES SUMMARY AND RECOMMENDATIONS

Summary

The major findings in this chapter are:

- Aircraft is long coupled;
- Flaps are not necessary based on a C_{Lmax} of 1.2.

Recommendations

The author recommends that:

- Flaperons be used if flaps are added;
- If the aircraft changes to a short-coupled design a different airfoil be selected to achieve a higher C_{Lmax}.

12. Class I Layout of the Empennage

This section will cover the design of the empennage. The empennage is responsible for providing both a down ,and a side force, to maintain longitudinal and directional stability during all phases of flight. The procedures followed come from Airplane Design Part III (Ref. 31).

12.1. Empennage Design Procedure

The empennage is an asymmetric "T-tail" design. The "T-tail" was chosen to allow the aircraft to be catapult launched. A classic tail design would require the catapult to be designed around the vehicle. The majority of the horizontal tail lies to the left of the main fuselage. This was done to limit the amount of roll caused by the elevator during pitch. The vertical and horizontal tail were designed using several aircraft of similar size and mission. Using three-views and CAD models of these aircraft the volume coefficient of both the vertical and horizontal tail could be derived. Table 12.1 shows each aircraft that was surveyed and the tail coefficients associated with each vehicle. Hand calculations for this procedure are located at the end of this chapter.

Table 12.1: Volume Coefficients of Similar Aircraft

Aircraft	$\overline{V}_v$	$\overline{V}_h$
Prion Mk3	0.07	1.07
BV 141	0.02	0.26
BAE Kingfisher	0.06	1.18
Mugin 3mh	0.04	1.35
Average	**0.05**	**1.30**

12.2. Design of Vertical Tail

The vertical tail is swept back which provides several advantages. Firstly, the sweep increases the distance between the quarter chords of the horizontal and vertical tails and the C.G. of the aircraft. These distances, known as X_h and X_v respectively, act as the moment arms of the empennage. Increasing these distances improves the performance of the empennage by reducing the force required to balance the aircraft. Secondly, sweeping the tail couples a small, positive,

Table 12.2: Vertical Tail Characteristics

Characteristic	Design Value
Aspect Ratio, AR_v (~)	1.5
Sweep Angle, $\Lambda_{c/4}$ (degrees)	15
Taper Ratio, λ_v (~)	1
Vertical Tail Chord, C_v (ft)	1
Vertical Tail Area, S_v (ft^2)	1.5
Vertical Tail Dihedral Angle, Γ_v (degrees)	0

pitching moment with rudder deflection in either direction (Ref. 37). The airfoil selected for the vertical tail is a NACA 0012. A symmetric airfoil was selected because the aircraft is not expected to have a large yawing moment due to drag. Table 12.2 shows the characteristics of the vertical tail.

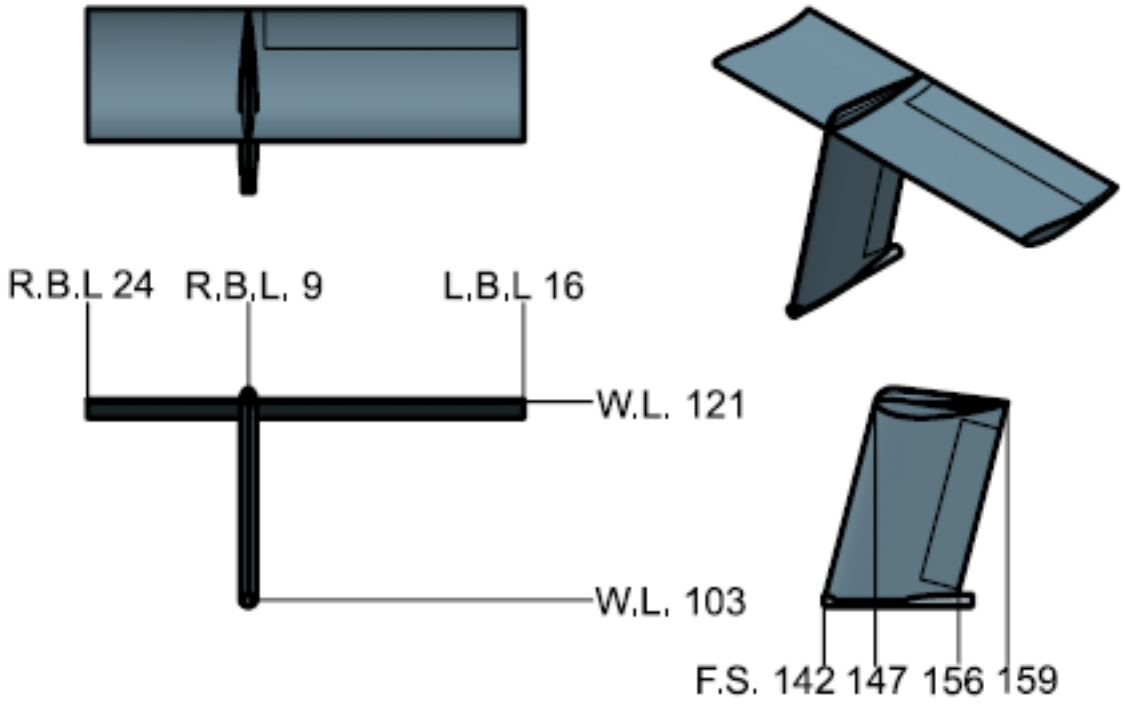

Fig. 12.1: DeHond V2.0: Empennage Three-View, All Dimensions in Inches (Scale 1:8)

12.3. DESIGN OF HORIZONTAL TAIL

The horizontal tail is straight with no taper. An inverted Selig 1210 airfoil was selected as it will always be providing a down force to counteract the pitching moment due to the wing. The quarter chord of the horizontal tail was collocated with the quarter chord of the vertical tail to place the center of lift further aft creating a larger moment arm. A horizontal tail volume coefficient of 1.3 was selected based on values collected from similar aircraft. Table 12.3 shows the characteristics of the horizontal tail.

Table 12.3: Horizontal Tail Characteristics

Characteristic	Design Value
Aspect Ratio, AR_h (~)	3.33
Sweep Angle, $\Lambda_{c/4}$ (degrees)	0
Taper Ratio, λ_h (~)	1
Horizontal Tail Chord, C_h (ft)	1
Horizontal Tail Area, S_h (ft^2)	3.3
Horizontal Tail Dihedral Angle, Γ_h (degrees)	0

12.4. Empennage Design Summary and Recommendations

Summary

The major findings in this chapter are:

- The horizontal tail aspect ratio, AR_h=3.33
- The vertical tail aspect ratio, AR_v=1
- The horizontal tail airfoil is an inverted Selig 1210
- The vertical tail airfoil is a NACA 0012
- The vertical tail is swept back 15°

Recommendations

This author recommends that:

- The placement of the horizontal tail be tested to prevent rolling moments caused by the elevator;
- More similar aircraft be surveyed to obtain more accurate volume coefficients.

Click to Enlarge

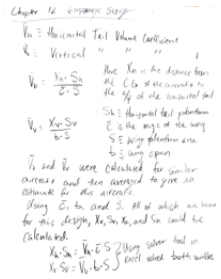

13. CLASS I DESIGN OF THE LAUNCH AND RECOVERY SYSTEMS

This section will describe the methods which will be used to launch and recover the aircraft. Due to the unconventional mission, unconventional methods for launch and recovery were selected. The procedures used for the determination of catapult energy is from a technical discussion with Dr. Barrett (Ref. 38).

13.1. CATAPULT SIZING AND GEOMETRY

The catapult was sized to launch the aircraft slightly faster than stall speed. This was chosen because the previous catapult sizing, shown in Chapter 6, resulted in a 25 ft long launcher. This would be heavy, difficult to transport, and would incur even higher costs. All hand calculations for the catapult were reworked for this length of catapult which determines the launch energy needed to be input by the catapult and also the load factor that the aircraft will experience on launch. The aircraft is planned to be launched about 20% faster than stall speed, approximately 58 fps. Using this launch speed and the mass of the vehicle the catapult energy was calculated, resulting in a 2.6 kJ launcher. Next the length of the catapult was found by setting the acceptable load factor along the X-axis of the aircraft to 5 (Ref. 38). Assuming that the catapult would accelerate the aircraft at constant velocity, the length was determined to be 10.6 ft which was rounded up to 11 ft. The catapult will launch the aircraft at a 12° angle. This angle was chosen to ensure that the would be safely off of the ground following launch and so that while resting on the catapult the tail would not drag on the ground. Figure 13 shows the planned geometry and dimensions of the catapult.

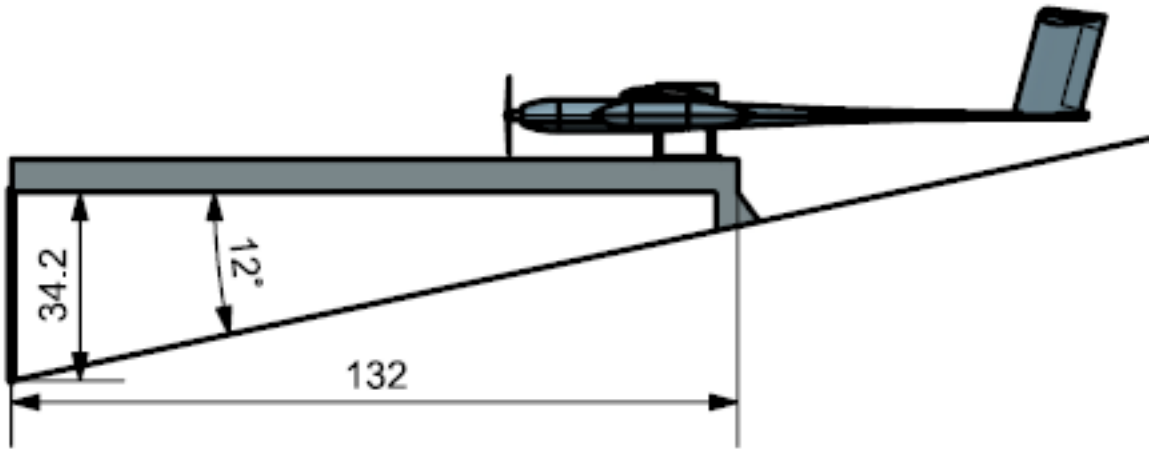

Fig. 13.1: Catapult Geometry, All Dimensions in Inches (Scale 1:40)

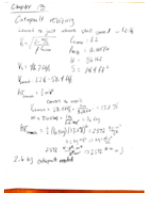
Click to Enlarge


13.2. Design of the Mount and Shuttle

Fig. 13.2: Catapult Clamps (Ref. 39)

The mount is designed to gently support the aircraft so that it does not damage the wings. This is accomplished by using two spring like clamps that are formed to the airfoil of the wing, Figure 13.2. Because the aircraft will be launched at a relatively low speed the mount was designed to allow the motor to be run while the aircraft is being launched. Figure 13.3 shows a front view of the aircraft on the catapult. The propeller has about 2.4 inches of clearance while on the catapult which should allow it to be spun during launch.

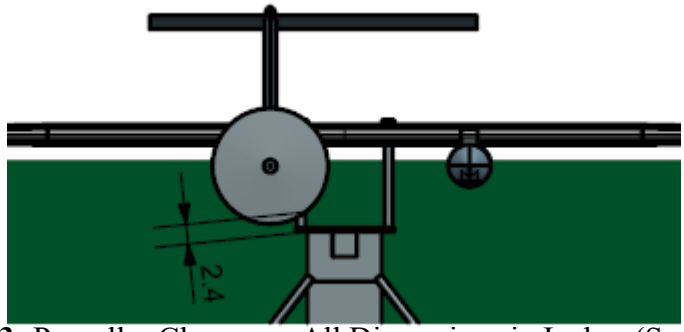

Fig. 13.3: Propeller Clearance, All Dimensions in Inches (Scale 1:20)

13.3. Parachute Selection

A wide selection of UAV parachutes is available through multiple vendors online. The parachute chosen for recovery of this aircraft comes from a vendor called Fruity Chutes. Online the company offers a sample calculator which gives the user the estimated energy the vehicle will have to absorb upon landing and the equivalent height of a free fall drop. The largest parachute that Fruity Chutes has available is a 120" diameter custom parachute rated for a 50 pound aircraft dropping at a constant 20 fps. Using their online calculator an aircraft weighing 36 lbf should fall at around 16 fps. At this descent rate an equivalent drop would be around four ft. (Ref. 40). The parachute will be stored in the main fuselage aft of the avionics. A small hatch in the fuselage will allow the parachute to be ejected when needed. The specifications of the selected parachute are listed below.

- Weight: 36 oz (2.25 lbf)
- Diameter: 120 in.
- Packed Dimensions: 5.5 in. diameter, 8 in. length (190.1 $in.^3$)

13.4. LANDING GEAR DESIGN SUMMARY AND RECOMMENDATIONS

Summary

The major findings in this chapter are:

- The design requires a catapult and parachute for launch and recovery;
- The catapult is planned to be 11 ft long;
- 2.6 kJ of energy will be delivered by the catapult;
- The parachute has a diameter of 120 in.

Recommendations

The author recommends that:

- A model for how the catapult will be stored be created;
- More analysis be dedicated to the calculation of the impact energy and how to absorb it on landing.

14. Class I Weight and Balance Analysis

This section will discuss the weight and balance analysis conducted on this aircraft. The methods used come from *Airplane Design Part V* by Dr. Jan Roskam (Ref. 41).

14.1. Preliminary Three-View

Figure 14.1shows the preliminary three-view of the Class I design. Figure 14.2 shows details of the center of gravity of all major components.

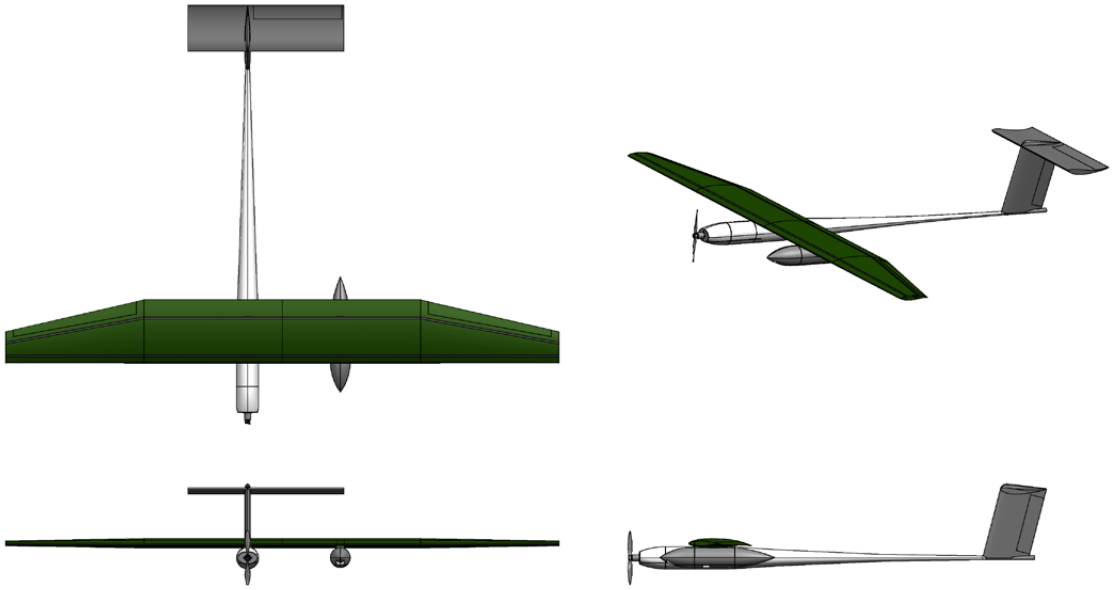

Fig. 10.4: Preliminary Three-View of DeHond, (Scale 1:50)

14.2. Class I Weights Breakdown

Weight analysis for this aircraft was determined using weight fractions from other UAVs as guidelines. These weight fractions were posted by Dr. Barrett (Ref. 42). Additionally, many of the components selected for use on this aircraft are commercially available so the weights of these items were known. Approximate weight fractions for the structure of various sections of the aircraft were found using similar aircraft. These weight fractions of the structure was then adjusted as needed so that the sum of all weight fractions was equal to one.

The wing accounted for roughly a quarter of the takeoff weight. The wing was given a large portion of the weight fraction because it is one of the largest items on the aircraft and will need to endure cyclic loading and unloading. The wing will also have two spars that attach to the fuselage and sensor pod. The main fuselage and sensor pod were also allocated a larger portion of the weight fraction as these will carry all avionics and sensors aboard the aircraft. Additionally, the aircraft will land on these after parachuting down so the bottom of both will need to be reinforced. The empennage weight fraction was considerably as both the horizontal and vertical tail can be

made of lightweight foam wrapped in either a plastic or other composite.

14.3. CLASS I WEIGHT AND BALANCE CALCULATION

Using both the CAD model of the aircraft and the weights determined from weight fractions the center of gravity could be approximated; Table 14.1. For most of the components within the aircraft, C.G. was simple to approximate as these objects are mostly symmetric so finding a halfway point between the height and length was suitable. For parts of the aircraft which have more complex geometry Airplane Design Part V (Ref. 41) outlines methods which can be used to approximate the C.G. Because this aircraft is asymmetric both the longitudinal and lateral C.G. needed to be found to ensure the aircraft will be stable in both planes. Figure 14.2 and Table 14.2 thoroughly detail the locations of all components, their weights, and their C.G. Hand calculations outlining the process used to calculate the aircraft C.G. are shown below.

Table 14.1: DeHond Weight Fractions and Weights of Major Components

Item	Weight Fraction, (~)	Weight, W (lbf)	Fuselage Station, F.S. (in.)	Butt Line, B.L. (in.)
Motor	0.015	0.53	52.00	9.02
Powerplant Battery	0.152	5.49	59.79	9.02
Avionics Battery	0.014	0.52	66.44	9.07
Auto-Pilot	0.001	0.05	66.07	9.07
Receiver	0.001	0.02	65.65	9.22
ADS-B	0.002	0.06	67.32	9.18
Parachute	0.063	2.25	73.14	9.02
FLIR	0.008	0.28	64.91	-14.96
LiDAR	0.094	3.40	71.06	-15.10
Sensor Battery	0.035	1.27	78.43	-15.02
Wing	0.213	7.67	71.92	0.00
Servos Aileron	0.008	0.28	75.71	0.00
Servos Tail	0.008	0.28	155.41	9.02
Main Fuselage	0.192	6.91	93.12	9.02
Sensor Pod	0.125	4.50	77.60	-15.10
Horizontal Tail	0.035	1.24	150.59	3.82
Vertical Tail	0.035	1.24	148.33	9.02
Total	1	36.00	80.66	0.52

Click to Enlarge

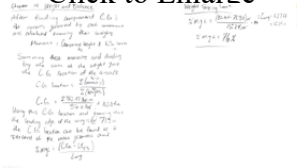

Table 14.2: DeHond Weight and Balance

	Item	Weight, W (lbf)	Weight Fraction, (~)	F.S. (in)	W*F.S. (lbf-in)	W.L. (in)	W*W.L. (lbf-in)	B.L. (in)	W*B.L. (lbf-in)
1	Motor	0.53	0.015	52.00	27.63	102.90	54.67	9.02	4.79
2	Main Battery	5.5	0.152	59.79	328.21	102.04	560.14	9.02	49.49
3	Aux Battery 2	0.52	0.014	66.44	34.42	102.04	52.87	9.07	4.70
4	Auto-Pilot	0.05	0.001	66.07	3.50	102.73	5.44	9.07	0.48
5	Receiver	0.02	0.001	65.65	1.35	103.30	2.12	9.22	0.19
6	ADS-B	0.06	0.002	67.32	4.04	103.28	6.20	9.18	0.55
7	Parachute	2.25	0.063	73.14	164.55	102.90	231.52	9.02	20.29
8	FLIR	0.28	0.008	72.31	20.47	103.06	29.17	-14.96	-4.24
9	LiDAR	3.40	0.094	78.46	266.76	102.97	350.09	-15.10	-51.35
10	Aux Battery 1	1.27	0.035	85.83	109.18	102.99	131.01	-15.02	-19.10
11	Wing	7.67	0.213	77.32	592.89	106.72	818.32	0.00	0.00
12	Servos Aileron	0.28	0.008	81.08	22.70	107.05	29.96	0.00	0.00
13	Servos Tail	0.28	0.008	155.41	43.50	120.69	33.78	9.02	2.52
14	Main Fuselage	6.91	0.192	93.12	643.63	102.90	711.24	9.02	62.33
15	Sensor Pod	4.50	0.125	77.42	348.38	102.97	463.37	-15.10	-67.96
16	Horizontal Tail	1.24	0.035	150.59	187.03	120.69	149.90	3.82	4.74
17	Vertical Tail	1.24	0.035	148.33	184.23	112.28	139.45	9.02	11.20
	C.G.	36.00	1.000	82.84		104.70		0.52	

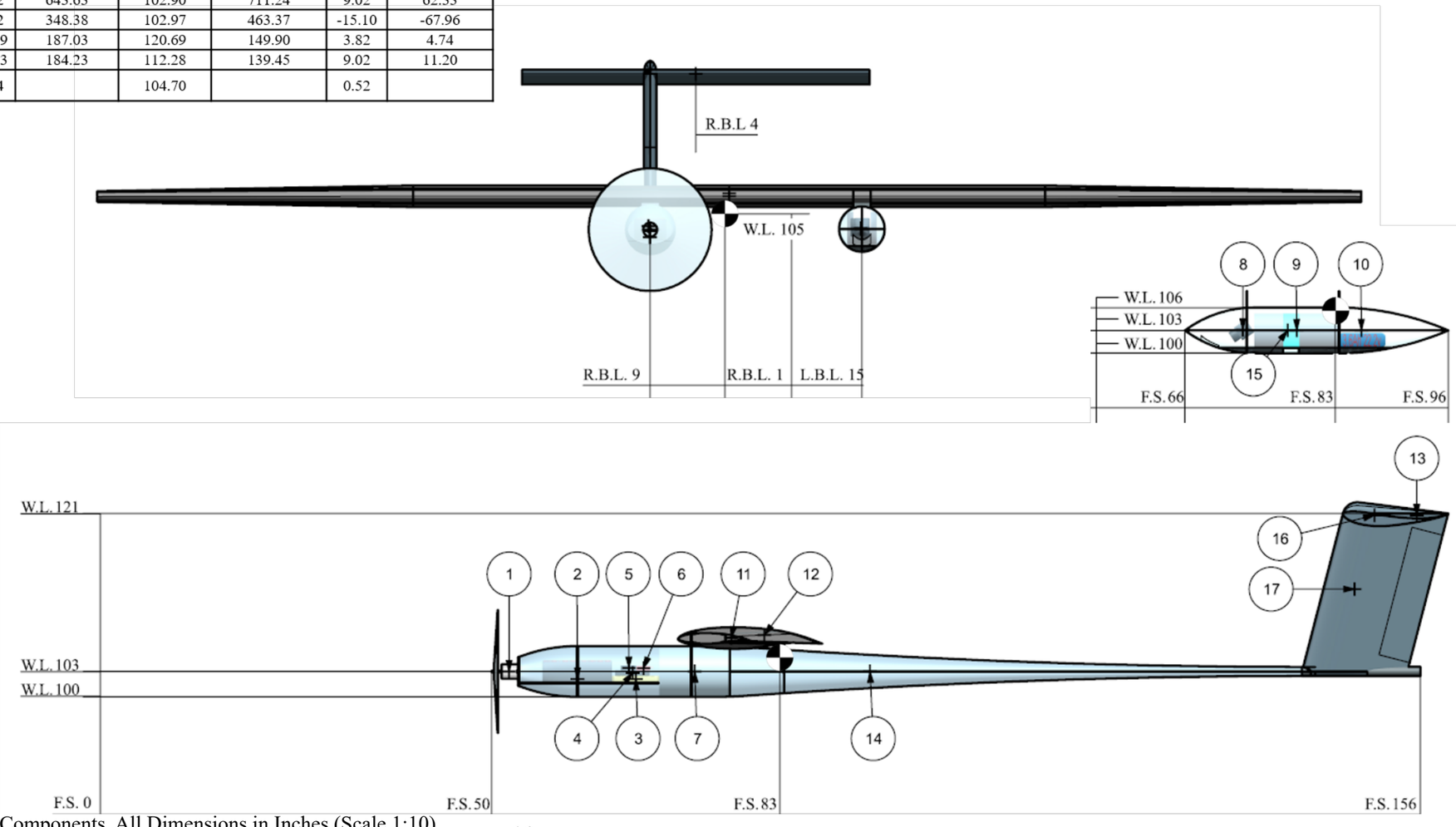

Fig. 14.1: DeHond V2.0: C.G. Location of Major Components, All Dimensions in Inches (Scale 1:10)

14.4. C.G. EXCURSION DIAGRAM

The C.G. excursion diagram is shown in Figure 14.2. This diagram shows how the location of the C.G. shifts during different loading conditions. This aircraft only has three different loading conditions because it is battery powered. Also, since none of the payload will be dropped or removed during or between flights there is no in-flight C.G. excursion. Currently the center of gravity resides approximately on the aft spar of the wing which is at about 75% of the mean geometric chord. It is possible that the C.G. is too far back. However, since the stability of the aircraft has not yet been determined the designer chose to not adjust the configuration.

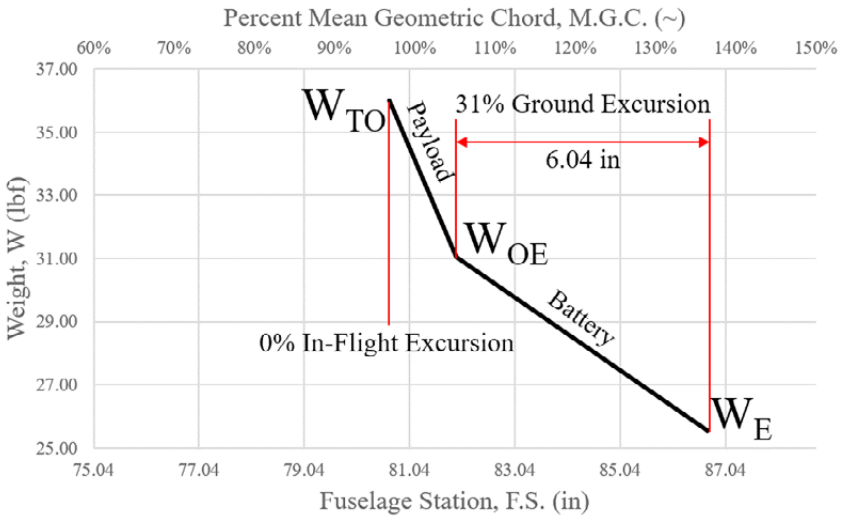

Fig. 14.2: C.G. Excursion Diagram

The maximum center of gravity shift occurs when the aircraft is in its empty configuration. Removing the battery results in a 33% shift aft of the operating empty weight C.G. Fortunately, this mission does not require the aircraft to ever operate fully unloaded. Because of the aft C.G. it may be possible for the aircraft to operate with a static margin of zero. Doing so would reduce the trim drag and improve battery economy while in flight.

14.5. SUMMARY AND RECOMMENDATIONS

Summary

The major findings of this chapter are:

- The in-flight C.G. is located at 75% of the M.G.C;
- There is no in-flight C.G. shift;
- The battery critically impacts the location of the C.G.

Recommendations

The author recommends that:

- The C.G. be adjusted after stability analysis is conducted.

15. V-n Diagram

This chapter covers how the V-n diagram for this aircraft was constructed. All methods used come from *Airplane Design Part V* (Ref. 41).

15.1. Presentation of the V-n Diagram

A V-n diagram, shown in Figure 15.1, is the flight envelope in which an aircraft can operate. The vertical axis depicts the load factor, given as a multiple of gravity. The horizontal axis represents the flight speed of the vehicle. The area under the solid curve is the envelope where the aircraft can fly, outside of that envelope the vehicle either stalls or breaks apart because it was not designed to take those loads. The dotted lines represents the gust loading at various flight speeds. This aircraft V-n diagram was created following rules from FAR 25 so gust speeds were set at 66, 50, and 25 feet per second. Neither the RFP, or Part 107 of the FAA restricts the load factor that the aircraft must be able to survive. The RFP listed "Capable of flight in 20 knot sustained winds and 35 knot gusting winds" as a tradeable requirement. However, this design is not capable of withstanding such loads. The aircraft was designed for a maximum positive load factor of 3.8 g's and a maximum negative load factor -1 g's. The diving speed, V_D, is 89 fps and the cruise speed, V_C, was calculated for cruise at maximum lift over drag as, 63 fps. Additionally, this aircraft may need to survive shock loads up to 30 g's. This was accounted for in Section 7.3.1 Concept of Operations. The aircraft is broken down for storage and placed in cushioned cases to help reduced the impact from the shock loads experienced in transit. Hand calculations for the graph are provided below.

Click to Enlarge

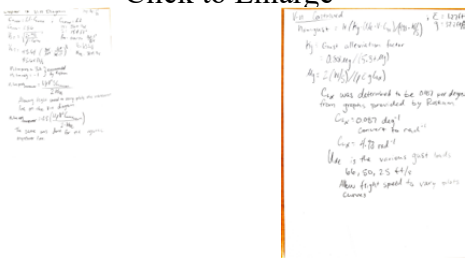

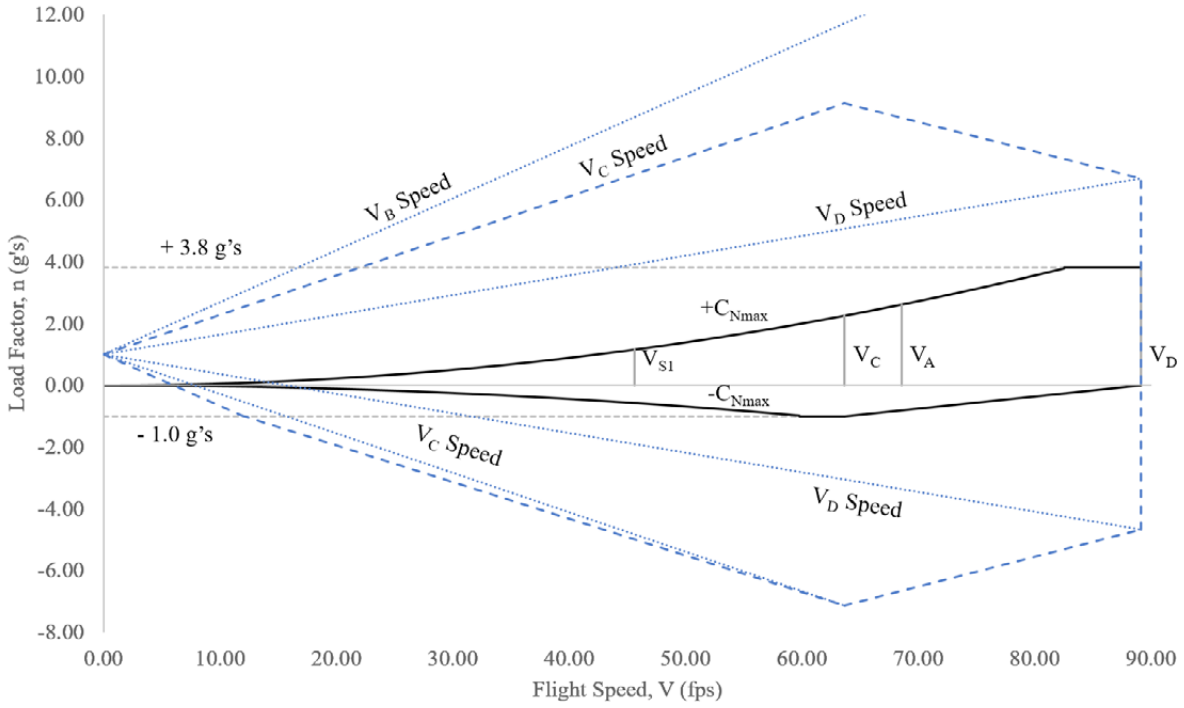

Fig. 15.1: V-n Diagram

16. Class I Stability and Control Analysis

This chapter will discuss the procedure for analyzing the stability of this aircraft. Both longitudinal and directional stability were analyzed. The yawing moment due to an engine out condition was considered as the engine does not act through the center axis of the vehicle. The procedures followed in this Chapter come from *Airplane Design Parts II* and *VI* (Ref. 28 & 43).

16.1. Longitudinal Stability Analysis

For the aircraft to be inherently stable it must have a positive static margin of approximately 10%. An aircraft with a static margin close to zero will be more maneuverable and responsive. Another benefit of a small static margin is the reduced trim drag the aircraft will experience. This occurs because a stable aircraft will have a tendency to pitch down. To counteract the downward pitching moment the elevator must be deflected to keep the nose level. A long range aircraft could be designed to have a static margin of zero and use a feedback loop to stabilize the aircraft. Thus, reducing the trim drag and increasing the efficiency of the aircraft. This aircraft was designed with this concept in mind. The aircraft has a design static margin of 0.2% and is stabilized with an SAS feedback gain, k_α, of 0.38 deg/deg.

Fig. 16.1: DeHond Multhopp Integration

The desired static margin was calculated by first finding the aerodynamic center of the wing and fuselage. Next, the lift-curve-slope of the horizontal tail was found based on the characteristics listed in Chapter 12. Using the horizontal tail lift-curve-slope and the characteristics of the empennage, the downwash on the horizontal tail was also be found. This will be needed to determine the aerodynamic center of the aircraft. Lastly, the Münk Shift for the fuselage was found by Multhopp integration. Due to the cylindrical shape of the fuselage the body will produce some lift and can cause the aerodynamic center of aircraft to shift forward. With all of these items found the aerodynamic center can be plotted as a function of the horizontal tail area, S_h. Figure 16.2 shows the longitudinal X-plot for this aircraft. The design point for this aircraft has a horizontal tail area of 3.46 ft^2 resulting in a static margin just over 0%. Since there is no in-flight center of gravity shift this aircraft will have a constant static margin barring any structural damage.

Table 16.1: Longitudinal Aerodynamic Coefficients

Wing-Fuselage Aerodynamic Center, $\bar{X}_{ac_{wf}}$(%MGC)	97%
Center of Gravity, C.G. (%MGC)	97%
Münk Shift, (%MGC)	-1%
Static Margin, SM (%MGC)	0.2%

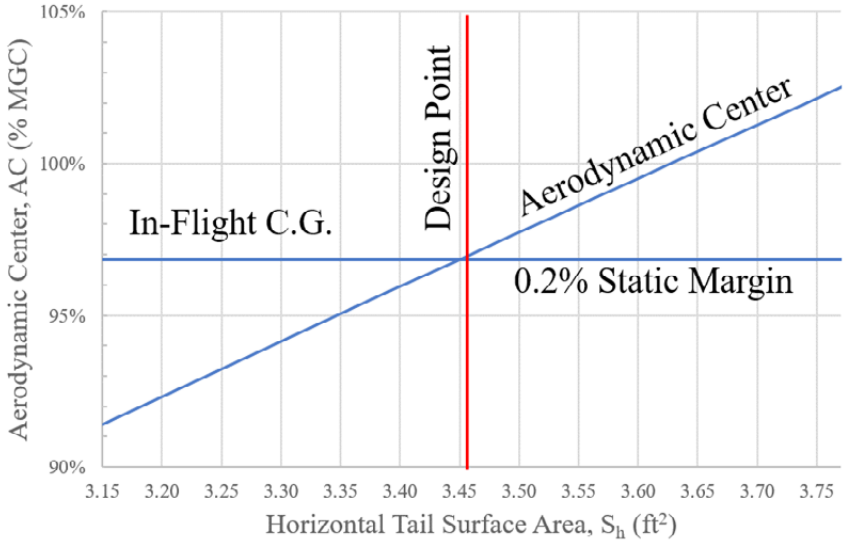

Fig. 16.2: Aerodynamic Center with Respect to Horizontal Tail Size

16.2. DIRECTIONAL STABILITY ANALYSIS

The directional stability was determined by the yawing moment due to sideslip, $C_{n\beta}$. The weathercock, or directional, stability of this aircraft was calculated by using the characteristics of both the fuselage and vertical tail. The fuselage largely contributes to the directional stability as it can cause a large, negative, yawing moment due to a sideslip. The effects of this were calculated by finding the effective area of the side of the fuselage. Then, the lift-curve-slope of the vertical tail was found to determine how effective it was at counteracting this yawing moment. Figure 16.3 shows the selected vertical tail area as well as the relationship between yawing due to sideslip with respect to the area of the vertical tail. Dr. Roskam recommends that $C_{n\beta}$ must be at least 0.001/deg for directional stability to be achieved (Ref. 43). This design has a vertical tail, S_v, area of 1.5 ft² as

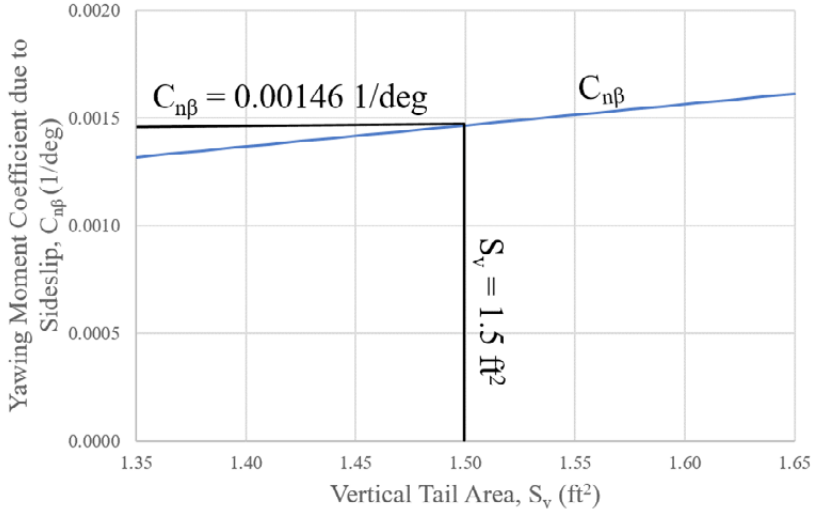

Fig. 16.3: Vertical Tail Sizing

Table 16.1: Vertical Tail Characteristics

S_v (ft²)	1.5
Vertical Tail Lift-Curve-Slope, $C_{L\alpha V}$ (deg⁻¹)	0.03
$C_{n\beta}$ (deg⁻¹)	1.46E-3

was chosen from similar aircraft in Chapter 12. Based on this tail area the yawing moment due to sideslip is 0.00146/deg which comfortably meets the criteria laid out by Dr. Roskam.

16.3. Engine Inoperative

This aircraft was also designed to meet the engine inoperative condition. This was calculated because there will be a small, positive yawing moment caused by the drag on the propeller. Normally, a single engine aircraft would not need to be concerned with this. However, because the motor does not act along the center line of the vehicle. This yawing moment must be counteracted by the tail and rudder. For a fixed pitch propeller the drag caused by an inoperative engine, N_D, is approximately 25% of the moment created by this same engine during its operating condition. The airspeed evaluated under this condition, V_{mc}, was 120% of the stall speed. This velocity is still 5 ft/s slower than the cruise speed and will rapidly decline. After determining these values the yawing moment due to the rudder, $C_{n\delta r}$, could be found and subsequently the rudder deflection, δ_r, needed.

Under the circumstance that the engine loses power, the rudder must deflect approximately 1° to keep the aircraft stable with the engine out. The engine out condition was evaluated and designed to ensure that the aircraft could be recovered safely, but also so it could be controlled to prevent harm to bystanders on the ground. Table 16.2 details values critical to important to the engine inoperative condition.

Table 16.2: Engine Out Values

N_D	0.51 ft-lbf
V_{mc}	58.4 ft/s
$C_{n_{\delta r}}$	0.07/rad
$\delta_{r_{required}}$	1°




16.4. STABILITY AND CONTROLS SUMMARY AND RECOMMENDATIONS

Summary

The major findings in this chapter are:

- The design SAS feedback gain, k_{α}, is 0.38 deg/deg;
- The Static Margin is 0.2%;
- The horizontal tail area, S_h=3.46ft^2;
- The yawing moment due to sideslip, $C_{n\beta}$ = 0.00146/deg;
- The vertical tail area, S_v = 1.5 ft^2;
- The rudder is sized for the one engine inoperative condition with $\delta_{r_{required}}$ = 1°.

Recommendations

The author recommends that:

- Testing be conducted to determine the in-flight effectiveness of the elevator and rudder.

17. Class I Drag Polar and Performance Analysis

This Chapter will discuss how the drag polar was recalculated for this aircraft. The updated drag polar is based on the final configuration of Class I design. Iterations made to get to this design will be discussed further in Chapter 18. The procedures followed in this section are found in Parts II and VI of *Airplane Design* by Dr. Roskam (Ref. 28 & 43).

17.1. Wetted Area Breakdown

The wetted area of this aircraft was determined by surface area measurements in the CAD model created in Siemens NX. Procedures detailed in *Airplane Design Part II* (Ref. 43) were followed as a rough order of magnitude check for the CAD. However, these equations often oversimplify the geometry of the aircraft and overestimate the wetted area. Because of this all final values presented in this section come from the CAD model. To ensure surfaces were not doubly accounted for intersections were subtracted. For example, sections where the wing and fuselage meet were subtracted from both wetted areas. One method suggested is a perimeter plot; such a plot is shown in Figure 17.1. Hand calculations at the end of this section will show a few examples of the equations Dr. Roskam provides. Table 17.1 details the wetted areas of each component of

Table 17.1: Component Wetted Area

Component	Wetted Area
Wing	28.5 ft^2
Fuselage	15.5 ft^2
Empennage	10.1 ft^2
Total	**54.1 ft^2**

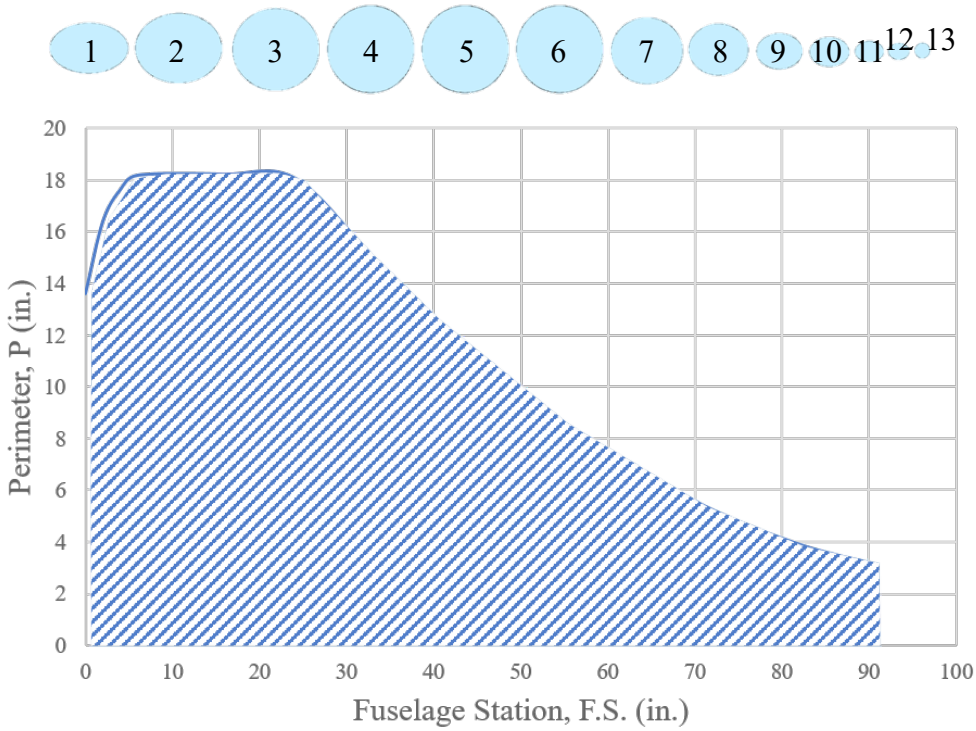

Fig. 17.1: Perimeter of Plot of the Main Fuselage

the aircraft.

Cross-sections one through four represent the nose of the main fuselage. Sections five through eight represent the main bay of the fuselage, and sections nine through thirteen represent the tail cone. This same process was followed for the sensor pod and a perimeter plot of this was also created, Figure 17.2. The sensor pod is symmetric across the XZ and XY plane of its own body so all cross sections are circular. Sections one through four and nine through thirteen represent the nose and tail cone respectively. Sections five through eight represent the main bay of the sensor

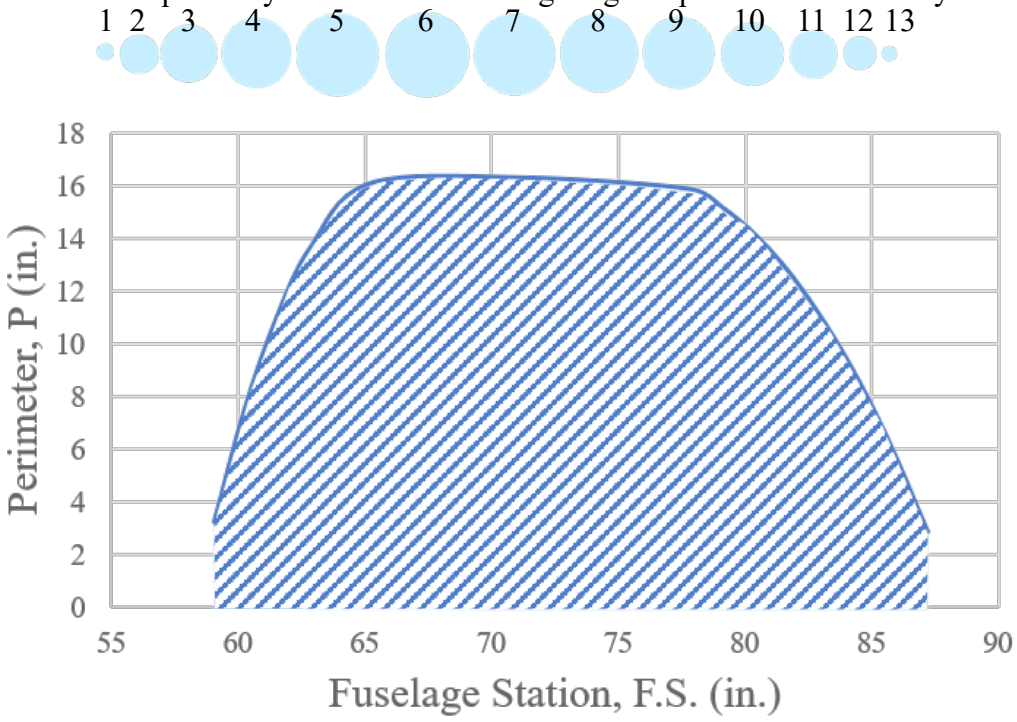

Fig. 17.2: Sensor Pod Perimeter Plot

pod.

17.2. DESIGN DRAG POLAR

Using the updated wetted area from the CAD model, the new drag polar charts could be created. First, the parasite area, f, had to be calculated so that the new zero lift drag coefficient, C_{D0}, could be found. This was accomplished using equation 3.21 from *Part I of Airplane Design* (Ref. 5). Normally, for a full sized aircraft this would not be necessary and the charts provided by Dr. Roskam could be used to approximate the parasite area. However, these charts do not scale down to the wetted area of smaller UAVs and because such could not be used. Equation 3.21 is dependent upon the equivalent skin friction coefficient, c_f. The final design c_f was dependent on the lift-to-drag ratio, L/D, that the aircraft needs to achieve. By first solving using a conservative c_f value, approximately

0.005, the corresponding C_{D0} could be found and used to determine L/D. Depending on whether this L/D was too high or too low a new c_f was selected until L/D converged to the desired cruise value of 19. This process is shown in further detail in the hand calculations. With C_{D0} found, the drag polar can be plotted; Figure 17.3. For this aircraft only a single curve is plotted as there are no landing gear or flaps.

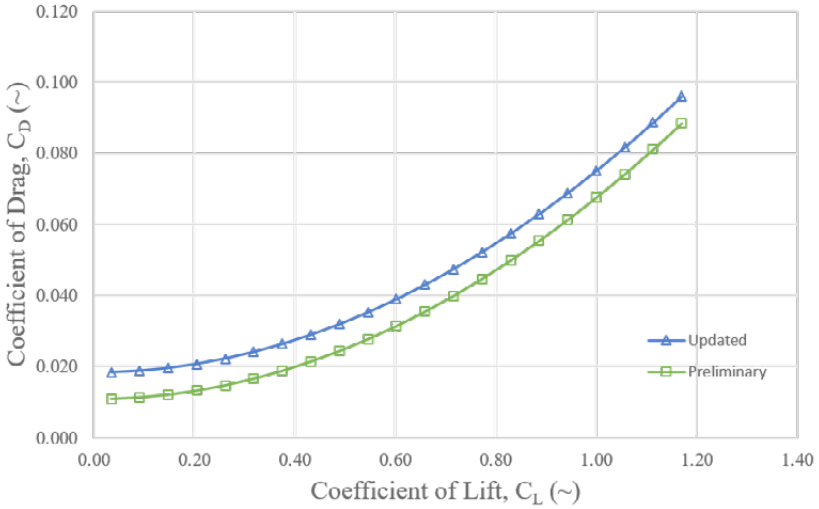

Fig. 17.3: Preliminary and Updated Drag Polar

Table 17.2: Design Parasite Coefficient

Equivalent Skin Friction Coefficient, c_f (~)	0.0049
Parasite Area, f (ft^2)	0.26 ft^2
Zero Lift Drag Coefficient, C_{D0} (~)	0.00489
Lift-to-Drag Ratio, L/D (~)	19.07

17.3. Drag Polar and Performance Summary and Recommendations

Summary

The major findings in this chapter are:

- The designed wetted area is 54.1 ft^2 with a parasite area of 0.26 ft^2;

- The equivalent skin friction coefficient, c_f, is 0.0049;
- The parasite drag coefficient, C_{D0} is 0.00489.

Recommendations

The author recommends that:

- Wetted area be reduced by converting the aft fuselage to a constant cross-section boom.

18. Analysis of Weight and Balance, Stability and Control

This Chapter will cover the analysis of weight and balance on the stability and control of the aircraft. Additionally, design iterations that were made to improve the stability of the aircraft will be discussed here. The procedures followed are from *Airplane Design Part II* (Ref. 28).

18.1. Impact of Weight and Balance, Stability and Control

Dr. Roskam highlights three major points which must be met in Class I design.

1. The aircraft must not have a "tip-over" problem on the ground.
2. The aircraft must not have too much travel between the forward and aft C.G.
3. The aircraft must be longitudinally and directionally stable.

This design meets both of the first two requirements as it does not have landing gear and it carries a static payload (i.e. no C.G. shift). However, the initial design was far from longitudinally stable. This was corrected by adjusting the location of payload and avionics and by moving the wing of the aircraft. Specific iterations that led to the aircraft meeting all criteria will be discussed in section 18.3.

18.2. Analysis of Critical L/D Results

Using the new drag polar, shown in Chapter 17, the lift-to-drag ratio was recalculate. To achieve the desired L/D of 19 the skin friction coefficient had to be reduced slightly to 0.0049. This value should still be attainable. However, depending on the maintenance of the aircraft and the environment it is flying in this skin friction coefficient could degrade due to bugs or dirt and this will cause the L/D to suffer. This could be improved by cutting down wetted area in components where it is not necessary. As mentioned in Chapter 17, the aft section of the fuselage could be converted into a constant cross-section boom which would reduce the wetted area slightly. Table 18.1 shows the design characteristics that impacted the L/D at 10,000 ft MSL.

Table 18.1: Design Lift to Drag Ratios

	alt. (ft)	W (lbf)	V (ft/s)	C_L	C_D	$(L/D)_{Designed}$	L/D
Inspection	10,000	36.0	300	0.63	0.027	19	19.07

As shown in Chapter 17 and the above table, the L/D of this configuration meets the design L/D. Because the design meets the needed L/D, the takeoff weight does not need to be changed from the originally planned 36 lbf. However, if the skin friction coefficient were to significantly degrade, the takeoff weight would need to be reduced in order to meet the mission requirements. However, as this design met the design lift-to-drag ratio within 5% this option has not yet been explored.

18.3. DESIGN ITERATIONS PERFORMED

The design of DeHond has changed largely over the course of Class I design. This can be highlighted by looking back to Chapter 8, where both the main fuselage and original sensor pod are shown. One of the earliest iterations made was the redesign of both of these components. Firstly, the main fuselage was converted to a more traditional fuselage extending back to the empennage; Figure 18.1. The sensor pod was also redesigned around static viewing windows for both the FLIR camera and the LiDAR as opposed to the originally planned mechanical doors. Finally, all avionics that were previously stored and powered in the sensor pod were relocated to the main fuselage, as was suggested in the recommendations in that section. This allows the sensor pod to be removed without significant performance impact on the aircraft. The redesigned sensor pod, Figure 18.2, also allows all the payload weight to be roughly collocated with the C.G. of the aircraft improving stability. A parachute was also added to the main fuselage, this helped slightly with weight and balance but was added for the purpose of recovery. The empennage was redesigned to allow the aircraft to clear the catapult. The horizontal tail was raised to t-tail shape.

The second set of iterations made were with respect to the stability of the aircraft. The benefit of this design is that it has been easy to relocate the wing along the main fuselage. This allows the designer to easily shift both the aerodynamic center and the center of gravity, C.G., of the vehicle. The wing was adjusted until the aerodynamic center of the vehicle lay close the C.G. At this point the horizontal tail area was grown slightly to make the static margin of the aircraft nearly zero. Designing for a static margin of zero reduces the carbon footprint of the vehicle by increasing the efficiency that it flies at.

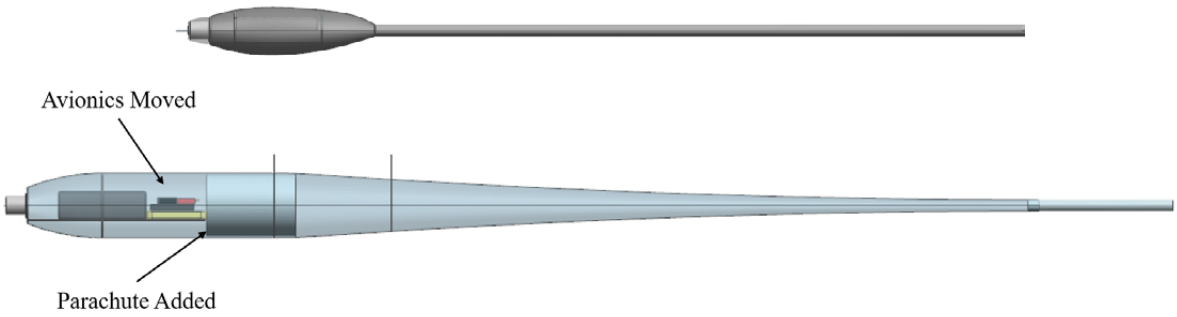

Fig. 18.1: Fuselage Iteration (Not to Scale)

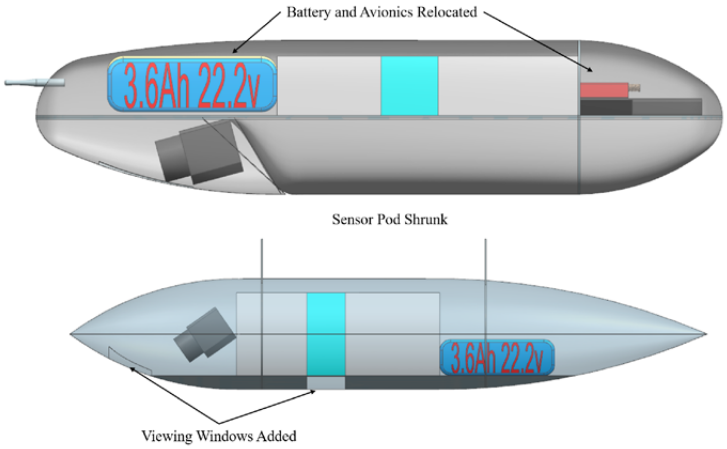

Fig. 18.1: Sensor Pod Iteration (Not to Scale)

18.4. Weight and Balance Summary and Recommendations

The major findings in this chapter are:

- The aircraft does not need to be reconfigured from the designed L/D of 19;
- The fuselage and sensor pod were completely redesigned to better meet the mission;
- The wing was shifted aft and the horizontal tail area grown to make the aircraft marginally stable.

Recommendations

The author recommends that:

- The design adjusted to reduce wetted area;
- The aircraft move into Class II design.

19. Class I Aircraft Characteristics

This is the final Chapter in Class I design. All major design characteristics will be summarized here, followed by a three-view, Figure 19.1, of the final Class I design configuration.

19.1. Table of Class I Aircraft Characteristics

Table 19.1: Summary of Class I Design Characteristics

	Wing	Horizontal Tail	Vertical Tail
Area	14.4 ft^2	3.46 ft^2	1.5 ft^2
Span	12 ft	3.375 ft	1.56 ft
MGC	1.27 ft	1.00 ft	1.00 ft
MGC L.E. F.S.	65.9 in	147 in	144.7 in
Aspect Ratio	10.08	3.33	1.5
Sweep Angle C/4	-2.5°	0°	15°
Taper Ratio	0.4	1	1
Thickness Ratio	12.1%	12.1%	12%
Airfoil	Eppler 403	Inverted Selig 1210	NACA 0012
Control Surface Chord Ratio	30%	30%	30%
Control Surface Span Ratio	44%	57%	81%
Control Surface Type	Single Hinge Plain Flap	Single Hinge Plain Flap	Single Hinge Plain Flap

Fuselage Length	90.8 in
Fuselage Maximum Height	5.8 in
Fuselage Maximum Width	5.8 in

19.2. Class I Aircraft Description

This design is an asymmetric aircraft that will conduct long range observation missions. Being asymmetric the aircraft has the capability of switching out equipment in the sensor pod, or switching out the sensor pod entirely. The aircraft will cruise within 150 feet of the transmission lines that it is designed to observe. This range is required to meet the mission based on the cruising speed of 63 ft/s. DeHond has been designed to fly at pressure altitudes up to 10,000 feet and has the power capacity to fly 100 miles at a time. The aircraft has also been designed to fly with no trim drag. This is achieved through the use of a feedback gain that augments the aircraft to fly at approximately 10% static margin. To simplify operation of the vehicle it can be easily broken down. The wings and fuselage and sensor pod detach from the wing at the spars. The wing can be further broken down at the midspan and breakspans. The entire empennage is capable of sliding off the end of the fuselage, and to make stowage of the fuselage easy it can be broken down at multiple

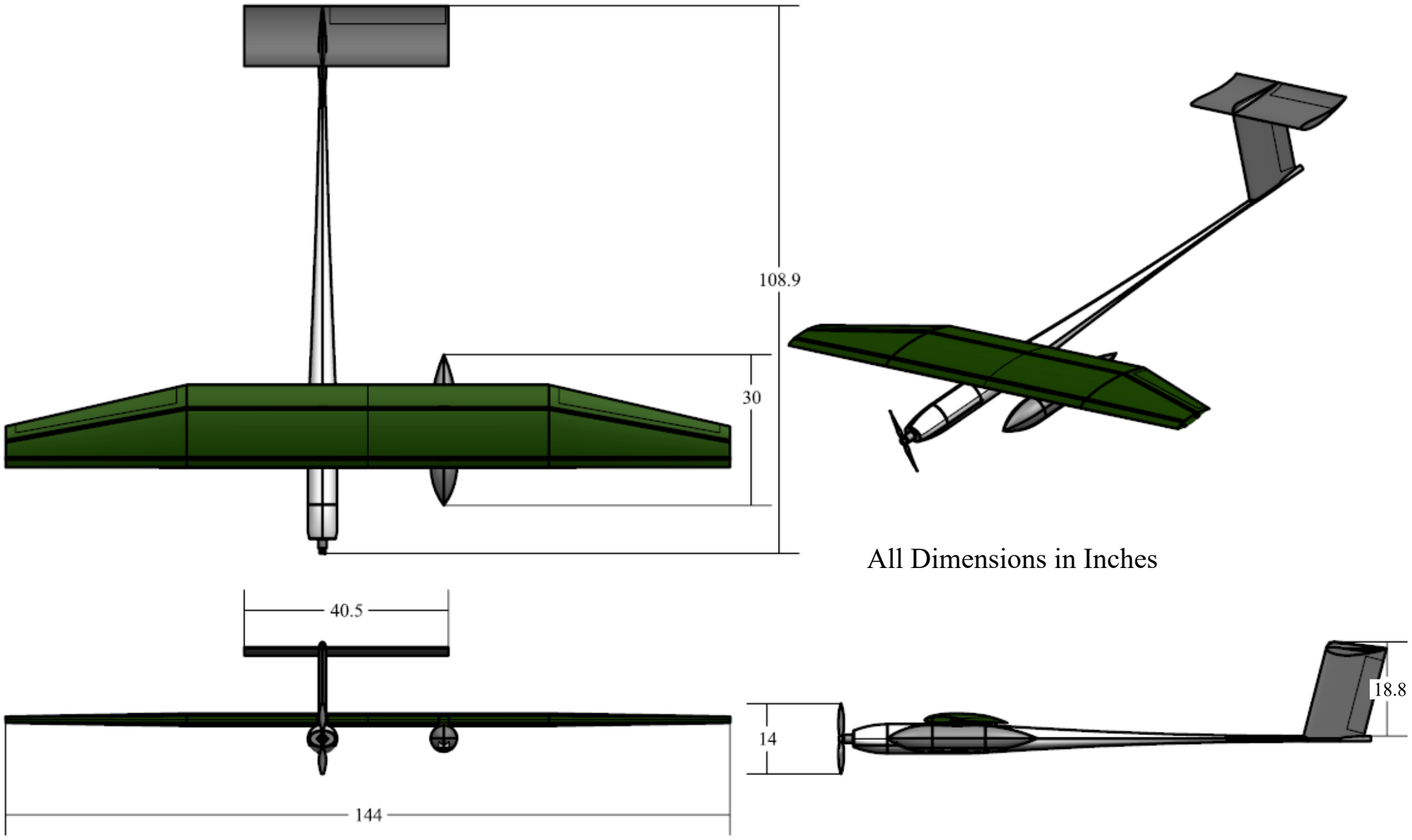

Fig. 18.1: Class I Design Three-View of DeHond (Scale 1:20) (Ref. 44)

20. DESCRIPTION OF MAJOR SYSTEMS

The purpose of this section is to clearly define major systems used in the design of DeHond. All procedures used in this section can be found in *Aircraft Design Part II* (Ref. 28).

20.1. LIST OF MAJOR SYSTEMS

Table 20.1 shows the major systems used on board the DeHond. Each of these systems will be explained in more depth throughout this section.

Table 20.1: List of Major Systems

System	Description
Flight Control	Servo Actuators, Control Surfaces and Avionics
Electrical	Provides Flight Control Systems and Sensors with Power
Environmental Control	Ventilation and Cooling for Electrical Systems and Sensors

20.2. DESCRIPTION OF THE FLIGHT CONTROL SYSTEM

DeHond relies on an entirely irreversible flight control system. This is accomplished by placing servos as close as possible to flight control surfaces and running the needed electrical wires back to the autopilot. The ailerons are of a single-hinge and plain flap design and are located on the outboard section past the break span of the wing. A single-hinged flap design was selected for simplicity and reliability. More complex designs are more prone to failure and require higher levels of maintenance to repair. This vehicle will fly long hours and operate in the field where it will be exposed to the elements and will not be given the same level of care as is required on full scale aircraft. If an aileron is damaged it can be easily repaired or replaced by a ground operator in the field. Servo actuators and control arms for the ailerons are located on the pressure face of the wing and attach together using a simple push rod between the two. Each aileron has three servos, two are needed to provide ample deflection at stall. Having three servos adds redundancy to the system and allows the operator to deflect the ailerons in the event of a servo failure.

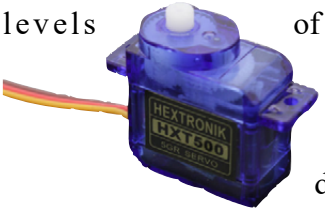

Fig. 20.1: HXT500 Aileron Servo (Ref. 45)

The elevator and rudder also employ a single hinge plain flap design for the control surfaces. The same thought process applied here, as replacing and/or repairing these components will be easier and less expensive than a more complex flap design. The servo actuator for the rudder uses a dual sided control arm and applies force in opposite directions on both sided of the

Fig. 20.2: TGY-9018MG Rudder Servo (Ref. 46)

Fig. 20.3: TGY-811 Elevator Servo (Ref. 47)

rudder hinge. While this does not provide as much redundancy as seen on the ailerons it is a cheap solution to a single control arm failure. Table 20.2 includes values associated with the selection of the servos.

Table 20.2: Servo Actuator Sizing

Control Surface	Servo	Range of Motion	Speed (sec/60°)	Torque (lb_f-in)
Aileron	HXT500 (Ref. 45)	±20°	0.08	1.06
Rudder	TGY-9018MG (Ref. 46)	±40°	0.09	1.28
Elevator	TGY-811 Slim (Ref. 47)	±60°	0.12	4.14

The remainder of the flight control system consists of the autopilot, receiver, ADS-B transponder, electronic speed controller (ESC), and navigation lights. The autopilot is the Micropilot MP2128^{g2} (Ref. 3) which will be responsible for controlling the aircraft during flight. The autopilot can be communicated with in flight via a ground station using the Horizon ground station software by Micropilot. (ge) This allows the user to set way points for flight and even control the aircraft using a joystick. The 8-channel receiver also with the servos and would allow the operator to take over control of the aircraft in the event of an autopilot failure. The ADS-B transponder selected for the DeHond is the Ping 2020 by uAvionix (Ref. 4). This ADS-B is the smallest available of system that could be found, weighing in at 25 grams (approximately 0.9 ounces or 0.05 lb_f). The transponder uses a transmitter and receiver antenna in combination with a global positioning system (GPS) antenna to broadcast the location of the DeHond and receive information on the location of other aircraft operating in the area. This then communicates with the autopilot to find a solution for flight deconfliction on the go. The ESC is controlled by the autopilot or receiver and dictates the how fast the motor runs. Finally, the navigation lights on board DeHond will emit a green colored light off the right wing and red on the left to visually represent the orientation of the aircraft. The navigation lights used are the battery powered PicoMax by Aveo Engineering (Ref. 51). The autopilot has the authority to disable the navigation lights outside of the line of sight (LOS) of the operator. This conserves the battery of the navigation lights for when they are needed. Additionally, when an aircraft is detected operating within 500 feet of DeHond the autopilot has the ability to activate the navigation lights to act as anti-collision lighting. Figure 20.6 shows an overview of the flight control system on board DeHond.

Fig. 20.4: uAvionix Ping 2020 (Ref. 4)

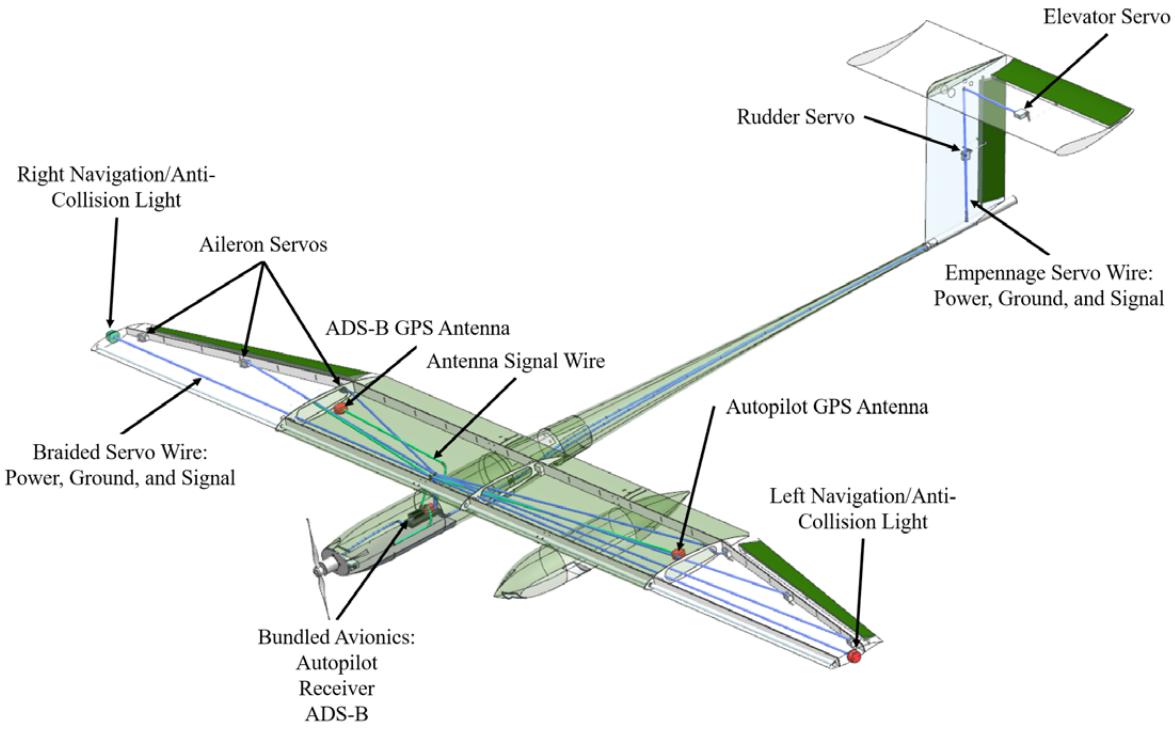

Fig. 20.5: Flight Control System Overview

20.3. DESCRIPTION OF THE ELECTRICAL SYSTEM

The electrical system consists of three different batteries which provide power to the flight control system (FCS), the sensors, and the powerplant. The electrical system was broken into three batteries for several reasons. First, many of the major components needed to run on different voltages and because of this were bundled into groups of similar input voltages. Secondly, using separate batteries allowed the sensors to be in a self contained pod that did not need to be powered from the main fuselage. Lastly, separating the batteries provides "clean" power to the flight control system and sensors so that data will not be impacted by feedback from the motor or servos. The largest battery, which powers the motor, is a 22,000 mAh LiPo battery (Ref. 34). The sensor and avionics both run off of smaller batteries needing 2300 and 5600 mAh respectively. Both batteries were well oversized to compensate in the event of a malfunction or flight error which extends the time of flight. Table 20.3 shows the pertinent characteristics of the electrical system. The powerplant and flight control system batteries have switches that need to be depressed before power is provided to these systems; see Figure 20.8. This is a safety feature that would be activated during the preflight of the aircraft which prevents the motor from receiving any power before the operator intends for the aircraft to fly. Due to the aircraft operating in a high electromagnetic environment all electrical systems are grounded to the front tube spar of the aircraft which is made

of aluminum. This should be a sufficient ground in the case of the aircraft being struck by lightning or contacting the transmission lines.

Wiring Schematic (Click to Enlarge)

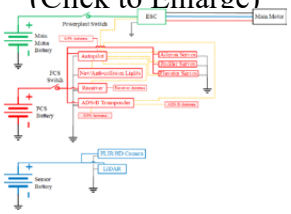

Table 20.3: Electrical System Characteristics

Powerplant Battery	Tattu 22,000 mAh LiPo (Ref. 34)
Flight Control System Battery	Turnigy 6000 mAh LiPo (Ref. 48)
Sensors Battery	Turnigy 3600 mAh LiPo (Ref. 49)
Grounding Plane	Wing Front Tube Spars, Aluminum

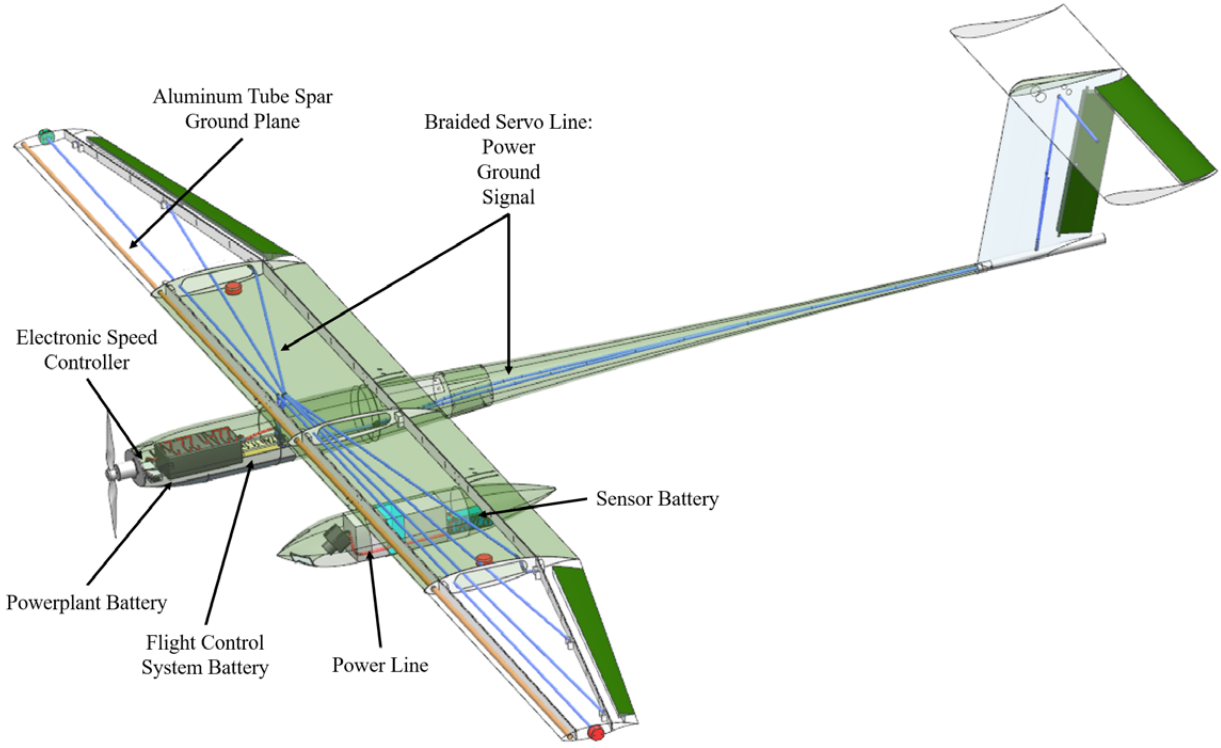

Fig. 20.6: Electrical System Overview

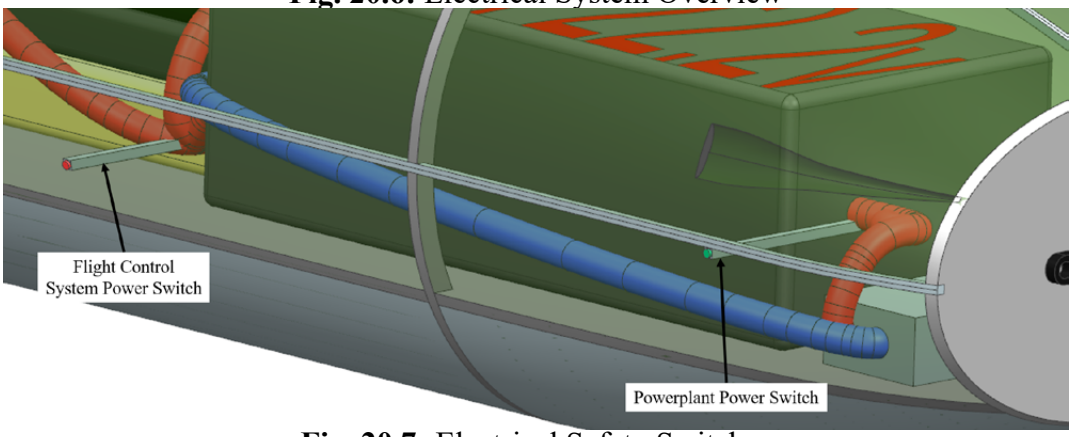

Fig. 20.7: Electrical Safety Switches

20.4. Electric Loading

The electrical loading profile for this aircraft was broken down into four phases of flight: Preflight, takeoff and climb out, cruise, and landing. The RFP specifies that the aircraft must be

assembled and ready for flight within 15 minutes of arriving on location. Due to this only five minutes was allocated for preflight checks during which all major flight systems will be checked before the aircraft is launched. During the takeoff and climb out phase the motor will be run at full throttle to provide maximum thrust to reduce the time it takes to climb to cruising altitude. The selected motor can provide a maximum of 6.1 lb_f of thrust which allows DeHond to climb at 442 feet per minute. To be conservative, a minute was assumed for takeoff and climb out. Cruise is the longest and most highly loaded phase of flight lasting nearly two and a half hours during which almost all systems are constantly running. The last phase is landing, here the sensors, motor and navigation lights are turned off. Based on the sink rate of the parachute, approximately 13.5 feet per second, the landing phase was set to 20 seconds. Table 20.4 shows the electrical load profile chart and this is plotted on Figure 20.8.

Table 20.4: Electrical Load Profile

Electrical Load Item	Preflight 5 min (W)	T/O & Climb 1 min (W)	Cruise 2.47 hr (W)	Landing 20 sec (W)
Autopilot (Ref. 3)	1.25	1.25	1.25	1.25
Servos (Ref. 45 - 47)	7.5	7.5	7.5	7.5
ADS-B Transponder (Ref. 4)	30	30	30	30
8 Channel Receiver (Ref. 50)	0.42	0.42	0.42	0.42
Navigation Lights (Ref. 51)	7	7	7	-
LiDAR (Ref. 2)	-	-	16	-
FLIR (Ref. 52)	-	-	4	-
Main Motor Power (Ref. 35)	-	425.2	143.4	-

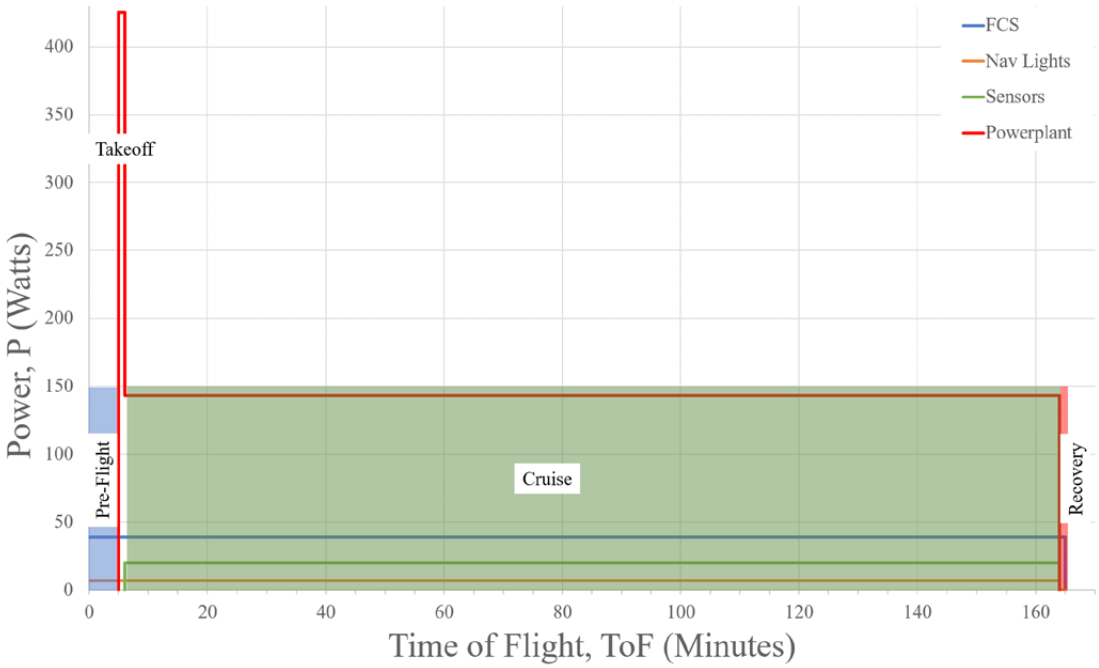

Fig. 20.8: Electrical Loading Profile

20.5. Description of the Environmental Control System

The environmental control system for DeHond relies on NACA inlets to provide cooling and ventilating air for the batteries, avionics and sensors. NACA ducts were selected due to the low external drag associated with this type of inlet. Additionally, these ducts allow for better pressure recovery from the boundary layer. More highly pressurized air is denser and contains more air particles which can absorb heat from the hot components within the aircraft to be transferred out via the exhaust vents (Ref. 53). The NACA inlets were formed using a calculator found online which output X and Y coordinates of the ramp (Ref. 54). This was then projected onto an offset surface of the fuselage and sensor pod skins. The curves on the offset surface could then be splined with the curves on the outer surface to achieve the desired ramp angle. Due to the location of the NACA inlets on the upper surface of the fuselage and sensor pod all inlets would be filtered to prevent the ingestion of excess moisture or insects in flight. The inlets for the fuselage and sensor pod are shown in Figure 20.10.

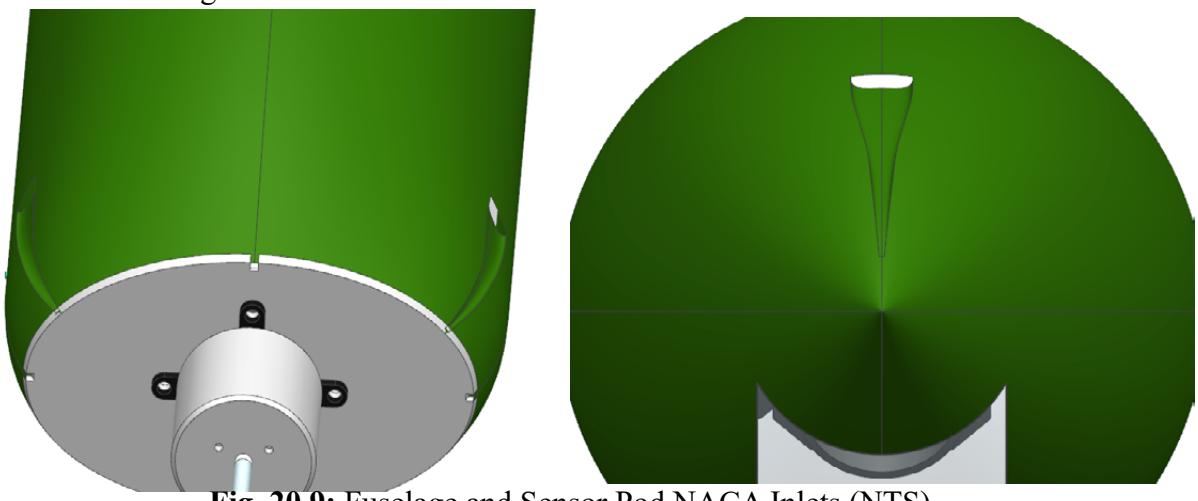

Fig. 20.9: Fuselage and Sensor Pod NACA Inlets (NTS)

The exhaust system for the fuselage is located aft of all major electronics which need to be cooled. Two cooling ports were cut out of the parachute door which simply allows the hot air to exit. As hot air naturally rises these holes were placed on the upper surface of the fuselage which should allow for more natural flow out of the aircraft. This is possible, because of the location of the exhaust. On manned aircraft exhaust ports are often placed on the underside of the aircraft to prevent the hot air from causing condensation on the windscreen of the aircraft obscuring the view of the pilot. On DeHond the sensors are located in a separate pod and the viewing windows are located on the underside of the pod. Exhausting hot air upwards on the fuselage will not negatively impact the mission. For the sensor pod the air enters on the upper surface of the fuselage and passes

over the FLIR camera and LiDAR. After passing the LiDAR the air will flow over the battery and exhaust out the back of the pod. The exhaust port for the sensor pod was formed by cutting the rearward section of the outer body. This formed a circular exhaust vent for hot air to flow through. Figure 20.11 shows the exhaust ports on the fuselage and sensor pod and Figure 20.12 shows how airflow would travel through both.

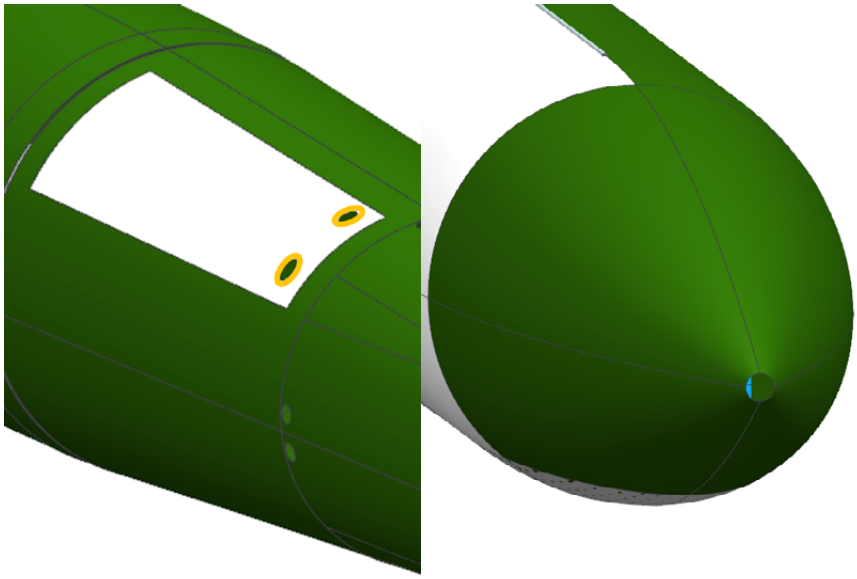

Fig. 20.10: Fuselage and Sensor Pod Exhaust

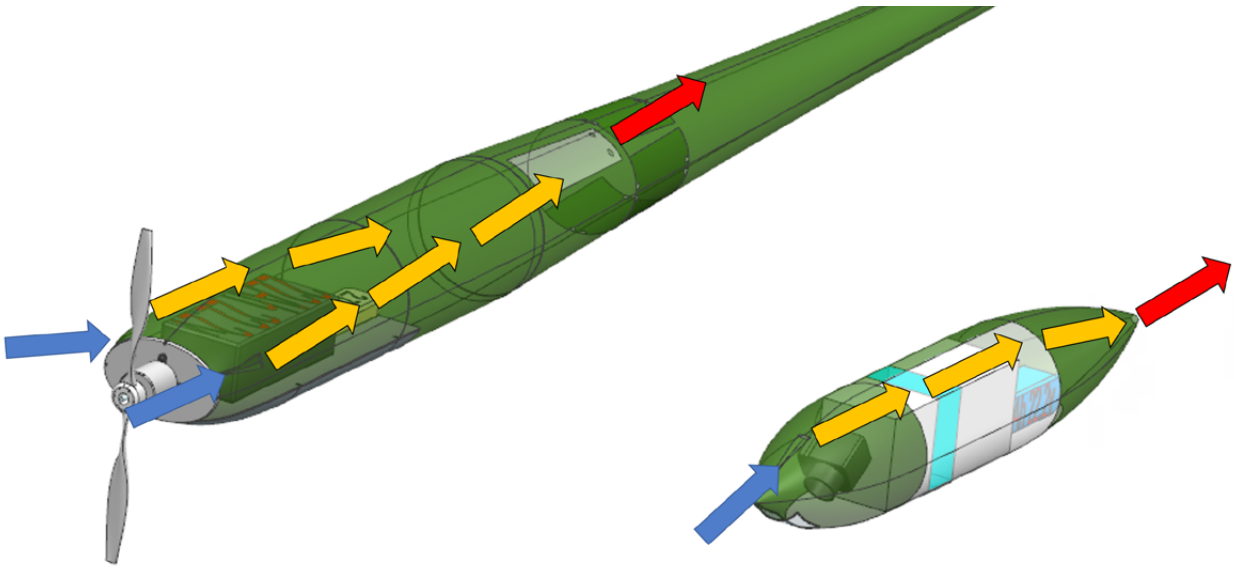

Fig. 20.11: Airflow Diagram

20.6. Conflict Analysis

In certain areas of the wing, wire bundles cross over each other or make contact with substructure. This could be resolved by using longer wires and insulating the wires to prevent electromagnetic interference. Due to the low voltages passing through the wires, even small amounts of electrical insulation should prevent interference. Airflow passing through the main fuselage could be partially block by the parachute in the fully compacted configuration; this could be resolved by allowing the parachute to be more loosely packed reducing the cross-sectional area it occupies and allowing for better airflow to the exhaust ports. Currently, the LiDAR is configured without the added cooling fan because the designer believes that the NACA inlet should provide sufficient cooling for the system. However, if in flight testing it is confirmed that the LiDAR needs more cooling more inlets could be added to improve cooling. Alternatively, the shell of the sensor pod could be grown in size to allow for the cooling fan to be added onto the LiDAR. Finally, if the frontal tube spar is not sufficient as the grounding plane ribs that extend through it could be made of thin aluminum to increase the size of this ground plane.

20.7. Description of Major Systems Summary and Recommendations

Summary

The major findings in this chapter are:

- The aircraft uses three servos per aileron to provide redundancy;
- The elevator and rudder has minimal redundancy to save on costs;
- All control surfaces are single-hinged plain flaps to reduce complexity of maintenance;
- The pertinent characteristics of the servo actuators are shown in Table 20.2;
- The Flight Control System consists of the servo actuators, autopilot, ADS-B transponder, all antennas, an 8-channel receiver, the ESC, and navigation lights;
- The 8-channel receiver offers single redundancy in the event of autopilot failure;
- Power, ground, and signal are all bundled together in braided cables for the servos to prevent electromagnetic interference (EMI);
- The ADS-B provides a second GPS antenna which can also pass data to the autopilot;
- The navigation lights follow standard convention for aircraft (green right wing, red left wing) and are capable of operating continuously for one hour;
- The navigation lights can be turned on or off by the autopilot/receiver as needed;
- The electrical system contains three separate batteries for the major systems;
- The electrical system provides power for the powerplant, flight control system, and the

sensors;

- Pertinent characteristics of the three batteries are shown in Table 20.3;
- Both the flight control system and powerplant are run through switches which should prevent the accidental activation of the propulsion system;
- A switch was not deemed necessary for the sensors as no dangerous equipment is powered by this system;
- The aircraft is grounded by the front tube spar which is made of aluminum;
- The electrical load profile consists of four phases: Preflight, T/O & Climb, Cruise, and Landing;
- Important values for the load profile diagram are shown in Table 20.4;
- Navigation lights would not be run during the entire flight but can be used if needed within LOS;
- The environment control system uses NACA inlets to provided cooling and ventilating air to the needed systems and batteries;
- The exhaust ports vent air upwards and out of the fuselage and sensor pod.

Recommendations

The author recommends that:

- More servos be added to the elevator and rudder to provide more redundancy;
- Shielded control arms and horns be added to reduce drag;
- Flight tests be performed in a high EMI environment to determine the effectiveness of wire shielding and the performance of GPS antennae;
- Testing be conducted to ensure that the batteries selected would indeed provide enough power in a non-theoretical environment;
- Ribs that extend into the front tube spar also be lined with aluminum to grow the size of the ground plane;
- Temperatures of heat producing components be monitored to ensure sufficient cooling is being provided;
- If not enough cooling is provided more inlets be added to allow for better airflow over components;
- All inlets be filtered to prevent moisture, debris, and insect ingestion.

21. Class II Sizing of the Launch and Recovery Systems

This section will discuss the Class II design of the catapult and parachute recovery systems. Additionally, the airbag that will be used to absorb impact load from the descent. The procedure comes from *Aircraft Design Part II & IV* (Ref. 28 & 55). Additionally, a technical discussion of catapult design by Dr. Barrett was used (Ref. 38).

21.1. Design of Catapult Launching System

By and large, the catapult was sized in Chapter 6. Provided in Chapter 6 is the simple kinematic approach that was used to find the needed energy for launch. The design of the catapult was further refined in Chapter 13; where the geometry of the launcher and shuttle was laid out. This section will discuss the launching mechanism and the how it would be employed. From the beginning the launcher was planned to be a pneumatic catapult. A pneumatic system requires an air compressor which, should be fairly simple to integrate with the Ford F-150 specified by the RFP. The bed can easily accommodate a gas powered air compressor similar to the one seen in Figure 21.1. This example is a 30 gallon gas powered air compressor which could be used to launch the aircraft. This compressor is capable of delivering 90 psi of pressure and filling up to 30 gallons of volume (Ref. 56). The piston that will launch DeHond requires 57.3 psi of pressure to propel the aircraft to 5g's on takeoff. This pressure came from the assumption of a constant acceleration 5g launch and a piston cross-section of two inches. The pressure was calculated by multiplying maximum takeoff weight by the load factor at take off and dividing by the cross-sectional area of the piston. The force required with this 5g assumption is 180 lb_f. Still assuming this 2 inch cross-section the length of the launcher is 127 inches resulting in a volume of 399 in^3 or 0.23 ft^3. Figure 21.2 shows the geometry of the catapult design. The force-stroke diagram for this launch system is shown in Figure 21.3, note that it is a horizontal line due to the constant acceleration launch. Table 21.1 highlights the pertinent characteristics of the catapult.

Fig. 21.1: Compressor (Ref. 56)

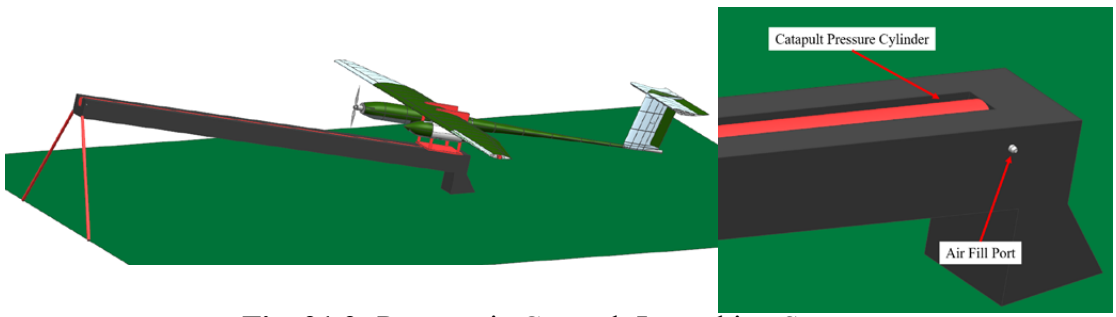

Fig. 21.2: Pneumatic Catapult Launching System

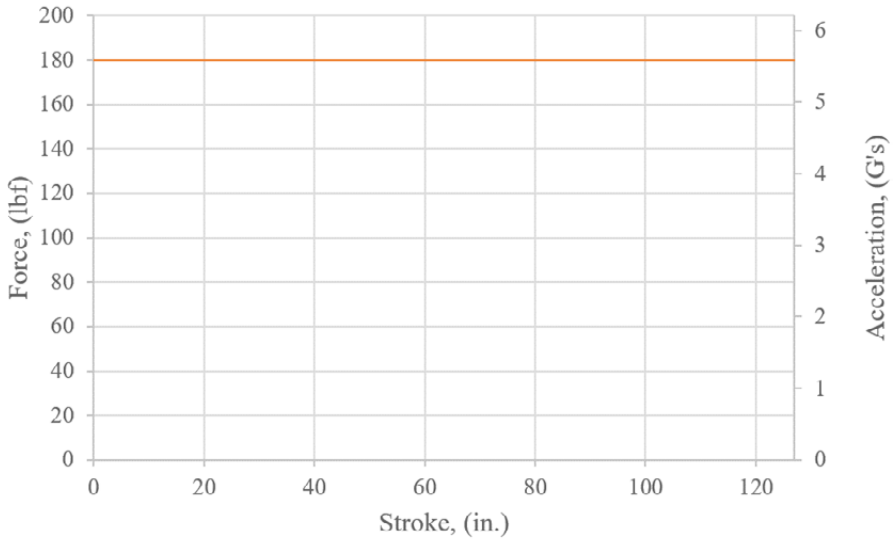

Fig. 21.3: Pneumatic Catapult Force-Stroke Diagram

(e)

Table 21.1: Pneumatic Catapult Salient Characteristics

Piston Diameter, D_{Piston} (in.)	2
Cylinder Length, $L_{Cylinder}$ (in.)	127
Pressure for Launch, $P_{Catapult}$ (psi)	57.3
Launching Force, F_{Launch} (lb_f)	180
Cylinder Volume, $V_{Cylinder}$ (Gallons)	1.72

21.2. DESIGN OF PARACHUTE RECOVERY SYSTEM

The parachute was sized based on the weight of the aircraft and data provided on the parachute by the manufacturer. The parachute selected for this aircraft is designed for a 13.5 foot per second sink rate based on an aircraft weight of 36 lb_f. The values provided by the manufacturer were then cross checked using hand calculations and formulas provided by NASA (Ref. 57). During the hand calculation check it was found that a slightly higher descent rate would be experienced by DeHond due to the conservative approach of sizing the parachute and aircraft for a maximum flight altitude of 10,000 feet mean sea level (MSL). The 120 inch diameter parachute that was originally planned to be used for recovery will still be used. However, because the descent rate is higher than anticipated the airbag impact system will have to absorb more energy at higher altitudes. Table 20.2 details the salient characteristics of the parachute.

Table 21.2: Parachute Salient Characteristics

Parachute Diameter, $D_{Parachute}$ (in.)	120
Descent Rate, $V_{Descent}$ (ft/s)	15.4
Impact Energy, (ft-lb_f)	132.4

(Click to Enlarge)

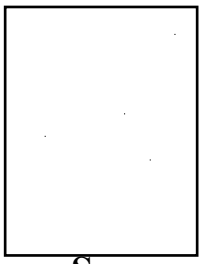

21.3. Design of Airbag Impact System

The mechanism that will be used to absorb impact loads experienced on landing will be a king sized air mattress. The air mattress can either be filled by the ground operator using the air compressor on a lower pressure setting or by using the built in two way pump that comes with the mattress. The air mattress selected has the dimensions of 82 by 75 by 19 inches resulting in a volume of 67.6 cubic feet (Ref. 58). The impact that the airbag must absorb was solved to meet the FAR 23 requirement of a 9.72 foot per second sink rate. This meant that air mattress only had to absorb the difference between the sink rate of the parachute and the standard set by FAR 23. This resulted in a 5.68 foot per second change in velocity due to the mattress. Using basic kinematic equations it was determined that the air mattress would need to be capable of a 7.72 inch deflection to dissipate this energy. 7.72 inches is approximately 40% of the max height of the air mattress. This means that on landing the air mattress would need to release approximately 60% of its volume to absorb the impact. Table 21.3 lists the salient characteristics of the air mattress.

Table 21.3: Air Mattress Salient Characteristics

Mattress Dimensions, (in.)	82x75x19
Mattress Volume, $V_{Mattress}$ (ft^3)	67.3
Deflection, (in.)	7.72
Energy Absorbed, (ft-lb_f)	18

(Click to Enlarge)

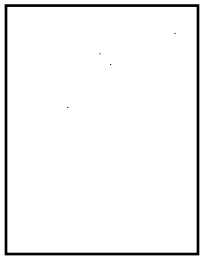

21.4. CLASS II DESIGN OF THE LAUNCH AND RECOVERY SYSTEMS SUMMARY AND RECOMMENDATIONS

Summary

The major findings in this chapter are:

- The aircraft will be launched using a pneumatic catapult that will be pressurized to 57.3 psi;
- The salient characteristics of the catapult are shown in Table 21.1;
- The aircraft relies upon a parachute and air mattress system to dissipate kinetic and potential energy;
- The salient characteristics of the parachute are shown in Table 21.2;
- The salient characteristics of the air mattress are shown in Table 21.3.

Recommendations

The author recommends that:

- Testing be conducted to ensure the reliability of landing on the air mattress and to determine if propulsive effects are needed to guide onto the landing spot;
- Testing be conducted to determine propulsive effects on the deployment of the parachute.

22. Initial Structural Arrangement

The initial structural arrangement of the aircraft follows the recommendations of Dr. Roskam as outlined in *Aircraft Design Part III* (Ref. 31).

22.1. Layout of Structural Components

The structure of DeHond was sized for subscale aircraft that would not experience extreme loads in flight. The aircraft is sized for a 1.25g maneuver stall in flight. However, in transit the aircraft could experience higher loading and this was mitigated through strictly enforcing padded cases that the aircraft must be transported in. With that said, the wing is made up of ribs and spars much like a full scale aircraft would have. The ribs are 3/32 inch thick and spacing was set at six inches between the midpoint of each rib. This should be more than sufficient to resist bending and shear moments in flight. The ribs were split between the forward main spar and the rear aft spar. Because the trailing edge of the wing will experience lower loading the aft sections of the ribs were separated and would connect to the rear spar to help maintain the shape of the wing. The leading edge of the majority of ribs were also cut out. This was replaced with a foam insert to maintain the shape of the wing. To reduce the weight of the wing structure all ribs have lightening holes cut through them. There are three spars that run the length of the wing. The two main spars are each an 1/8th inch thick would be made of plastic or some form of polymer based composite. However, more analysis could lead to the conclusion that main spars be constructed of aluminum. If this is the case the thickness of the spars could likely be reduced, this would have the added benefit of growing the ground plane for the aircraft. The spars need to be strong enough to resist bending moments generated by lift on the wing. A frontal tube spar, made of aluminum, was added through the leading edge insert to bear the majority of bending loads due to how the wing was to be broken up for storage. Figure 22.1 shows half of the symmetric wing substructure.

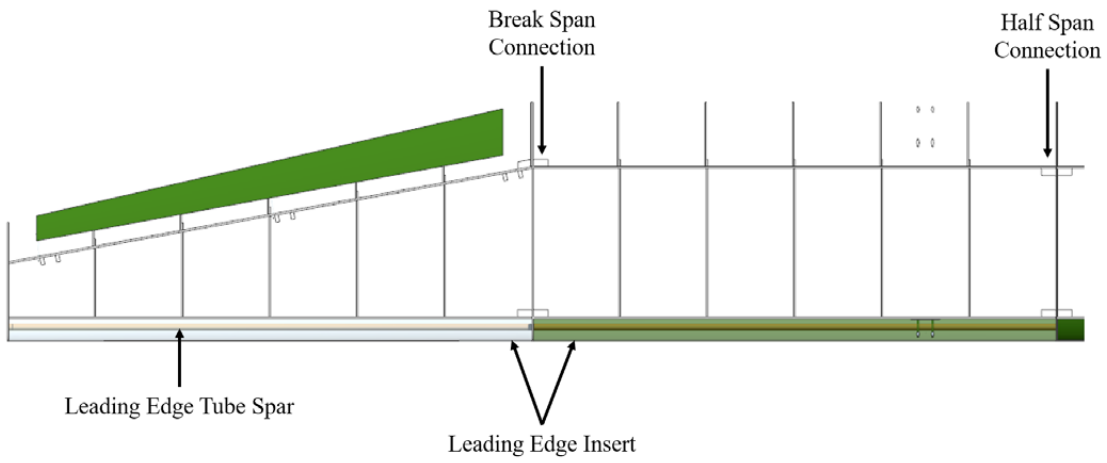

Fig. 22.1: Wing Structure (NTS)

The empennage followed similar procedures for substructure design as the wing. For the horizontal tail a two tube spar design was used. This was selected because it is intended for the horizontal tail to break in two for storage. The tube design allows for easy assembly and is also strong in a cantilever design without adding excess and unnecessary weight. Ribs are continuous along the chord line with holes through them to allow for connection to the tube spar. In areas where the elevator would connect ribs were cut short to allow for movement of the control surface. These cut ribs still have to provide a structural attachment for the elevator and maintain the shape of the airfoil. Lightening holes were cut through ribs wherever possible to save weight. The vertical tail consists of three spars and has a rib design similar to the horizontal tail. The vertical tail does not need to break. However, it does have to accommodate the tube spars of the horizontal tail. This was resolved by adding a 1/8th inch thick extrusion between the upper two ribs that allows the tubes spars to pass through and connect. The three main spars also continue down to the connection tube where empennage connects to the fuselage. Figure 22.2 shows the horizontal tail structure and Figure 22.3 shows the vertical tail structure.

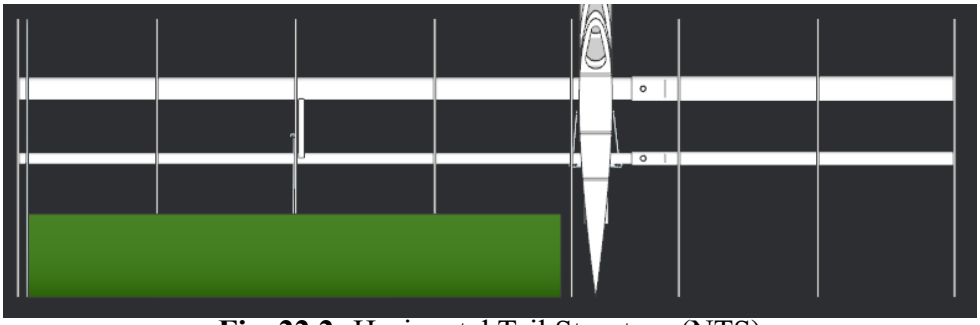

Fig. 22.2: Horizontal Tail Structure (NTS)

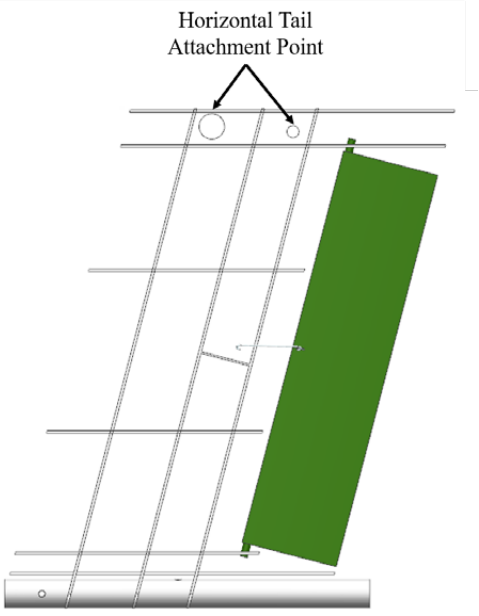

Fig. 22.3: Vertical Tail Structure (NTS)

The main fuselage was designed with ring frames and longerons. This design style was chosen, while unorthodox for UAV design, because of the necessity of breaking the fuselage into two parts. This style of substructure layout seemed the most accommodating for this requirement. Ring frames were unevenly spaced and placed at points that were necessary for major connection. The two main ring frames in the fuselage are used to connect to the rectangular spars of the wings. This connection is made by fittings placed through the upper surface of the ring frames and the spars. The fuselage has four longerons spaced 90° apart that run the length of the fuselage. These were added to help maintain the shape of the skin both in flight and when the fuselage was broken apart for storage. The fuselage connection is made approximately three feet aft of the firewall. This allows the fuselage to be broken into two sections, both smaller than six feet long. The connections consist of two broken up ring frames, each with a longeron running through it. The fuselage assembly requires 12 screws to make the connection. Figure 22.4 shows the fuselage structure and key attachment points. Figure 22.5 shows how the wing and fuselage connect.

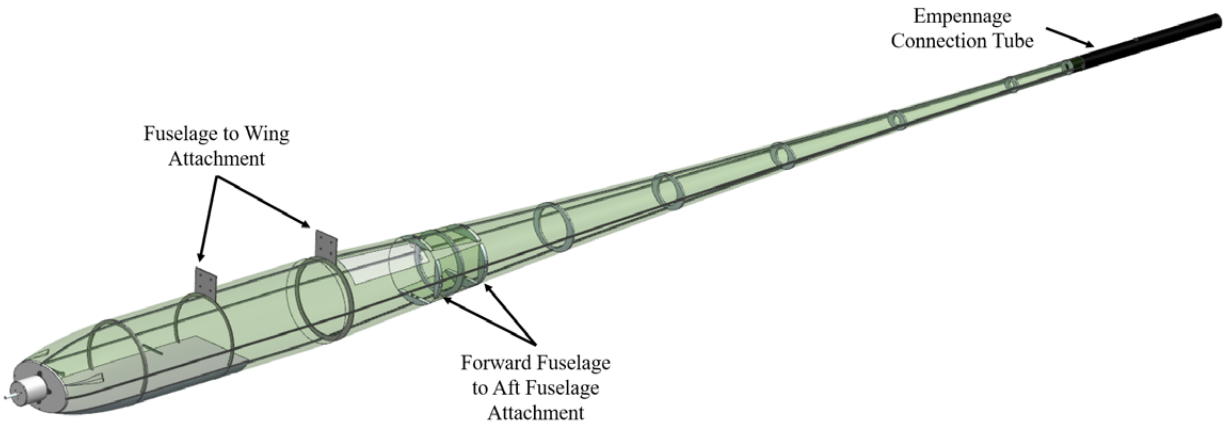

Fig. 22.4: Fuselage Structure

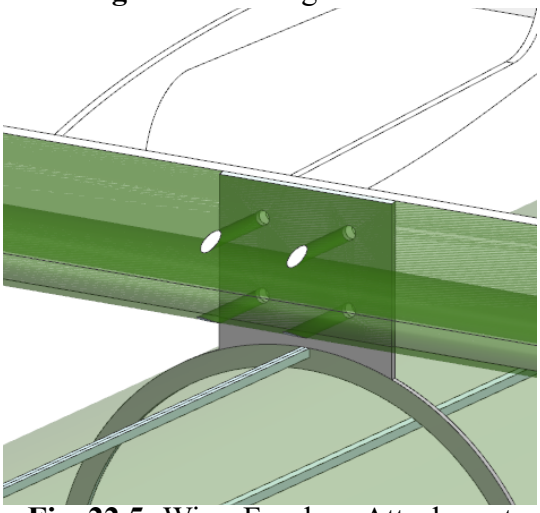

Fig. 22.5: Wing-Fuselage Attachment

The sensor pod was designed to be fully monocoque with two outer ring frames that facilitates the connection of the pod to the wing. The "floor" of the sensor pod has a foam insert to dampen the impact felt by the LiDAR and FLIR camera. Additionally, the sensor pod has two windows on the lower surface to allow the cameras to inspect the transmission lines and surrounding areas.

22.2. CAD DRAWINGS OF STRUCTURAL LAYOUT

Figure 22.6 shows a full view of the structure for DeHond as this is an asymmetric aircraft.

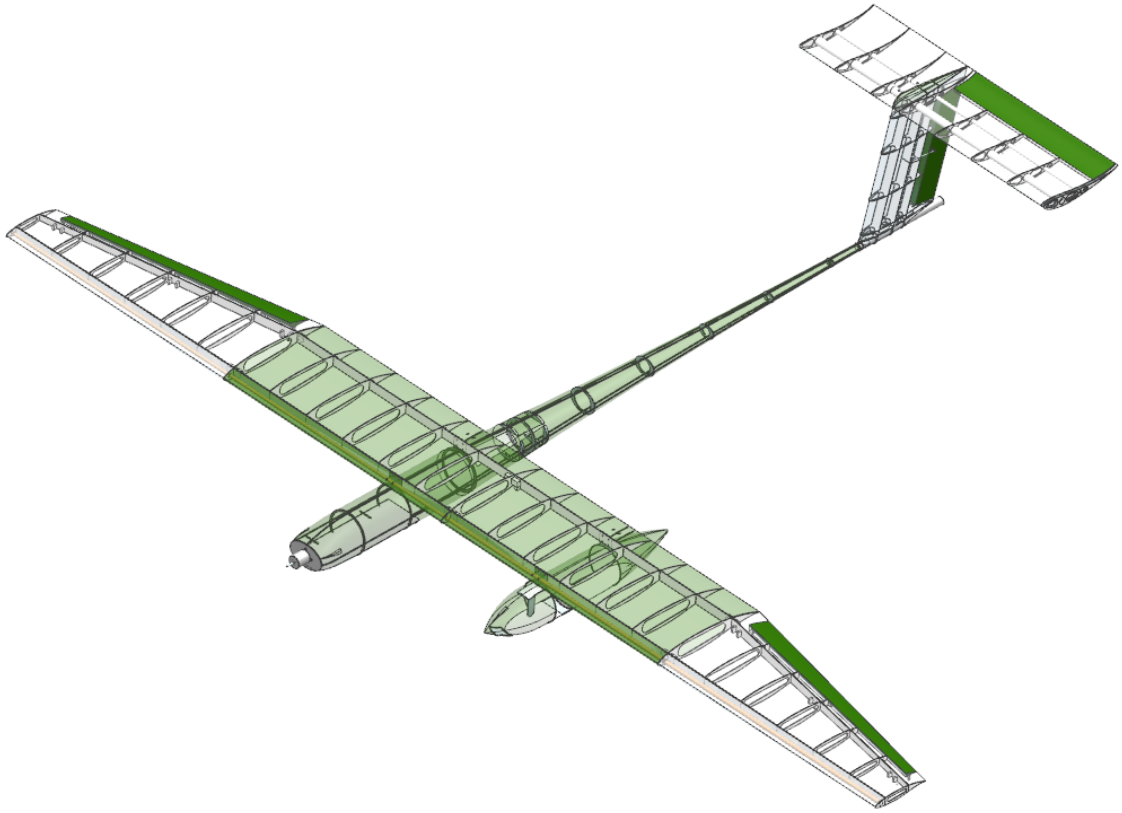

Fig. 22.6: Off-Axis Structure Overview

22.3. STRUCTURAL ARRANGEMENT SUMMARY AND RECOMMENDATIONS

Summary

The major findings in this chapter are:

- The wing rib spacing is six inches and all ribs have lightening holes;
- There are three total spars in the wing, the front tube spar will endure the majority of bending loads;
- The horizontal tail uses two tube spars along with traditional ribs;
- The vertical tail relies on three spars in addition to traditional ribs;
- The vertical tail facilitates the connection of the horizontal tail and supports the structure;
- The fuselage is made of longerons and ring frames;

- The sensor pod is fully monocoque;
- The fuselage and sensor pod both attach to the wing via extended ring frames;
- The ring frames for the sensor pod lie outside of the pod.

Recommendations

The author recommends that:

- Analysis be conducted to determine if the current rib spacing for the wing and emppenage is over or under designed;
- Testing with the fuselage connection be conducted to determine if a redesign of this attachment is necessary.

23. CLASS III WEIGHT AND BALANCE

This section will discuss the detailed weight and balance calculations conducted for DeHond. All procedures followed for these calculations come from *Airplane Design Part II* (Ref. 28).

23.1. CLASS III WEIGHT AND BALANCE CALCULATIONS

The class III weight and balance was calculated "by hand" using Siemens NX and a large Excel spreadsheet to determine the weight of all components placed within the aircraft and their centers of mass (CoM). Using these locations, along with known weights of components the center of gravity of the aircraft could be accurately determined. On items such as the substructure, the weight needed to be calculated. This was accomplished by taking the known volume of each component and multiplying it by the density of the material the component will be made from. Table 23.1 shows the materials and their respective densities used for the weight and balance calculations.

Table 23.1: Material Densities (Ref. 59 - 67)

Material	lb_f/in^3
Coroplast	0.0091
3M Scotch Weld	0.074
AA8090 Aluminum	0.092
Polyurethane Foam	0.0011
Kevlar 49	0.052
Zinc Sulfide	0.15
	lb_f/in^2
Monokote	0.0001
	lb_f
#8 Screw	0.0018
	lb_f/in
Med-Light Servo Wire	0.0004

23.2. CLASS III CG POSITIONS ON THE AIRFRAME, CG EXCURSION

Using geometry of substructure, skin, control surfaces, control arms, et cetera NX provides an accurate estimate of the center of mass of each object (Ref. 68). This does assume that each item is homogeneous which, for this aircraft, should be fairly accurate. NX was also used to determine the volume of each component, this was then multiplied by the density of the material to provide an accurate weight approximation. Table 23.2 details the weights and CG locations of major components of DeHond. With the new CG of the takeoff weight, operating-empty weight, and empty weight found the CG excursion plot could be plotted. Figure 23.1 shows the class

III CG excursion plot for DeHond. As was mentioned in Chapter 14, this aircraft still has no CG excursion during flight. Furthermore, this aircraft is catapult launched and will never operate without the propulsion battery. For this reason the large ground excursion will not negatively impact DeHond and was not rectified. Figure 23.2 shows the CG locations of all major components depicted graphically on the aircraft.

Table 23.2: Major Component CG Breakdown

Component	Weight (lb_f)	F.S. (in.)	B.L. (in.)	W.L. (in.)
Wing	6.96	71.5	-0.21	107
Fuselage	8.27	92.7	9.02	103
Sensor Pod	2.84	76.4	-15.1	103
Horizontal Tail	1.03	151	4.22	120
Vertical Tail	1.15	150	9.02	113
LiDAR	3.4	71.1	-15.1	103
FLIR	0.28	64.9	-15.0	103
Parachute & Launcher	3.53	72.5	9.02	103
Motor	0.45	52.0	9.02	103
Powerplant Battery	5.49	59.8	9.02	103
Avionics Battery	0.52	66.4	9.07	102
Sensor Battery	1.27	78.4	-15.03	102
Avionics	0.34	67.3	9.18	103
DeHond	**35.9**	**79.9**	**1.80**	**104**

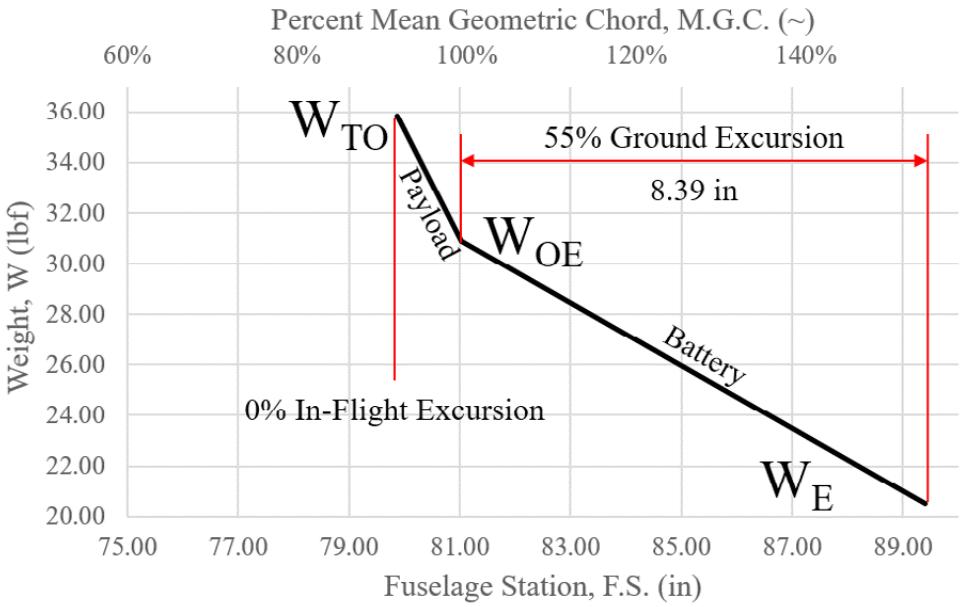

Fig. 23.1: Class III CG Excursion Diagram

Item	Weight (lb_f)	F.S. (in.)	B.L. (in.)	W.L. (in.)
1. Wing	6.97	71.5	-0.21	107
2. Fuselage	8.27	92.7	9.02	103
3. Sensor Pod	2.84	76.4	-15.1	103
4. Horizontal Tail	1.03	151	4.22	120
5. Vertical Tail	1.15	150	9.02	113
6. LiDAR	3.40	71.1	-15.1	103
7. FLIR	0.28	64.9	-15.0	103
8. Parachute	3.53	72.5	9.02	103
9. MT3520 Motor	0.45	52.0	9.02	103
10. Main Battery	5.49	59.8	9.02	103

Item	Weight (lb_f)	F.S. (in.)	B.L. (in.)	W.L. (in.)
11. Avionics Battery	0.52	66.4	9.07	102
12. Sensor Battery	1.27	78.4	-15.0	102
13. ADS-B	0.06	67.3	9.18	103
14. ADS-B GPS Ant	0.06	73.4	-33.0	107
15. ADS-B Ant	0.05	72.7	39.0	107
16. Receiver	0.02	65.6	9.22	103
17. Autopilot	0.09	66.1	9.07	103
18. Autopilot GPS Ant	0.06	73.4	33.0	107
19. Right Nav Light	0.03	69.4	72.4	107
20. Left Nav Light	0.03	69.4	-72.4	107
21. CG	**35.8**	**79.9**	**1.80**	**104**

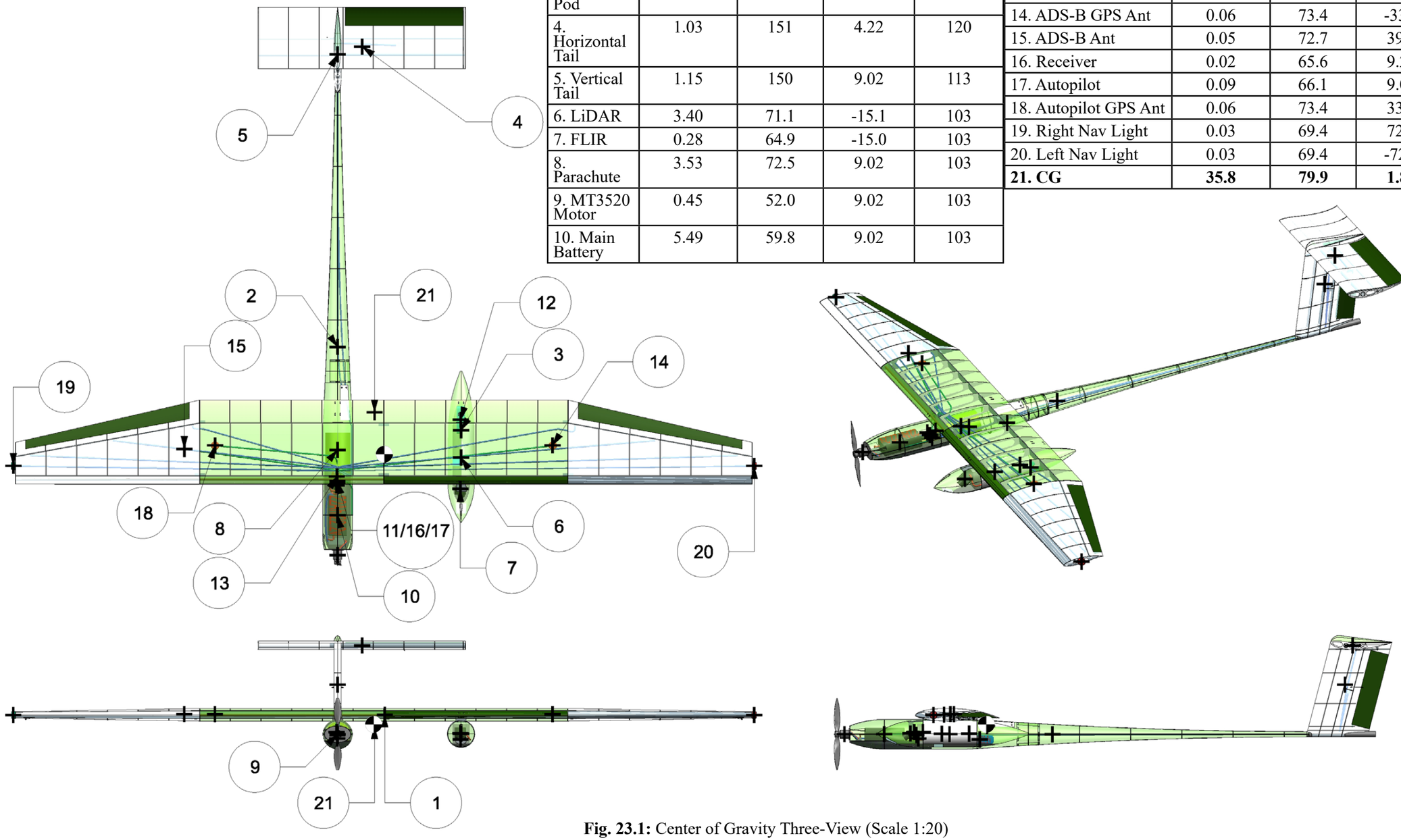

Fig. 23.1: Center of Gravity Three-View (Scale 1:20)

23.3. CLASS III WEIGHT AND BALANCE SUMMARY AND RECOMMENDATIONS

The major findings in this chapter are:

- The operating CG is now at F.S. 79.9 from 80.8 in Class II;
- The weight of the aircraft is within 0.5% of the predicted weight;
- The CG excursion is still irrelevant for this aircraft;
- Figure 23.1 shows the CG excursion plot;
- Figure 23.2 shows the CG locations of all major components.

Recommendations

The author recommends that:

- Some structural weight be sacrificed for a larger battery;
- The CG be wingtip tested on production built aircraft to verify CG estimation.

24. CLASS III WEIGHT AND BALANCE ANALYSIS

This section will discuss the implications of the class II weight and balance calculations and how this could affect the aircraft in the air. All procedures followed in this section can be found in *Airplane Design Part II* by Dr. Jan Roskam (Ref. 28).

24.1. CLASS III WEIGHT & BALANCE ANALYSIS

Using the CG location determined from Chapter 23 the weight and balance analysis for DeHond was performed a second time. This aircraft has no landing gear, so it cannot have a tip-over problem. As mentioned previously, there is a large CG excursion on the ground. While this may be concerning for aircraft with a ground mission, DeHond will likely never operate without payload and will never operate without its powerplant. For this reason the large ground excursion was not adjusted and will not cause problems for this aircraft. DeHond has no in-flight CG excursion because the motor is battery powered and there is no payload drop. The only case where the aircraft would experience any shift in the CG is during the deployment of the parachute. However, as the aircraft will no longer be controllable using traditional control surfaces this scenario was not evaluated in the CG excursion plot.

This aircraft was determined to have a static margin of 5.5% which requires it to be artificially stabilized to 10%. To accomplish this a SAS feedback gain was calculated. The needed value is 0.17 deg/deg. This size of static margin should allow a human operator to control the aircraft with relative ease. The benefit of flying with a static margin closer to 0 comes from reduced trim drag. Trimming the aircraft out to level flight causes drag; both induced, and profile penalties are paid for deflecting control surfaces. Flying without trimming any control surfaces eliminates this source of drag and can allow the aircraft to fly longer endurance missions. This is particularly key for this mission set as the RFP requires the aircraft to fly 200 miles a day.

24.2. STRUCTURAL ARRANGEMENT SUMMARY AND RECOMMENDATIONS

Summary

The major findings in this chapter are:

- The aircraft has a static margin of 5.5%;
- The aircraft is longitudinally stable with a SAS Feedback gain of 0.17 deg/deg.

Recommendations

The author recommends that:

- The aircraft be adjusted to reduce the static margin to 0.

25. Variant Models

The most updated three-view of DeHond can be seen in Figure 25.4. This section will also discuss the family of aircraft that is intended to be designed around DeHond.

The -200 series of this aircraft, DeBom, will be targeted towards the military sector. This variant will have an upgraded powerplant for increased speed. The sensor pod is replaced with high explosive anti-tank (HEAT) shaped charge. In this case the weapon selected is the warhead from the TOW II missile. A total weight of 8.65 lbf is gained back from removing LiDAR, FLIR, ADS-B, and parachute. An additional two pounds is saved by removing the sensor pod altogether. Guidance to target includes waypoint following and/or laser designation. Lightweight construction using basswood as a replacement for aluminum could increase payload to nearly 16 lbf and reduce RADAR signature due to a more electrically transparent design. This aircraft would also become extremely cheap and could be used in a swarm configuration to overwhelm air defense assets. The shaped charge allows for precision strikes compared to traditional high explosive warheads. Additionally, shaped charges allow for high penetration against rolled homogenous armor (RHA) relative to their size. For example, the 15 lbf warhead of the BGM-71D can penetrate up to 900mm of RHA (Ref. 69). This would be enough for a top down or straight in side attack on most modern main battle tanks (MBT). More than enough for armored vehicles, self-propelled anti-air (SPAA), and infantry. For comparison the Browning machine gun (BMG) .50 caliber (12.7 mm) round is capable of penetrating up to 19mm of RHA. The aircraft is small enough it could be easily transported and setup in the field. Having relatively long-range capabilities and catapult launching means the aircraft could fly out nearly 80 miles before engaging a target improving the standoff capabilities of our military. This long endurance could also allow the aircraft to loiter while searching for a target. Figure 25.1 shows DeBom.

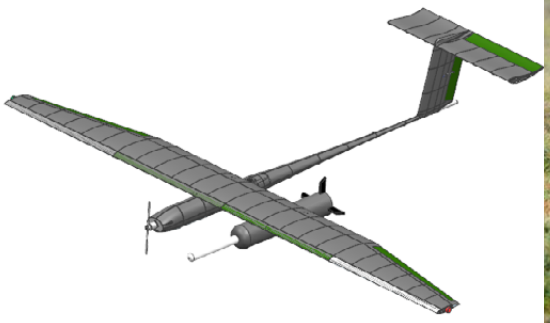

Fig. 25.1: DeBom

Fig. 25.2: DeBom Attacking a ZSU-23-4 (Ref. 70)

The -300 series of this aircraft will be the DeHond Long. This aircraft will have a longer sensor pod allowing the aircraft to carry more and better sensors. Depending on the mission set this aircraft could also have an improved motor, reducing endurance but increasing flight speed. This could better perform the transmission line inspection mission by gathering more data. Alternatively, the sensor package could be replaced entirely and the larger pod could be used to transport goods, food, or medicine. The DeHond Long is shown in Figure 25.3.

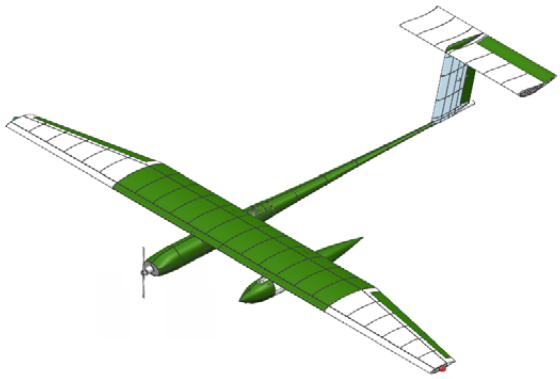

Fig. 25.3: DeHond LongClass III Design

25.1. VARIANT MODELS SUMMARY AND RECOMMENDATIONS

Summary

The major findings in this chapter are:

- Two variant models are available;
- DeBom military targeted UAV;
- DeBom carries a TOW II warhead;
- DeHond Long has increased e and endurance.

Recommendations

The author recommends that:

- Research be conducted on a more powerful motor;
- Other sensor packages be explored.

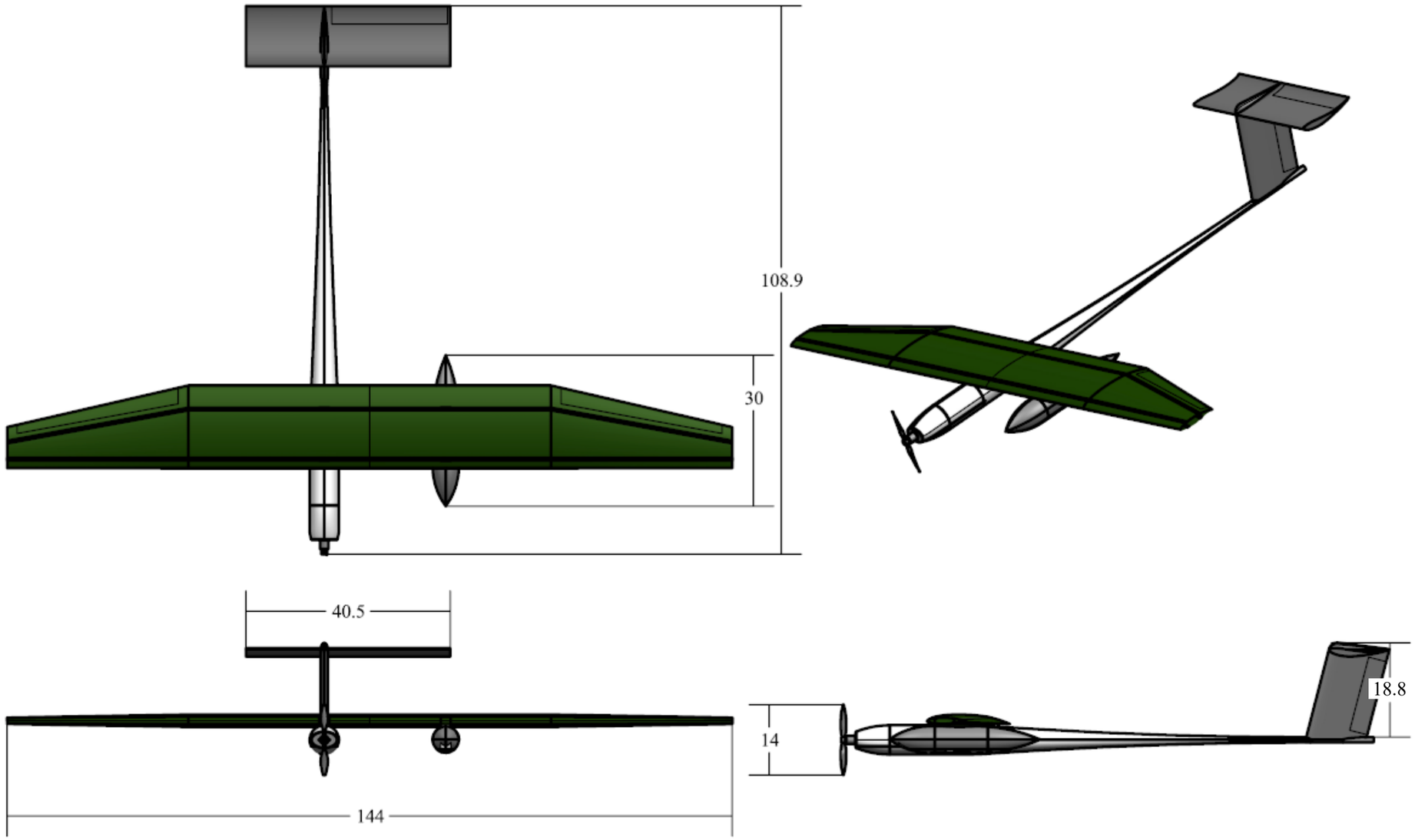

Fig. 25.4: Three-View of DeHond (Scale 1:20) (Ref. 44)

26. ADVANCED TECHNOLOGIES

This section will review the advanced technologies that are available to the design.

26.1. ADVANCED TARGETING

Using cameras already carried by DeHond, and subsitituting the LiDAR for a high powered electro-optical camera DeHond could be used to identify targets. This would require a more powerful processor onboard the aircraft and would also require a significant amount of memory storage onboard as well. With inprovements in solid state memory, up to 100 TB in a 3.5-inch form factor, could allow DeHond to perform a mission similar to the one naval systems perform now. Currently, camera based target recognition for maritime awareness is being explored as a more robust method of tracking naval vessel traffic in congested areas. This system is capable of distinguishing ships from the background and can also compare hull shapes it sees via cameras with hull outlines stored of known vessels in its database, Figure 26.1. This has the potential to expand to identification of military aircraft, armored vehicles, or tanks. This could also be used in the civilian vehicle market but, as there are many of the same model vehicle in the consumer market, this system would struggle to perform as well.

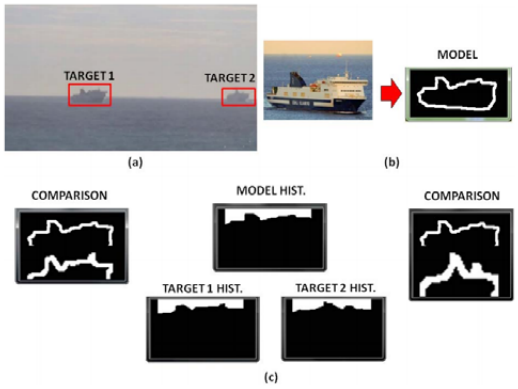

Fig. 26.1: Target Distinction (Ref. 71)

26.2. HYDROGEN FUEL CELLS

Another emerging technology in avation is the use of hydrogen as a clean fuel source. As improvements in the storage of liquid hydrogen is made DeHond could make the switch to a fuel cell that could potentially allow for day long flights. If a closed loop system were to be used, and enough energy stored, DeHond could perform electrolysis and split water (H_2O) back into hydrogen and oxygen. This could then be used to power the fuel cell and the cycle repeated. This is a clean form of energy and could improve DeHond's capability to perform its mission. Figure 26.2 shows an example of a regenerative fuel cell.

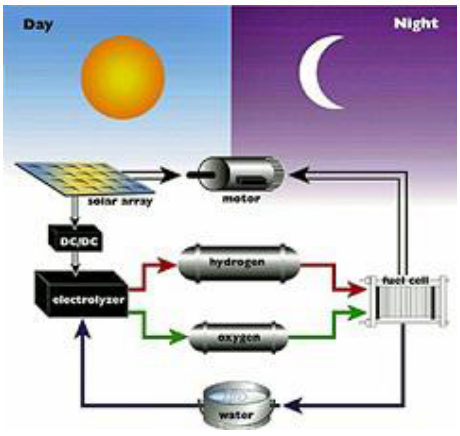

Fig. 26.1: Regenerative Fuel Cell (Ref. 72)

26.3. Advanced Technologies Summary and Recommendations

Summary

The major findings in this chapter are:

- Target recognition systems could be used to facilitate military mission;
- A hydrogen fuel cell could be used to extend mission times.

Recommendations

The author recommends that:

- Solid state memory and lightweight processors be explored;
- Small liquid hydrogen storage tanks be evaluated for use on DeHond.

27. RISK MITIGATION

This section will discuss the potential risks involved with this aircraft design. Specifically, the launch and recovery systems. Additionally, this section will discuss some of the risks involved with the materials selected for the manufacture of this aircraft.

27.1. LAUNCH AND RECOVERY RISKS

DeHond could encounter several major issues if the launch and recovery systems do not perform as expected. Firstly, the catapult will need to hold the needed pressure to allow for launch. In the event of a major air leak in this system the aircraft will not reach stall speed and will never generate enough lift to prevent it from crashing into the ground. This risk has been considered in the structural design of the aircraft be manufacturing with shock absorbing materials to at least protect the sensory equipment in the event of a crash. Additionally, buying the catapult from a reputeable vendor will be very important as the catapult will need to operate twice every flight and will likely experience significant wear and tear.

During the recovery phase of flight a parachute is deployed allowing the aircraft to slowly sink back towards the earth. An obvious risk with this recovery method is the proximity of the aircraft to the powerlines. This risk has been considered and could be mitigated by performing a power on recovery allowing he aircraft to have marginal control on descent. Another major risk is high winds. A recovery in high winds would likely blow the aircraft of course during descent and could lead to structural damage. This can be avoided by performing a stall recovery onto the large air matress carried by the ground crew (see Chapter 21).

27.2. STRUCTURAL AND ENVIRONMENTAL RISKS

The major structural issue facing this aircraft is the use of materials with dissimilar coefficients of thermal expansion (CTEs). Obviously, while desiging it is prefferred to avoid using materials that expand at different rates when exposed to temperature variances. However, this was somewhat unavoidable in this mission specification. Due to the aircraft operating in close proximity to high power transmission lines the aircraft was built with aluminum spars, ribs, longerons, and ring frames that would act as a grounding plane in the event of the aircraft stricking the power lines and completing a circuit or in the event of lightning strike.

28. Manufacturing Plan

This section will discuss the manufacturing plan and process for DeHond. Additionally, the bill of materials will be shown and discussed based on its relevance to major components.

28.1. Discussion of Manufacturing Process

Figure 28.1 shows a rough overview of the bill of materials in an exploded view. For the manufacturing of DeHond most parts will be bought pre-cut so that the majority of the process conducted at the local factory will be assembly. For this to be accomplished the designer must provide tooling to the company which will be manufacturing all of the kevlar skins. Figure 28.2 shows an example of the tooling that will be needed to layup the kevlar fuselage and sensor pod skins.

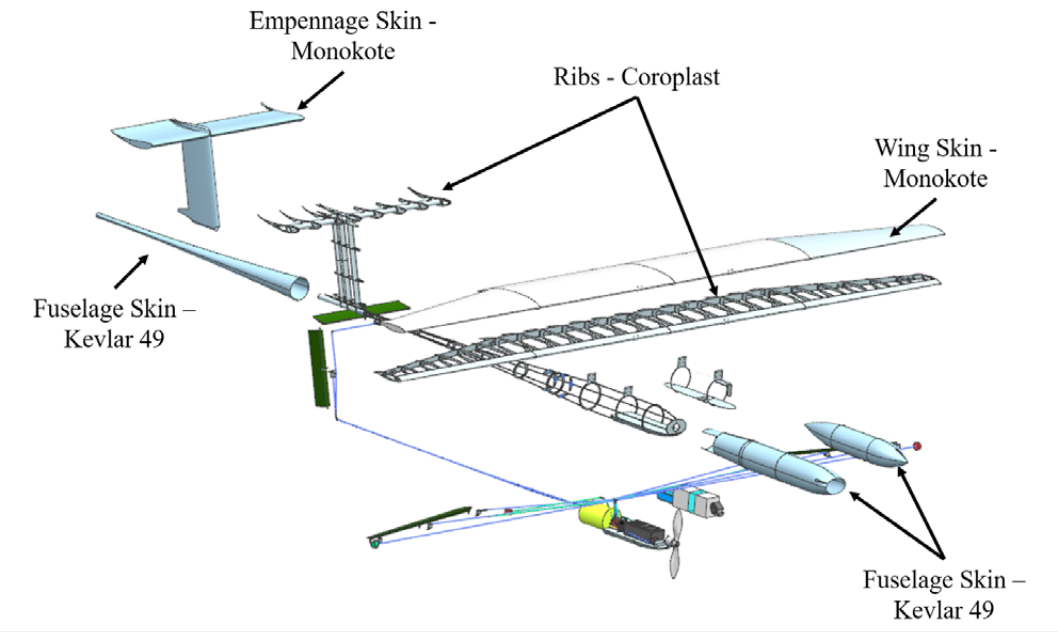

Fig. 28.1: Major Components and Materials

The bill of materials shown in Table 28.1 is a very brief overview of the detailed analysis that was conducted to determine the material for each individual structure. Materials were selected for their ease of procurement as well as the ability for relatively unskilled workers to work with the aircraft. With that said the fuselage is made of kevlar but this was outsourced to ensure quality manufacturing for this vital part of the aircraft. The majority of ribs were made of a corrugated plastic which has decent strength while also being incredibly light. Other, more load bearing ribs, as well as all spars, longerons, and threaded connections were made out of

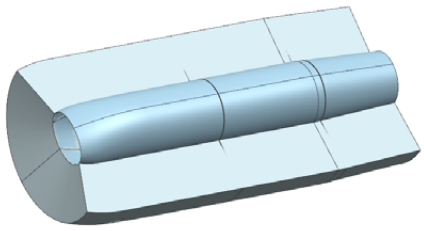

Fig. 28.2: Fuselage Kevlar Layup Tool

a lightweight aluminum. This gives strength to the structure where needed and also acts as a grounding plane for the aircraft. Figure 28.3 shows the manufacturing diagram. The manufacturing process will begin with the influx of ordered parts and materials. Workers begin to breakout parts for the assembly and manufacture ribs, ring frames, and other shape holding parts from coroplast. After this has been completed each component is individually assembled and then undergoes its respective systems integration. Following this the aircraft is fully assembled and a full systems check is performed. After this has been completed to satisfaction the aircraft is broken down for shipping to the customer.

Table 28.1: Bill of Materials for Major Components

Item	Material	Supplier
Spars (Wing and Empennage)	AA8090 Aluminum	Smith Metal
Connecting Ribs (Wings and Empennage)	AA8090 Aluminum	Smith Metal
Longerons	AA8090 Aluminum	Smith Metal
Ribs	Corrugated Plastic	Coroplast
Shock Absorbing Foam	Polyurethane Foam	HomeDepot
Fuselage	Kevlar 49	DuPont
Sensor Pod	Kevlar 49	DuPont

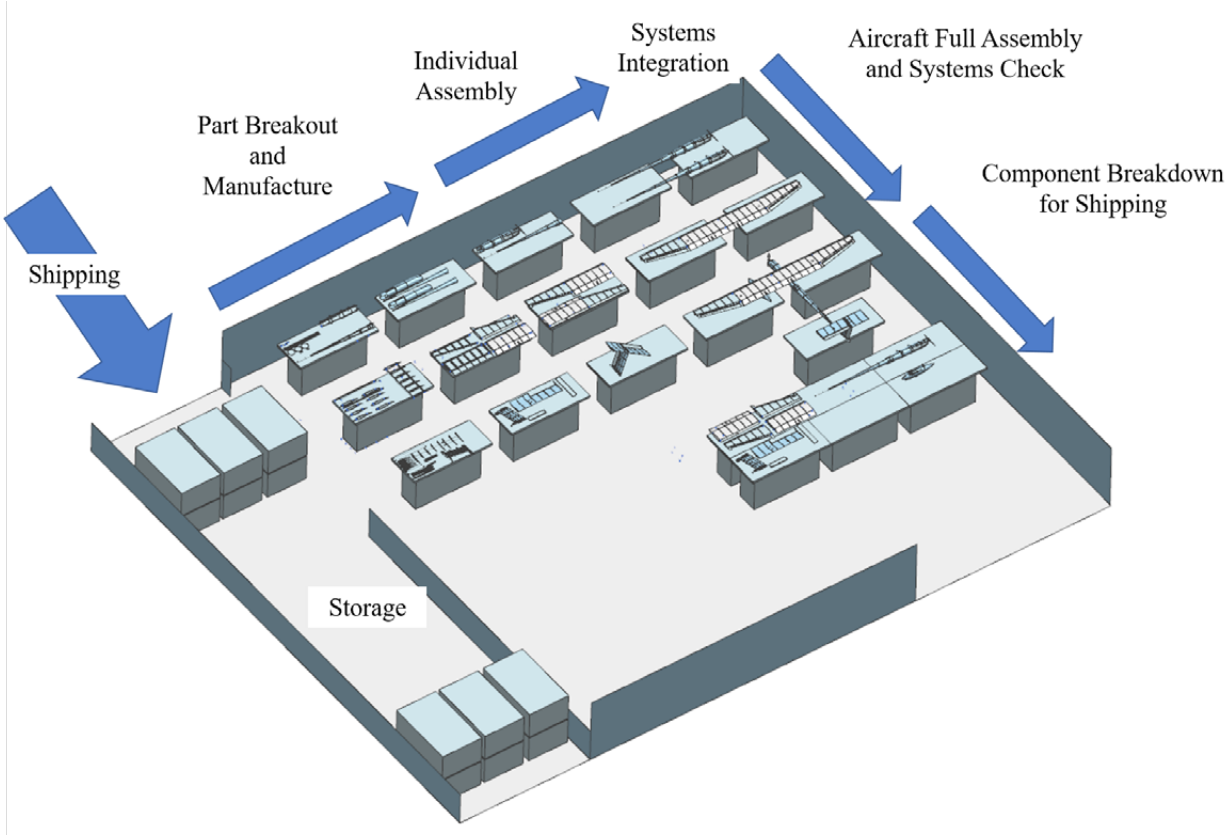

Fig. 28.3: Manufacturing Floor Plan

29. Specification Compliance

This section is a review of the RFP (Ref. 1) as stated in Chapter 1. Here the designer will demonstrate how DeHond has and has not met the requirements orginally specified within the RFP.

Specification Requirements/ Aircraft Characteristics	Aircraft Performance	Spec., or Requirement Threshold , Objective Met	Page #
Capable of taking off and landing from unimproved dirt roads or clearings.	Catapult launced/ airbag recovery	Yes	61
System shall be able to survey 100 linear miles of power transmission lines in one day.	Capable of 200 miles/ day	Yes	46
Capable of autonomous flight with an autopilot under lost link conditions.	Micropilot UAV Autopilot	Yes	53
Carry RIEGL miniVUX-1UAV weight 1.55 kg. LiDAR point clouds should have a density of 25 points per square meter.	>25 Points per square meter	Yes	14
The aircraft will have an ADS-B with broadcast capability.	Ping2020 ADS-B	Yes	53
The aircraft must have the ability to perform an emergency recovery in the event of a propulsion failure.	Redundant flight control battery and parachute recovery method	Yes	54/62
The entire system must be contained within the truck.	Design breaks down into boxes	Yes	65

30. Marketing Plan and Aircraft Design Summary

This section will evaluate the marketing plan for DeHond. Following this section will be a small brochure showcasing the unique design and mission capability of DeHond.

DeHond finds itself in the middle ground between the high end expensive UAV and the dirt cheap. This aircraft is redundant and capable of flying long endurance missions while also not busting the budget. This can be marketed to smaller transmission companies which may not be able to afford the higher end systems or a company that is still unsure of adotping the UAV solution. DeHond can conduct autonomous flights due to its Micropilot autopilot allowing less experienced ground crews to easily inspect damaged powerlines. Additionally, DeHond has been designed to withstand impacts and the Kevlar structure can protect the valuable sensors held within the sensor pod. Being asymmetric, DeHond is great for observation and surveillance missions as there is no structure obscuring sensor view in front of or below the aircraft.

Other variants of DeHond can be marketed in the civilian and military sectors. In the civilian market a scaled down aircraft with a higher thrust to weight ratio could be marketed as a novelty aircraft that is forgiving and easy to fly. In the military sector DeBom could be used to target integrated air defense systems (IADS) or DeHond could be used in its traditional role as a surveillance aircraft.

DeHond Asymmetric Sensing

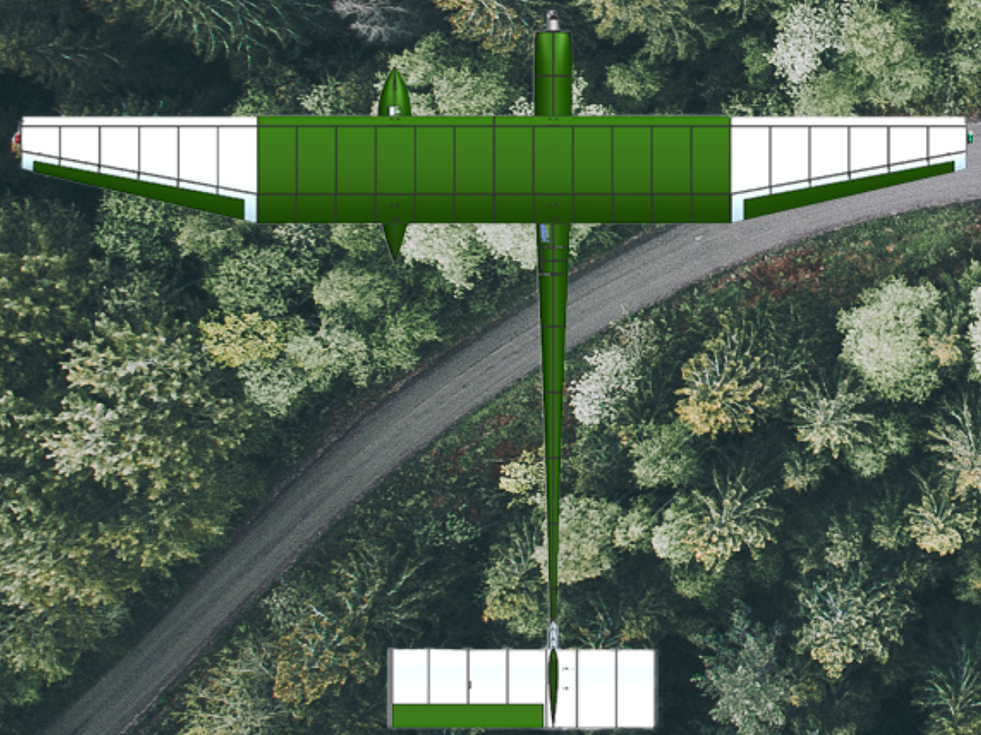

Weight.....36 lbf
Payload.....5 lbf
Span.....12 ft
Aspect Ratio.....10
Cruise Speed.....63.3 ft/s
Endurance.....2.5 hr
Range.....100 miles

References

1. Anon., "2018 - 2019 Undergraduate Individual Aircraft - Power Line Inspection Unmanned Aircraft System," AIAA, Design Competitions Page, [https://www.aiaa.org] Ameircan Institute of Aeronautics and Astronautics, Reston, VA 20191, 21 August 2018.

2. RIEGL, "RIEGL miniVUX-1UAV," RIEGL Laser Measurement Systems, URL: [http://www.riegl.com], September 2018.

3. Anon., "MP2128^{g2} Advanced UAV Autopilot," MicroPilot, URL: [http://store.micropilot.com/product-p/a-2128-g2.htm], 9 September 2018.

4. Anon., "uAvionix PING-2020 ADS-B Transceiver," uAvionix, URL: [https://uavionix.com/products/ping2020/], 9 September 2018.

5. Roskam, Jan, *Airplane Design: Part I: Preliminary Sizing of Airplanes*, DARcorp, Lawrence, KS, 2005.

6. Anon., "Transmission Maintenance," Westar Energy, URL: [hhttps://www.westarenergy.com/transmission-maintenance], 3 September 2018.

7. Anon., "Practice Power Line Inspection Ends in Wire Strike," AOPA, URL: [https://www.aopa.org/training-and-safety/air-safety-institute/accident-analysis/featured-accidents/practice-power-line-inspection-ends-in-wire-strike], 3 September 2018.

8. Anon., "Bird Diverter Helicopter Installation" URL: [http://www.capx2020.com/gallery/images/bird-diverter-helicopter-installation-closeup-web.jpg], 5 September 2018.

9. Anon., "Powerline Inspection Helicopter Crash Highlights Importance of Fuel Cross Checking, Says ATSB," Austrailian Aviation, [http://australianaviation.com.au/2018/08/powerline-inspection-helicopter-crash-highlights-importance-of-fuel-cross-checking-says-atsb/], 5 September 2018.

10. Anon., "Penguin C UAS," UAV Factory, Penguin C Specifications Page, [http://www.uavfactory.com], 25 August 2018.

11. Anon., "Prion MK3 Specifications," UAVE$_{LTD}$, Prion Mk3 Page, [https://www.uave.co.uk], 25 August 2018.

12. Anon., "Delair DT26x LiDAR," DELAIR Aerial Intelligence, DT26x LiDAR Specifications, [https://delair.aero], 27 August 2018.

13. Anon., " Atlantic Crossing II," Barnard Microsystems, Trans-Atlantic Model 5, [http://www.barnardmicrosystems.com/UAV/milestones/atlantic_crossing_2.html], 30 August 2018.

14. Anon., "AL-20," Aeroland UAV, AL-20 Specifications, [http://aerolanduav1.blogspot.com/2010/11/aeroland-al-20.html], 30 August 2018.

15. Anon., "AR4 Evolution," Tekever, AR4 Evolution Page, [http://airray.tekever.com/], 30 August 2018.

16. Anon., "CSV 20," Tasuma, CSV 20 Page, [http://www.tasuma-uk.com/tasuma.php?p=2], 30 August 2018.

17. Anon., "Penguin B UAS," UAV Factory, Penguin B Specifications Page, [http://www.uavfactory.com], 25 August 2018.

18. Anon., "Penguin BE Electric Platform," UAV Factory, Penguin BE Electric Specifications Page, [http://www.uavfactory.com], 25 August 2018.

19. Anon., "UAS: RQ-20B Puma™ AE," AeroVironment, RQ-20B Puma Page, [https://www.avinc.com], 30 August 2018.

20. Anon., "UAS: RQ-11B Raven™," AeroVironment, RQ-11B Raven Page, [https://www.avinc.com], 30 August 2018.

21. Anon., "ScanEagle," Boeing, ScanEagle Page, [https://www.boeing.com/defense/autonomous-systems/scaneagle/index.page], 30 August 2018.

22. Anon., "Coyote UAS," Raytheon, Coyote UAS Page, [https://www.raytheon.com], 30 August 2018.

23. Anon., "Silent Falcon," Silent Falcon, URL: [http://www.silentfalconuas.com/], 30 August 2018.

24. Anon., "Silver Fox UAS," Raytheon, Silver Fox UAS Page, [https://www.raytheon.com], 30 August 2018.

25. Anon., "Warmate: Polish Loitering Munition," Defence24, URL: [https://www.defence24.com/warmate-polish-loitering-munition-two-export-agreements-have-been-already-signed], 30 August 2018.

26. Anon., "IP Rating Chart," DSM&T, URL: [http://www.dsmt.com/resources/ip-rating-chart/], 24 September 2018.

27. Barrett, Ronald, "Report Block 1, Video1, rev. 8_30_18," The University of Kansas, URL: [https://vimeo.com/230399161], 21 August 2018.

28. Roskam, J., *Airplane Design Part II: Preliminary Configuration Design and Integration of the Propulsion System*, DARcorp, Lawrence, KS, 2005.

29. Pop, Sebastian, "RECOVERY SYSTEM OF THE MULTI-HELICOPTER UAV". Review Report, URL: [http://www.afahc.ro/ro/revista/2016_1/Prisacariu_Pop_Circiu_2016_1.pdf], 1 October 2018.

30. Lietzau, Zak, "Aircraft Intuitive Design (AID)," MATHWORKS, URL: [https://www.mathworks.com/matlabcentral/fileexchange/66770-aircraft-intuitive-design-aid], 15 September 2018.

31. Roskam, J., *Airplane Design Part III: Layout Design of Cockpit, Fuselage, Wing and Empennage*, DARcorp, Lawrence, KS, 2005.

32. Anon., "The Correct Material for Infrared (IR) Applications," Edmund Optics Worldwide, URL: [https://www.edmundoptics.com/resources/application-notes/optics/the-correct-material-for-infrared-applications/] 1 October 2018.

33. Muller, Markus, "eCalc," eCalc, URL: [https://ecalc.ch/index.htm], 26 September 2018.

34. Anon., "Tattu 22000 mAh 25C," Amazon.com, URL: [https://www.amazon.com/Tattu-22000mAh-22-2V-Battery-Multicopter/dp/B017NJTHJU], 26 September 2018.

35. Anon., "T-Motor MT3520," OMGFly, URL: [http://www.omgfly.com/tmotor-mt3520-kv300-400-p-2508.html] 1 October 2018.

36. Anon., "Advanced Aircraft Analysis," DARcorp, URL: [http://www.darcorp.com/Software/AAA/] 1 October 2018.

37. Barrett, R. "Technical Discussion of Swept Vertical Tails," The University of Kansas, Aerospace Engineering Department, Lawrence, KS, 18 October 2018.

38. Barrett, R. "Technical Discussion of Catapult Kinematics," The University of Kansas, Aerospace Engineering Department, Lawrence, KS, September 2018.

39. Anon., "*AVA Catapult,*" Air-Vision-Air, URL: [http://www.air-vision-air.com/products-for-you/asm300-2-5-6kg-catapult/], 20 October 2018.

40. Anon., "*Parachute Descent Rate Calculator,*" Fruity Chutes, URL: [https://fruitychutes.com/help_for_parachutes/parachute-descent-rate-calculator.htm], 20 October 2018.

41. Roskam, J., *Airplane Design Part V: Component Weight Estimation*, DARcorp, Lawrence, KS, 2005.

42. Barrett, Ronald, "Report Block 3, Video, rev. 10/15/18," The University of Kansas, URL: [https://vimeo.com/295262380], October 2018.

43. Roskam, J., *Airplane Design Part VI: Preliminary Calculation of Aerodynamic Thrust and Power Characteristics*, DARcorp, Lawrence, KS, 2005.

44. Gupta, S., "Propeller," GrabCAD, URL: [https://grabcad.com/library/propeller-308], 31 October 2018.

45. Anon., "Hextronik HXT500," HobbyKing, URL: [https://hobbyking.com], November 2018.

46. Anon., "Turnigy TGY-9018MG," HobbyKing, URL: [https://hobbyking.com], November 2018.

47. Anon., "Turnigy TGY-811 Slim," HobbyKing, URL: [https://hobbyking.com], November 2018.

48. Anon., "Turnigy Nano-Tech 6000 mAh LiPo Pack," HobbyKing, URL: [https://hobbyking.com], November 2018.

49. Anon., "Turnigy 3600 mAh LiPo Pack," HobbyKing, URL: [https://hobbyking.com], November 2018.

50. Anon., "FrSky 8-Channel Receiver," HobbyKing, URL: [https://hobbyking.com], September 2018.

51. Anon., "PicoMax," Aveo Engineering, URL: [http://www.aveoengineering.com], November 2018.

52. Anon., "FLIR Vue Pro and Vue Pro R," FLIR, URL: [https://www.flir.com], September 2018.

53. Frick, C. W., Davis, W. F., Randall, L., and Mossman, E. A., "An Experimental Investigation of NACA Submerged Duct Entrances," NACA, found via NASA Publications [https://ntrs.nasa.gov/search.jsp?R=20090012113], May 1945.

54. Clayton, S., "NACA_profile_calculator," Sports Racer Network, URL: [http://dsr.racer.net/], January 2005.

55. Roskam, J., *Airplane Design Part IV: Layout Design of Landing Gear & Systems*, DARcorp, Lawrence, KS, 2005.

56. Anon., "CENTRALPNEUMATIC 30 Gal. Truck Bed Air Compressor," Harbor Freight, URL: [https://www.harborfreight.com/30-gal-420cc-truck-bed-air-compressor-epa-iii-62779.html], 25 November 2018.

57. Anon., "Velocity During Recovery," NASA Glenn Research Center, URL: [https://www.grc.nasa.gov/www/k-12/VirtualAero/BottleRocket/airplane/rktvrecv.html], 25 November 2018.

58. Anon., "Fox Airbeds King Size," Amazon.com, URL: [https://www.amazon.com/Best-Inflatable-Bed-Fox-Airbeds/dp/B00QQVBGC8/ref=sr_1_2_sspa?ie=UTF8&qid=1543175151&sr=8-2-spons&keywords=king+sized+air+mattress&psc=1], 25 November 2018.

59. Anon., "Coroplast Tolerance Specs," Coroplast, URL: [https://www.coroplast.com/technicalinfo/tolspecs.htm], December 2018.

60. Anon., "3M™ Scotch-Weld™ Metal Bonder Acrylic Adhesive DP8407NS Gray," 3M, URL: [https://3m.citrination.com/pif/000926?locale=en-US], December 2018.

61. Anon., "Aluminum 8090 Alloy (UNS A98090)," AZO Materials, URL: [https://www.azom.com/article.aspx?ArticleID=8789], December 2018.

62. Anon., "Spray Polyurethane Foam Statistics," AmericanChemistry.com, URL: [https://polyurethane.americanchemistry.com/Spray-Foam-Coalition/SPF-Stats-Brochure.pdf], December 2018.

63. Anon., "KEVLAR ARAMID FIBER TECHNICAL GUIDE," DuPont, URL: [http://www.dupont.com/content/dam/dupont/products-and-services/fabrics-fibers-and-nonwovens/fibers/documents/Kevlar_Technical_Guide.pdf], December 2018.

64. Anon., "ZINC Sulfide," PubChem, URL: [https://pubchem.ncbi.nlm.nih.gov/compound/zinc_sulfide#section=Top], December 2018.

65. Bien, F., Perez, H., "Covering and Painting Weights," FatlLion.com, URL: [http://www.fatlion.com/sailplanes/weights.html], December 2018.

66. Anon., "Weights per Thousand for Pan Head Industrial Screws," Elgin Fastener Group, URL: [https://elginfasteners.com/resources/weights-per-thousand-for-pan-head-industrial-screws/], December 2018.

67. Anon., "Medium-Light Servo Extension Cable," Hyperflight.co.uk, URL: [https://www.hyperflight.co.uk/products.asp?code=MLW-SERVO-EXT&name=medium-light-servo-extension-cable], December 2018.

68. Anon., "Siemens NX", Version 12.0.0.27, URL: [www.plm.automation.siemens.com], December 2018.

69. Anon., "TOW Anti-Tank Guided Missiles," Military Today, URL: [http://www.military-today.com/missiles/tow.htm], December 2018.

70. Anon., "Mongolian Shilka AAA gun system during joint RUssian-Mongolian exercises" Deagel.com, URL: [http://www.deagel.com/library/Mongolian-Shilka-AAA-gun-system-during-joint-Russian-Mongolian-exercises-Selenga-2016-at-polygon-Burdun-Republic-of-Buryatia-on-August-31-2016_m02016083100004.aspx], December 2018.

71. Bloisi, D., Iocchi, L., Fiorni, M., Graziano, G., "Camera Based Rarget Recognition for Maritime Awareness," Sapienza University of Rome, Italy, June 2014.

72. Anon., "Global Regenerative Fuel Cell (RFC)," OpenPR, URL: [https://www.openpr.com/news/570587/Global-Regenerative-Fuel-Cell-RFC-Market-2017-SFC-Power-Polyfuel-Sharp-Corp-Toshiba-Corp.html], December 2018.